NASA CONTRACTOR
REPORT

NASA CR-2

NASA CR-2678

ATMOSPHERIC STRUCTURE AND VARIABILITY
IN AREAS OF CONVECTIVE STORMS
DETERMINED FROM 3-h RAWINSONDE DATA

Gregory S. Wilson and James R. Scoggins

NATIONAL AERONAUTICS AND SPACE ADMINISTRATION • WASHINGTON, D. C. • APRIL 1976

1. REPORT NO. NASA CR-2678	2. GOVERNMENT ACCESSION NO.	3. RECIPIENT'S CATALOG NO.
4. TITLE AND SUBTITLE Atmospheric Structure and Variability in Areas of Convective Storms Determined from 3-h Rawinsonde Data		5. REPORT DATE April 1976
		6. PERFORMING ORGANIZATION CODE M167
7. AUTHOR(S) Gregory S. Wilson and James R. Scoggins		8. PERFORMING ORGANIZATION REPORT #
9. PERFORMING ORGANIZATION NAME AND ADDRESS Texas A&M University College Station, Texas 77840		10. WORK UNIT NO.
		11. CONTRACT OR GRANT NO. NAS8-26751
12. SPONSORING AGENCY NAME AND ADDRESS National Aeronautics and Space Administration Washington, D. C. 20546 .		13. TYPE OF REPORT & PERIOD COVERED Contractor
		14. SPONSORING AGENCY CODE

15 SUPPLEMENTARY NOTES

16. ABSTRACT

The structure and variability of the atmosphere in areas of radar-observed convection are established by using the unique 3-h rawinsonde and surface data from NASA's second Atmospheric Variability Experiment (AVE II) conducted on May 11 and 12, 1974.

Convective activity is shown to exist in areas where the low and middle troposphere is moist and the air is potentially and convectively unstable and has upward motion, in combination with positive moisture advection, at either the surface or within the boundary layer. The large variability of the parameters associated with convective storms over time intervals less than 12 h is also demonstrated so as to possibly produce a change in the probability of convective activity by a factor of 8 or more in 3 h. Between 30 and 60 percent of the total changes in parameters associated with convective activity over a 12-h period is shown to take place during a 3-h period. These large changes in parameters, normally measured with 12-h data, are related to subsynoptic-scale systems that many times produced convective storms.

17. KEY WORDS	18. DISTRIBUTION STATEMENT Category 47

19. SECURITY CLASSIF. (of this report) Unclassified	20. SECURITY CLASSIF. (of this page) Unclassified	21. NO. OF PAGES 128	22. PRICE $5.75

For sale by the National Technical Information Service, Springfield, Virginia 22161

FOREWORD

This report is one of several to be published from research conducted under NASA Contract NAS8-26751 entitled "Atmospheric Variability and Vertical Motion." This effort is sponsored by the NASA Office of Applications under the direction of Marshall Space Flight Center's Aerospace Environment Division. The results presented in this report represent only a portion of the total research effort. Other reports will be published as the research progresses. Data used in the report were taken from the AVE II Experiment conducted during a 24-h period beginning at 1200 GMT on May 11, 1974, and ending at 1200 GMT on May 12, 1974.

AUTHORS' ACKNOWLEDGMENTS

TABLE OF CONTENTS

TABLE OF CONTENTS (Continued)

LIST OF FIGURES

LIST OF FIGURES (Continued)

ATMOSPHERIC STRUCTURE AND VARIABILITY IN AREAS OF CONVECTIVE

STORMS DETERMINED FROM 3-H RAWINSONDE DATA

by

Gregory S. Wilson[1]

and

James R. Scoggins[2]

Center for Applied Geosciences
Texas A&M University

1. INTRODUCTION

Convective systems are important in meteorology for many reasons.
They provide a mechanism for the vertical transport of moisture and
heat (Palmen and Newton, 1969), are responsible for much of the needed
precipitation during the summer months over large regions of the
United States, cause much of the severe weather such as tornadoes,
hail, and damaging surface wind, and influence large-scale circulations
in the atmosphere (Ninomiya, 1971). The importance of convective
systems has been recognized by the general scientific community as
evidenced by the emphasis placed upon convective systems in GATE and
other programs. Yet, even with the sophisticated data provided by
satellites, aircraft, and other meteorological observing systems
including the synoptic network, insufficient knowledge exists on the
relationships between convective- and synoptic-scale systems. Because
of the type of available data, it is necessary to assume that such a
relationship exists to forecast convective systems.

A study of the interrelationships between large-scale synoptic or
subsynoptic systems and small-scale convective systems offers definite
benefits in terms of increasing forecasting skills and furthering the
understanding of atmospheric processes. In fact, these interrelation-
ships must be understood better if forecasts of small-scale convective

systems and severe thunderstorms are to be improved since present measurements and numerical forecast models are unable to operationally define and predict these important weather producers.

In this research, the variability and structure of large-scale synoptic systems are related to radar-observed convection using the second Atmospheric Variability Experiment (AVE II) data obtained by NASA between 1200 GMT, 11 May and 1200 GMT, 12 May 1974. By using the unique 3-h consecutive rawinsonde soundings, the primary purpose of the study is to better establish the interrelationships between synoptic- and convective-scale systems by determining the atmospheric structure and variability in areas of radar-observed convection that could not be measured from 12-h rawinsonde data. Convection, as referred to in this study, denotes the existence of convective clouds observed by radar.

2. BACKGROUND AND STATEMENT OF PROBLEM

a. Statement of problem

A basic assumption made by some atmospheric scientists is that an interrelationship exists between convective- and synoptic-scale systems outside the tropics. Some general relationships already have been established from the 12-h synoptic rawinsonde data measured operationally, but forecasts of convective activity still fail to consistently verify in space and time. The primary reason for the failure of the forecasts is that relationships between convective- and synoptic-scale systems have not been established well or resolved from 12-h synoptic rawinsonde data.

The underlying problem in understanding the interactions between synoptic- and convective-scale systems is that the time and space scales of motion of convective systems cannot be consistently measured from the synoptic rawinsonde network. Even so, large-scale synoptic distributions of potential instability and vertical motion have been related directly to the formation of convection. However, the variability of these and other parameters over time periods shorter than the normal 12-h synoptic time interval must be understood and predicted if convective activity is to be forecasted accurately. Therefore, the basic problem in this study was to determine what changes in atmospheric structure occur when convective systems develop and interact with the large-scale synoptic environment. The use of 3-h rawinsonde data allowed better resolution of convective systems whose time scales of motion usually are much less than 12-h.

b. Previous studies

The first step in determining the relationships between convective- and synoptic-scale systems is to establish the large-scale atmospheric structure in areas where convection is present. Previous research to determine this structure has concentrated upon objective methods which relate synoptic-scale parameters to the observed convection.

Endlich and Mancuso (1968) studied the relationships between objectively analyzed synoptic data and severe convective storms. They

were able to identify accurately areas in which severe weather occurred by establishing those parameters that correlated best in space with the observed convection. A basic conclusion reached in the paper was that boundary layer fluxes of temperature and moisture appeared to be more directly related to severe storm occurrence than lapse rates of temperature or parcel instabilities. In addition, the usefulness of objective analysis techniques to resolve subsynoptic-scale features that delineated areas where convection formed, was demonstrated.

Scoggins and Wood (1971) studied those factors responsible for the formation and prediction of convection from synoptic-scale data. They concluded that potential instability and positive vertical motion were the two most important synoptic-scale parameters responsible for the formation of convection.

Ninomiya (1971) examined the structure of the atmosphere in an area of severe convection by using two consecutive 12-h synoptic time periods. Detailed synoptic and dynamic analysis of the data was used to clarify the physical interactions between the large-scale synoptic flow and the severe thunderstorm areas. A primary conclusion was that convective systems interact with and modify the large-scale synoptic field mainly through the release of latent heat. The resulting warm core observed by the author in the middle and upper troposphere above the convection area was apparently responsible for intensifying the horizontal temperature gradient that resulted in a strong upper-level jet. The jet maintained the convective system by creating strong upper-level divergence over the convective area. An entire interaction model was developed to explain the formation and development of the convective system through the transfer of energy between the synoptic- and convective-scale systems.

Probability forecasts of convection have been developed recently by Bonner et al. (1971), Reap and Foster (1975), and David (1973) using screening regression with forecast parameters from numerical models. Statistical correlations between observed convection and forecasted parameters have helped in establishing the relationships between convective- and synoptic-scale systems, but the inability of the present models to resolve and forecast subsynoptic-scale systems has limited the accuracy of forecasts of convection. Even so, the best forecast

parameters determined from the correlations of parameters with convective activity indicate that the layer of air between the surface and 10,000 ft should be moist and convectively unstable with positive vertical motion occurring within the layer.

A short range forecasting technique for severe weather, developed by Charba (1975), has demonstrated the importance of surface effects in the formation and prediction of convective activity. Surface data are used primarily to better define subsynoptic and mesoscale features usually associated with convective systems.

Research at the National Severe Storms Laboratory (NSSL) has emphasized the importance of subsynoptic and mesoscale systems in creating specific regions within the large-scale synoptic field where the release of instability resulted in convection. Lewis et al. (1974) examined a specific case of squall line formation within an area of large-scale upslope motion above a frontal surface. The results indicated that the large-scale synoptic field created a shallow layer of convectively unstable air above the frontal surface, and subsynoptic-scale features of strong, low level, wind shear and surface wind convergence produced a small region where strong, positive, vertical motion released the instability and produced convection.

Fankhauser (1969) was able to identify subsynoptic and mesoscale systems moving through the NSSL mesoscale rawinsonde network that were responsible for producing convection. Fankhauser concluded that many convective processes could be resolved from rawinsonde data measured at 1.5-h intervals within a mesoscale network.

Finally, mesoscale numerical models, initialized with synoptic rawinsonde data, have been used successfully to forecast subsynoptic-scale systems that produced convection. Kaplan et al. (1973) developed a subsynoptic-scale, primitive-equation model that was able to predict the movement and development of subsynoptic-scale systems and features that resulted in the severe convection associated with the Palm Sunday Tornadoes of 1965. The results indicated that synoptic-scale rawinsonde data could be used to establish and predict the interrelationships between synoptic- and convective-scale systems.

c.   Objectives

The primary objective of this research is to use the unique 3-h
AVE II rawinsonde and surface data to determine the structure and
variability of the large-scale synoptic conditions relative to radar-
observed convection.

The following is a list of specific objectives:

(1)   Establish the spatial and temporal relationships between
      parameters measured or computed from 3-h rawinsonde data
      and radar-observed convection.

(2)   Determine the variability of parameters associated with
      convection over time intervals of 3, 6, 9, and 12 h.

(3)   Determine the interrelationships between various synoptic-
      scale conditions and radar-observed convection.

(4)   Examine the interactions of synoptic- and convective-
      scale systems.

3. DATA AND SYNOPTIC CONDITIONS

a. <u>AVE II Pilot Experiment</u>

    1. <u>Rawinsonde and surface data</u>

The data utilized in this study consists of rawinsonde soundings taken at intervals of 3 h at 54 stations over the United States east of approximately 105° west longitude. Soundings began at 1200 GMT on May 11 and ended at 1200 GMT on May 12, 1974. These data constitute the AVE II pilot experiment conducted by NASA (Scoggins and Turner, 1975). Figure 1 shows the locations and station identifiers* of the participating stations.

To supplement the rawinsonde data within the AVE II network, all available surface data were obtained from the National Climatic Center. Figure 2 shows the locations of the 310 surface stations used within the AVE II area.

The data reduction procedure used in processing the AVE II rawinsonde data is considerably different from that usually employed with operational rawinsonde data. Asimuth and elevation angles were read at 30-s intervals and thermodynamic quantities were determined for each pressure contact. The raw data were keypunched and checked for errors by computer before calculating the soundings. The computed soundings were then rechecked for errors and corrections made as required.

The entire master reduction program was designed to obtain the most accurate data possible from rawinsonde soundings. Estimates of the RMS errors of the thermodynamic quantities are as follows (Scoggins and Smith, 1973; Fuelberg, 1974):

<u>Parameter</u>	<u>Approximate RMS Error</u>
Temperature	1°C
Pressure	1.3 mb surface to 400 mb; 1.1 mb between 400 and 100 mb; 0.7 mb between 100 and 10 mb
Humidity	10%
Pressure Altitude	10 gpm at 500 mb; 20 gpm at 300 mb; 50 gpm at 50 mb.

---

*Station names are given in Appendix I.
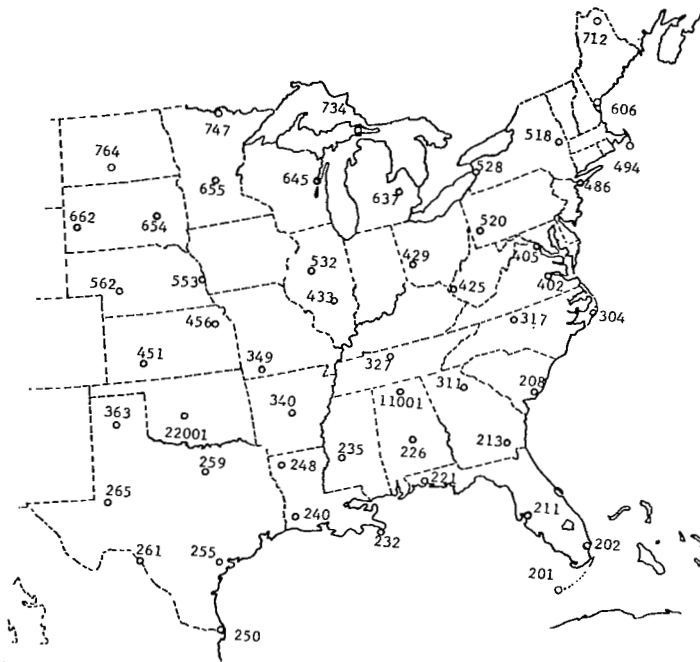
Fig. 1. Location of rawinsonde stations for AVE II.
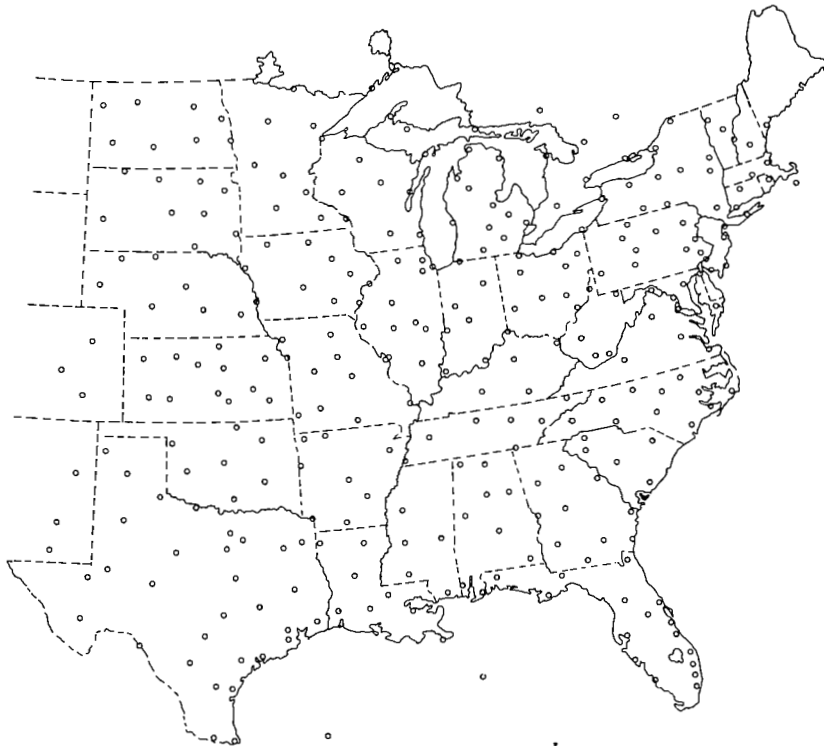
Fig. 2. Locations of surface stations in AVE II.

An error analysis conducted by Fuelberg (1974) indicates RMS
vector errors in wind speed for the AVE II data as follows:

Level	Elevation Angle	
	40°	10°
700 mb	0.5 m s^{-1}	2.5 m s^{-1}
500 mb	0.8 m s^{-1}	4.5 m s^{-1}
300 mb	1.0 m s^{-1}	7.8 m s^{-1}

These RMS errors agree closely with those presented by Reiter (1963)
and those determined at the Air Force Missile Test Center in Florida.*
The data reduction program and the complete error analysis are presented
by Fuelberg (1974), and the AVE II data are given at 25-mb intervals
by Scoggins and Turner (1975).

All surface data were read and keypunched for the nine release
times of the AVE II experiment from the hourly service "A" observations.
Vector winds, temperature, dew point temperature, and surface pressure
were the surface parameters used in this study. All data were checked
carefully both manually and by computer for inaccurate or unrepresenta-
tive measurements and corrections made as needed.

2. Digital radar data

To determine accurately the intensity and position of radar-
observed convection in the AVE II experiment, the Manually Digitized
Radar (MDR) data were obtained from NOAA's Techniques Development
Laboratory and plotted for every hour during the experiment. Figure 3
shows the MDR grid network which covers almost the entire AVE II
experimental area. Each MDR radar block is approximately a square
83 km on a side.

MDR data are in coded form with a single digit between 1 and 9
indicating the areal coverage and echo intensity within each square.
The following is an explanation of the MDR code (Foster and Reap, 1973):

---

*Meteorological Handbook, AFMTCP 105-1, 4th Weather Group, Patrick
Air Force Base, Florida, June 1963.
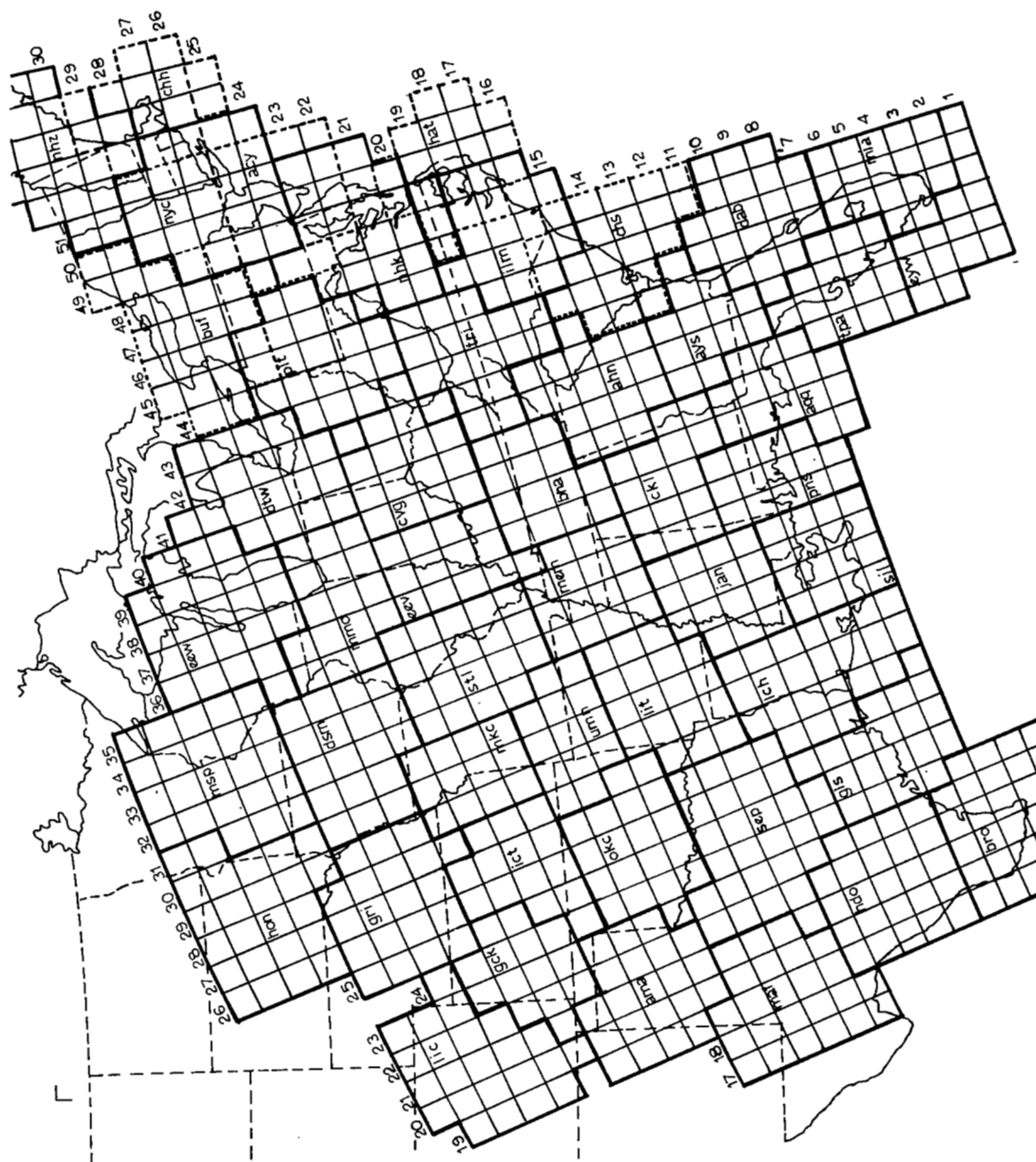
Fig. 3. Manually digitized radar (MDR) grid network.

Code No.	Maximum Observed VIP[1] Values	Coverage In Box	Maximum Rainfall Rate (in./hr)	Intensity Category
0	No Echoes			
1	1	Any VIP1	<.1	Weak
2	2	≤ 50% of VIP2	.1-.5	Moderate
3	2	> 50% of VIP2	.5-1.0	Moderate
4	3	≤ 50% of VIP3	1.0-2.0	Strong
5	3	> 50% of VIP3	1.0-2.0	Strong
6	4	≤ 50% of VIP3 and 4	1.0-2.0	Very Strong
7	4	> 50% of VIP3 and 4	1.0-2.0	Very Strong
8	5 or 6	≤ 50% of VIP3, 4, 5 and 6	>2.0	Intense or Extreme
9	5 or 6	> 50% of VIP3, 4, 5 and 6	>2.0	Intense or Extreme

[1]Video Integrator Processor

Areas of convection for each of the 3-h rawinsonde periods in AVE II were determined by combining 3 hourly plots of MDR data surrounding a given rawinsonde release time into a composite radar chart. The highest coded value during the 3-h period was used when echoes were observed in a given block at consecutive hourly observations. The intensity of convection was separated by assuming that rainshowers exist for $2 \leq MDR \leq 3$, and thunderstorms for $MDR \geq 4$ (Reap, 1975).

b. Synoptic conditions

The synoptic situation at the beginning of the AVE II experiment (1200 GMT 11 May) consisted of a large push of cold polar air moving southeastward through the Northern Plains States, a retreating cold air mass moving northeastward over the Northeast U.S., and a flow of warm, moist air moving northeastward through the Mississippi Valley ahead of the polar air. Figures 4 and 5 show surface-, 850-, 700-, 500-, and 300-mb charts for the periods 1800 GMT, 11 May 1974, and 0600 GMT, 12 May 1974, six hours after the start and preceeding the end of the experiment, respectively.

(a) Surface

(b)   850 mb

Fig. 4.   Synoptic charts for 1800 GMT, 11 May 1974.
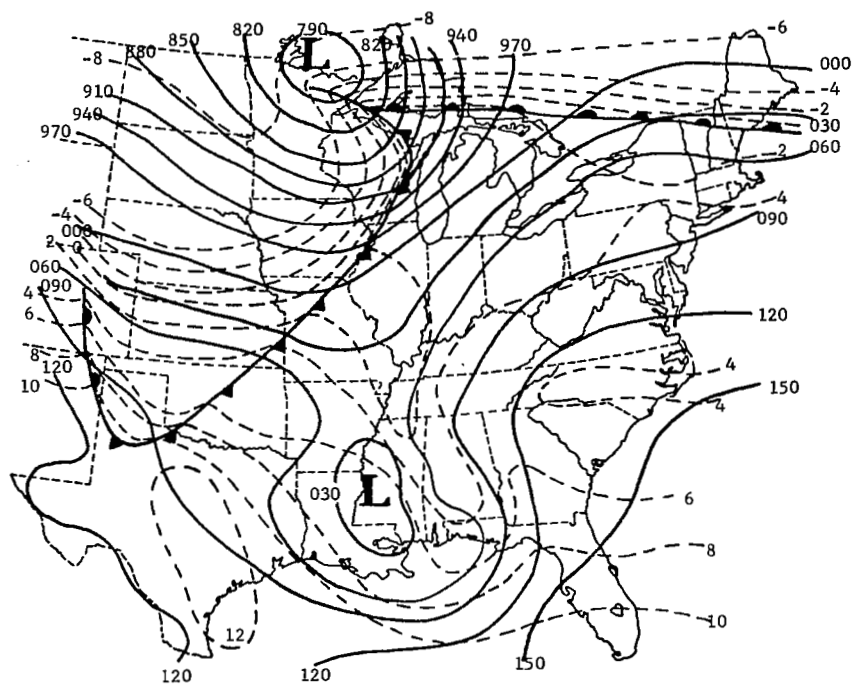
(c) 700 mb
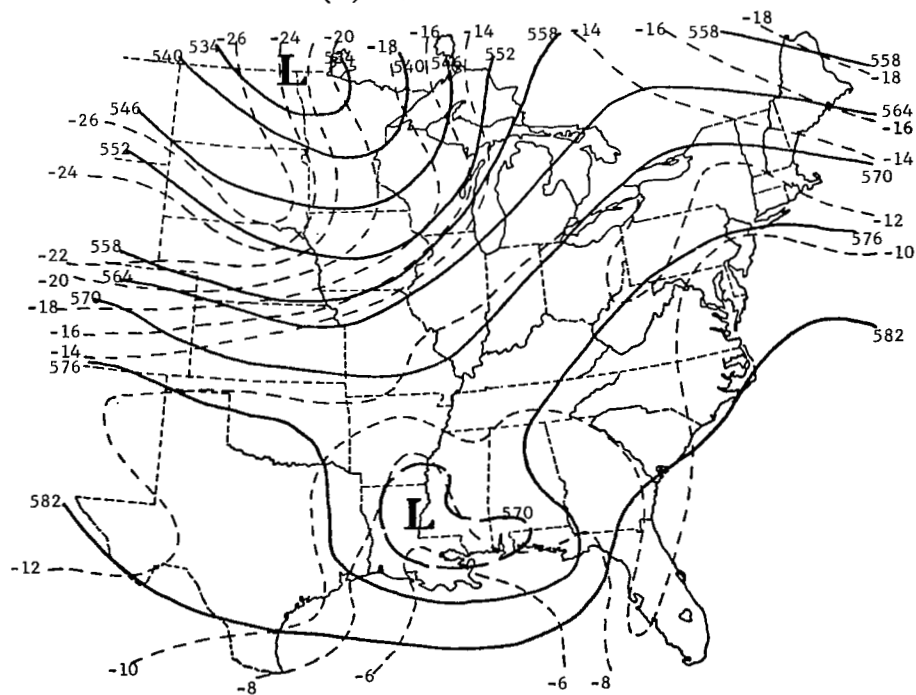
(d) 500 mb

Fig. 4. (Continued)
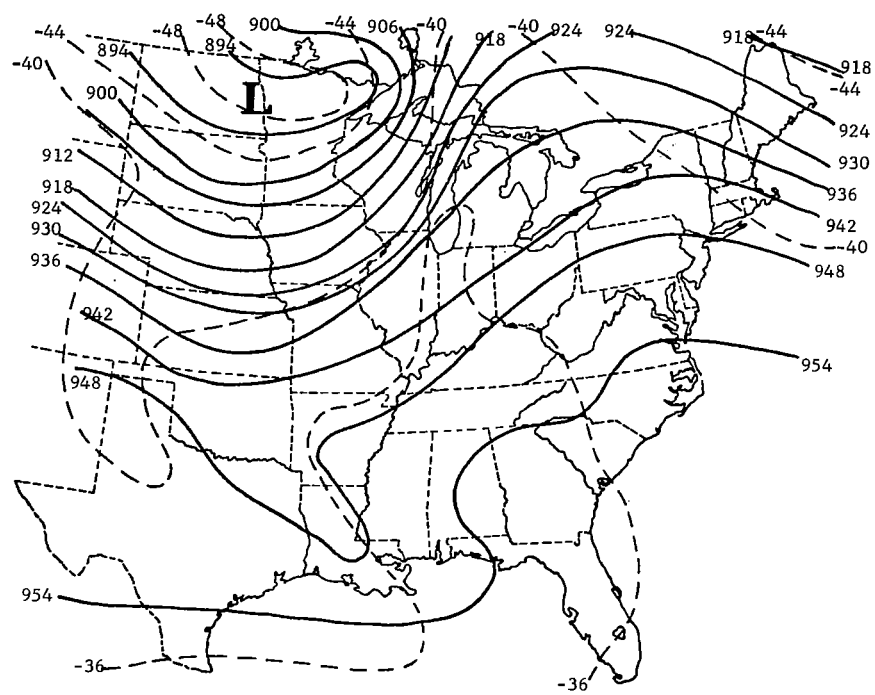
(e)   300 mb

Fig. 4.   (Continued)
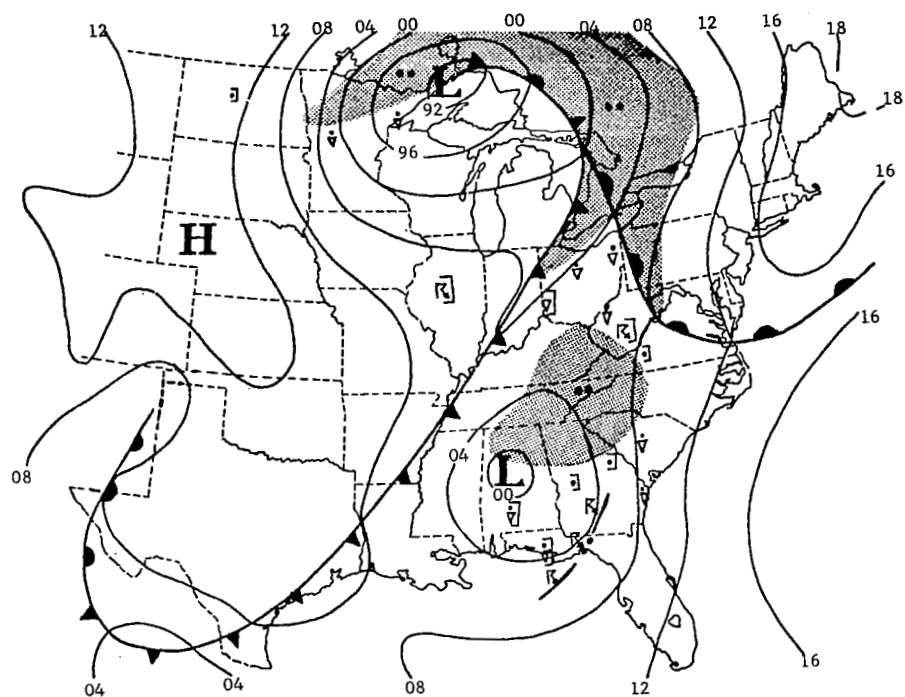
(a) Surface
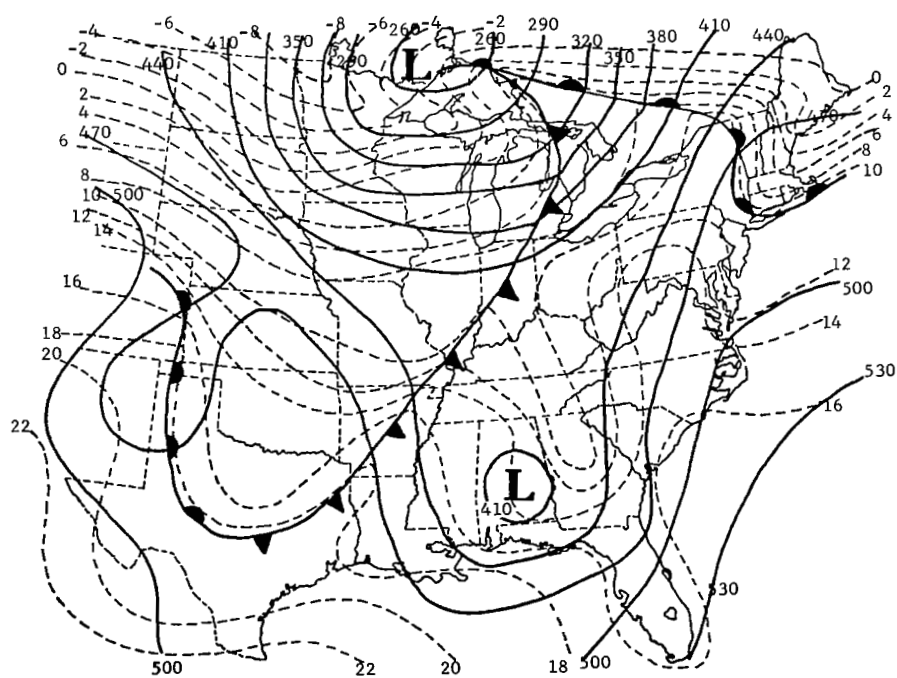
(b) 850 mb

Fig. 5. Synoptic charts for 0600 GMT, 12 May 1974.

(c)   700 mb

(d)   500 mb
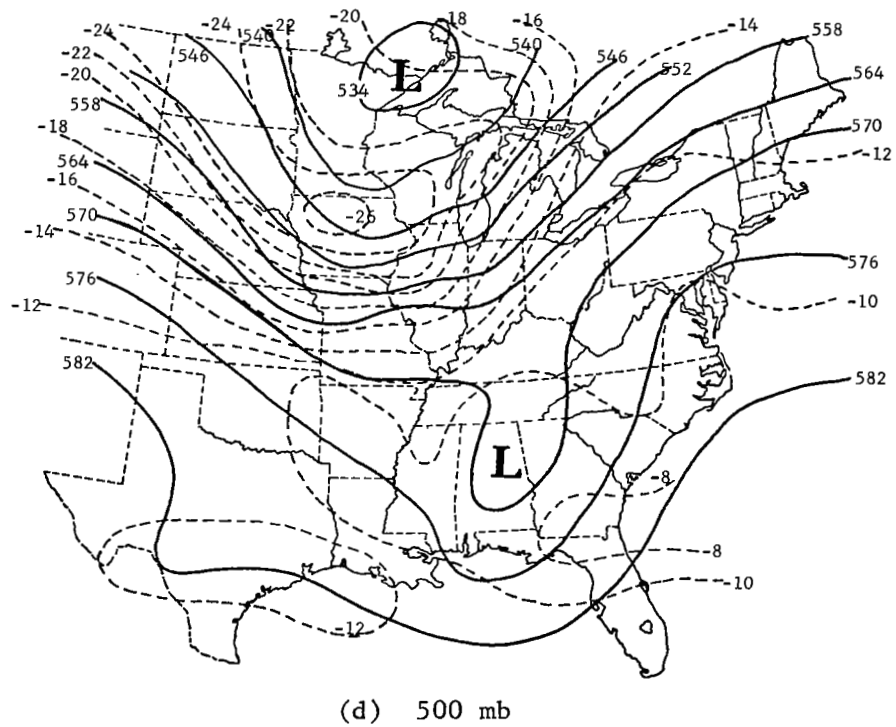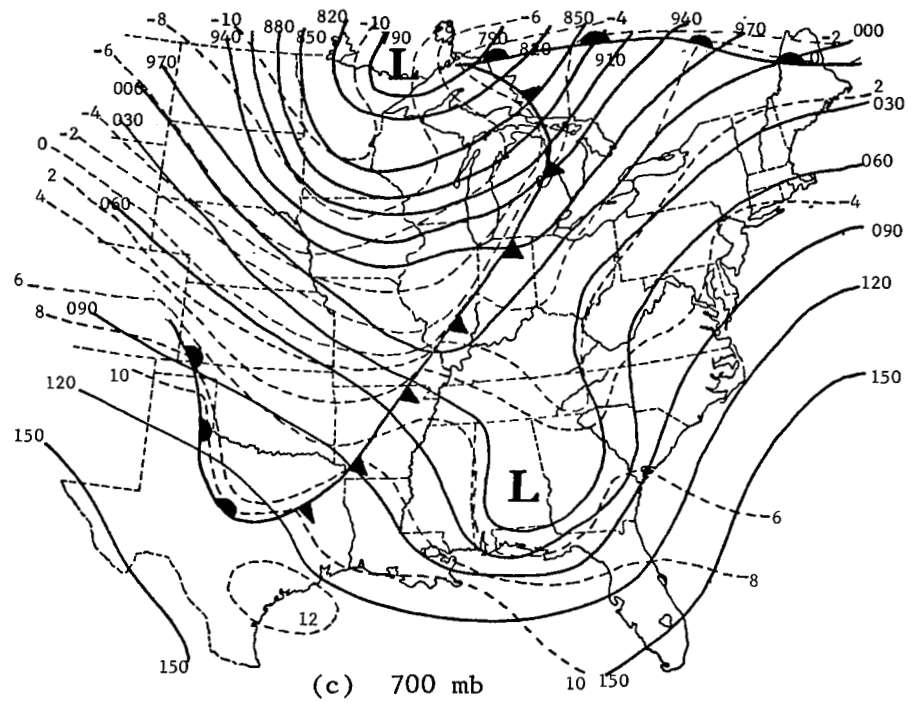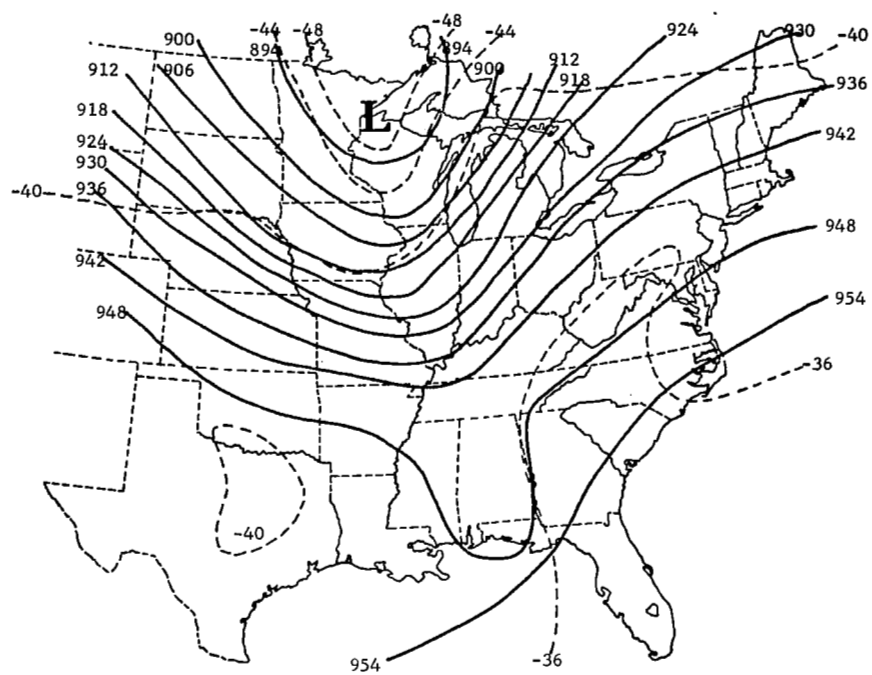
Fig. 5.   (Continued)

(e)   300 mb

Fig. 5.   (Continued)

Two major weather systems were moving through the AVE II network during the 24-h experiment. A strong and partially-occluded cold front, which connected with a deep cyclone, moved eastward through the Great Lakes and Mississippi Valley as the cyclone itself moved slowly northeastward across Minnesota and Lake Superior. A warm-sector surface low with an almost vertical structure moved eastward across Louisiana, Mississippi, and Georgia ahead of the cold front.

Widespread rain and thundershower activity were present during the entire experiment ahead of the cold front and on top of the warm frontal surface. Mostly stratiform-type precipitation occurred within the occluded part of the cyclone over the Great Lakes. Heavy shower and thunderstorm activity was predominant over the southeast U.S. as the surface low there produced strong vertical motion within the warm and moist air ahead of the front.

Two smaller-scale disturbances developed during the experiment that were particularly interesting. A post-frontal line of thunderstorms formed within the cold air over Nebraska and South Dakota around 2100 GMT on 11 May in association with an upper-level cold pocket and short wave. In addition, a squall line containing heavy to severe thunderstorms developed at 0600 GMT, 12 May 1974 from southeast Georgia southwestward into the Gulf of Mexico. Maximum radar tops along the squall line were above 55,000 ft.

4. ANALYTICAL APPROACH

a. Objective analysis scheme

An objective analysis scheme developed by Barnes (1964) was used
to interpolate the 25-mb rawinsonde and surface data to a grid (Fig. 6)
with approximately a 160-km spacing between grid points. This grid
point spacing essentially produces the maximum horizontal resolution
possible from randomly spaced rawinsonde stations (Barr et al. 1971).
The data from each rawinsonde station were allowed to influence grid-
points within a radius of only three grid distances so that major
subsynoptic-scale features were not eliminated. A radius of influence
of 2 grid points was used in the surface analysis which produced
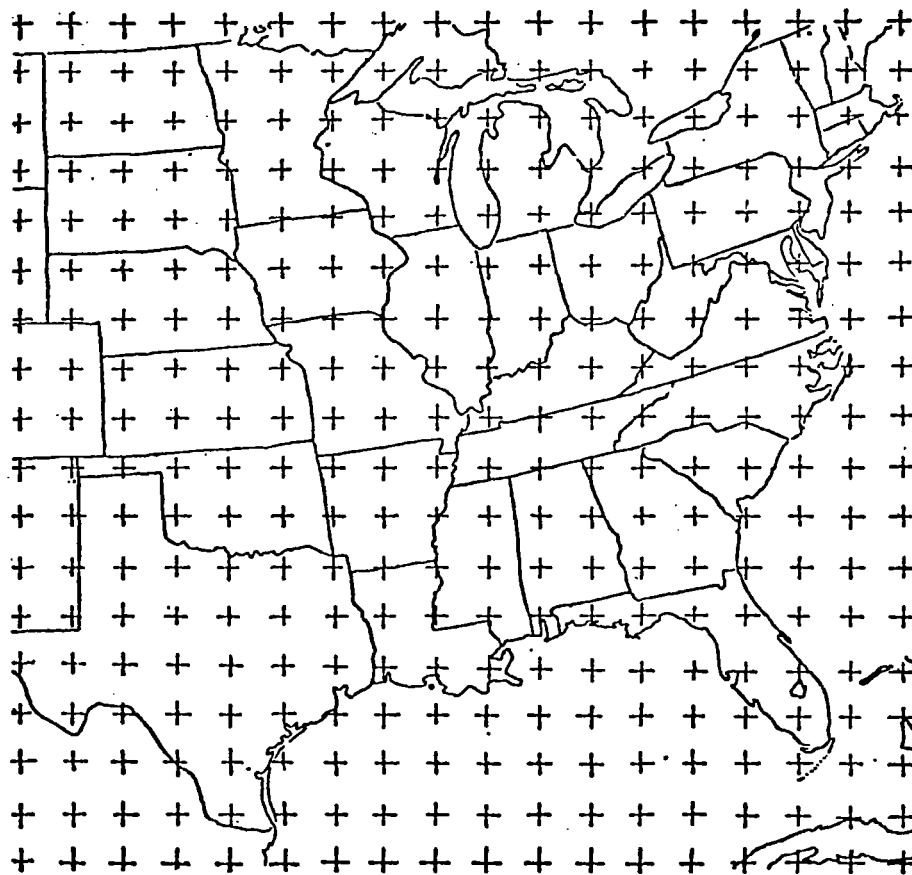
Fig. 6. Grid used for numerical computations.

smooth fields from the high density surface data that meshed with the large-scale rawinsonde data. Four iterations were allowed in the Barnes method to maintain all possible resolution while still keeping small-scale noise low.

b. Surface analysis

Surface data have become an integral part of research and forecasting on convective storms during the past few years since it allows somewhat better resolution of subsynoptic and mesoscale systems usually associated with convection. Miller (1967) has shown a high correlation between high surface dew point temperatures and areas of convection, and Lewis et al. (1974) have shown that surface data can be used to define strong areas of wind convergence along surface frontal zones. A stability index also was recently developed by Maddox (1973) using the surface static energy field as a measure of potential instability, and Charba (1975) used surface data as input for an operational forecast of severe weather over short time periods.

1. Surface vertical motion

In this study, surface fields of vector wind and dew point temperature were objectively analyzed for the nine time periods of the experiment using the surface data within the AVE II rawinsonde network. Terrain-induced vertical motion was calculated from the equation:

$$w_T = u_s \left(\frac{\partial h}{\partial x} \right) + v_s \left(\frac{\partial h}{\partial y} \right) \tag{1}$$

where w_T is the terrain-induced vertical motion, u_s and v_s are the components of the surface wind in the x- and y-directions, respectively, and $\frac{\partial h}{\partial x}$ and $\frac{\partial h}{\partial y}$ are the slopes of the terrain in the x- and y-directions, respectively.

The terrain height for each grid point is shown in Fig. 7. These heights were determined from a smoothed terrain field given by Berkofsky and Bertoni (1955). The gradients of terrain height in Eq. 1 were calculated by use of centered finite differences over 2 grid distances. As can be seen from Fig. 7, small scale surface effects such as small hills or tall mountain peaks were not considered so that the magnitudes of the terrain-induced vertical velocities would be similar in scale to those calculated from the rawinsonde data.

20 18 16 14 12 11 11 10 9 10 10 10 10 10 10 9 11 3
24 20 17 15 12 11 11 9 9 8 8 8 10 11 12 12 7 0
27 23 20 15 13 12 12 11 9 8 5 8 8 10 8 10 13 8 0
33 25 22 17 13 12 12 10 8 8 8 8 9 13 13 13 0 0
43 30 24 20 14 12 11 10 9 8 8 9 11 13 14 15 0 0
50 37 27 20 15 12 10 9 8 8 8 10 12 12 15 12 0 0
60 45 30 22 15 12 10 8 7 7 9 10 12 16 10 2 0 0
66 50 35 25 15 12 9 7 7 5 6 10 12 16 7 2 0 0
69 54 40 25 13 10 10 10 4 5 9 12 18 10 4 1 0 0
65 53 40 25 11 9 11 8 4 4 9 10 11 6 3 0 0 0
58 50 37 25 11 9 10 4 4 4 5 8 6 4 0 0 0 0
54 46 35 20 10 7 5 4 4 4 4 5 3 2 0 0 0 0
48 43 35 20 11 7 5 4 4 4 2 2 2 2 1 0 0 0
43 40 33 20 11 4 5 3 2 2 0 0 0 0 1 1 0 0
40 38 34 20 10 3 0 0 0 0 0 0 0 0 0 1 0 0
40 40 35 22 6 0 0 0 0 0 0 0 0 0 0 0 0 0
50 52 40 29 5 0 0 0 0 0 0 0 0 0 0 0 0 0
55 55 50 35 20 0 0 0 0 0 0 0 0 0 0 0 0

Fig. 7. Terrain heights at each grid point (hundreds of feet).

Surface wind divergence was calculated using the expression

$$\text{Div}_2 \vec{V}_{SFC} = \frac{\partial u_s}{\partial x} + \frac{\partial v_s}{\partial y} \tag{2}$$

where $\text{Div}_2 \vec{V}_{SFC}$ is the 2-dimensional surface wind divergence, and the subscript s refers to the surface. The partial derivatives were evaluated by centered finite differences over 2 grid distances.

In computations of vertical motion just above the surface, both terrain-induced vertical motion and divergence of the surface wind must be considered (Jarvis and Agnew, 1970). By assuming the surface wind field as representative of the mean wind through a 50-mb deep layer above the surface, the equation of continuity in pressure coordinates

$$\text{Div}_2\vec{V}_{\text{SFC}} = -\frac{\partial \omega}{\partial p} = \frac{\partial u_s}{\partial x} + \frac{\partial v_s}{\partial y} \qquad (3)$$

can be integrated from the surface to the top of the 50-mb layer to give the vertical motion through the top of the layer. Thus,

$$\omega_{(P_s - 50 \text{ mb})} = \omega_{P_s} + \int_{(P_s - 50 \text{ mb})}^{P_s} \text{Div}_2\vec{V}_{\text{SFC}}\, dp \qquad (4)$$

where $\omega = \frac{dp}{dt}$ and P_s is the surface pressure. Since ω_{SFC} is not known, it can be approximated by the terrain-induced vertical motion w_T from Eq. 1 using the relation

$$\omega \simeq -g\rho w_T \qquad (5)$$

where g is the acceleration of gravity and ρ is the air density. For the range of surface temperatures and pressures in the AVE II experiment, the above relation can further be simplified so that

$$\left| \omega_{P_s} (\mu\text{bar s}^{-1}) \right| \simeq -\left| w_T (\text{cm s}^{-1}) \right|. \qquad (6)$$

Therefore, the resultant vertical motion at 50 mb above the surface was calculated using the expression

$$\omega_{(P_s - 50 \text{ mb})} = \omega_{P_s} + (\text{Div}_2\vec{V}_{\text{SFC}})\, \Delta p. \qquad (7)$$

where $\Delta p = 50$ mb and $\left| \omega_{\text{SFC}} \right| = -\left| w_T \right|$.

2. Surface moisture divergence

Charba (1975) has reported that one of the primary parameters used to produce accurate short-range forecasts of severe weather is surface moisture divergence. In this study the surface dew point temperature field was used as a measure of the moisture distribution so that the 2-dimensional surface moisture divergence is given by

$$D_{ms} = \frac{\partial (T_D u_s)}{\partial x} + \frac{\partial (T_D v_s)}{\partial y} = \text{Div}_2(T_D\vec{V}_{\text{SFC}}) \qquad (8)$$

where D_{ms} is the surface moisture divergence and T_D is the surface dew point temperature. Equation 8 may be written:

$$D_{ms} = \text{Div}_2(T_D\vec{V}_{\text{SFC}}) = \vec{\nabla}_2 \cdot T_D\vec{V}_{\text{SFC}} = \vec{V}_{\text{SFC}} \cdot \vec{\nabla}_2 T_D + T_D(\vec{\nabla}_2 \cdot \vec{V}_{\text{SFC}}) \qquad (9)$$

where $\vec{V}_2$ is the horizontal gradient operator, and $\vec{V}_{SFC}$ is the surface vector wind. This form of the equation shows that surface moisture divergence is a measure of the horizontal advection of moisture and surface wind convergence (negative of divergence), and that the largest negative values (convergence) occur where moisture advection $(-\vec{V}_{SFC} \cdot \vec{V}_2 T_D)$ and surface wind convergence times high surface T_D values $[T_D(-\vec{V}_2 \cdot \vec{V}_{SFC})]$ are large. By considering vertical motion only, convective activity should occur where strong surface wind convergence, in combination with high surface T_D values, produces upward air motion just above the surface and the distribution of surface moisture is such that positive moisture advection is occurring and D_{ms} is negative.

c. Rawinsonde analysis

The AVE II 25-mb data were objectively analyzed for all nine time periods to determine the horizontal distributions of moisture, stability, and the kinematic fields of velocity divergence, moisture divergence, and vertical motion. Since layer-averaged quantities appear to be more representative of a given field than point values (Endlich and Mancuso, 1968), average values for a given layer of wind, moisture, and temperature were computed from the 25-mb data whenever possible.

The vertical soundings of temperature, moisture, and wind were plotted by computer in the form of an emagram using the AVE II contact data. These soundings provided the maximum vertical resolution possible from the rawinsonde data and were used to locate stable layers and frontal zones sometimes lost in the 25-mb data.

1. Moisture

The average relative humidity for various layers was computed by averaging the 25-mb values as follows:

$$\overline{RH]}_{P_1}^{P_2} = \frac{1}{\left(\dfrac{P_2 - P_1}{25 \text{ mb}}\right)} \sum_{P_1}^{P_2} RH \tag{10}$$

where $\overline{RH]}_{P_1}^{P_2}$ is the average relative humidity in the layer from pressure P_1 to P_2 and $\sum_{P_1}^{P_2} RH$ is the summation of the individual 25-mb relative humidity values in the layer from P_1 to P_2. Fields of average relative humidity were objectively calculated and analyzed for the following

layers:

(1) $\overline{\text{RH}}$ (SFC - 500 mb),

(2) $\overline{\text{RH}}$ (SFC - 850 mb),

(3) $\overline{\text{RH}}$ (850 - 700 mb), and

(4) $\overline{\text{RH}}$ (700 - 500 mb).

2. Stability

Four measures of stability were considered in the delineation of areas of convective activity indicated by MDR data. They were the Total Totals Index (TTI) (Miller, 1967), "K" Index (KI) (George, 1960), Lifted Index (LI) (Galway, 1956), and the convective instability index (CII), $-\dfrac{\partial \Theta_e}{\partial p}$.

The TTI was computed from the equation:

$$\text{TTI} = 2 \cdot (T_{850} - T_{500}) - \overline{(T - T_D)}_{\text{SFC - 850 mb}} \tag{11}$$

where T_{500} and T_{850} are temperatures (°C) at 500 and 850 mb, respectively, T and T_D are temperatures and dew point temperatures (°C), respectively, and $\overline{(T - T_D)}_{\text{SFC - 850 mb}}$ is the average dew point depression between the surface and 850 mb (°C). This equation is slightly different from that given by Miller since the average dew point depression below 850 mb and not the point value at 850 mb is used as a measure of low level moisture. Values > 45 are usually associated with convective activity.

The "K" Index was computed from the equation:

$$K = (T_{850} - T_{500}) + \overline{T}_{D_{\text{SFC - 850}}} - (T - T_D)_{700} \tag{12}$$

where T_{500}, T_{850} and T_D are as defined previously, $\overline{T}_{D_{\text{SFC - 850}}}$ is the average dew point temperature from the surface to 850 mb (°C), and $(T - T_D)$ is the dew point depression at 700 mb (°C). Again, this expression is different from the "K" Index defined by George since the average dew point temperature below 850 mb and not the point value at 850 mb is used. Values > 24 usually are associated with convection.

The Lifted Index in this study was also calculated slightly differently from the original definition. First, the 25-mb data at each station were scanned from the surface to 850 mb and the pressure

level at which the temperature and moisture combined to give the highest equivalent potential temperature (Θ_e) was determined. The parcel at this level was then lifted dry adiabatically until saturation occurred, then along the saturated adiabat up to 500 mb. The index value was computed by subtracting the 500-mb lifted temperature from the environmental 500 mb temperature where both temperatures are in degrees Celcius. Values < +2 are usually associated with convective activity.

Finally, a convective instability index (CII) was computed by scanning the equivalent potential temperatures from the surface to 700 mb and calculating $\frac{-\Delta\Theta_e}{\Delta p}$ over all 25-mb layers. The CII value was taken to be the minimum value of $\frac{-\Delta\Theta_e}{\Delta p}$ where $\Delta p = 25$. This method gives a good approximation to $\frac{\partial\Theta_e}{\partial z}$ in the lower troposphere.

3. Horizontal kinematic fields

The vertical structure of the kinematic fields was represented by 17 layers between 950 mb and 100 mb (Fig. 8). Wind measurements in each layer were determined by averaging the wind over each 50-mb layer using the 25-mb data. Layer 1 was allowed to have a varying depth so that the surface layer remained 50-mb deep and the variations in surface pressure from different station elevations were adjusted within this first rawinsonde level. In addition, since the boundary layer (BL) usually is approximately 1.5 km in depth, the layer between the surface and 850 mb is called the boundary layer.

Vector wind fields for all layers were first calculated on the grid using the layer-averaged winds. Horizontal velocity divergence was then computed for every layer using the expression

$$(\overline{\vec{\nabla}_p \cdot \vec{V}_p})_k = \left(\frac{\partial u}{\partial x}\right)_k + \left(\frac{\partial v}{\partial y}\right)_k \tag{13}$$

where u and v represent average velocity components through a given pressure layer, and $(\overline{\vec{\nabla}_p \cdot V_p})_k$ is the average horizontal velocity divergence within layer k where $1 \leq k \leq 17$.

4. Vertical motion

The three-dimensional distribution of vertical motion is perhaps the single most important parameter needed in the study of convection since the release of potential instability is dependent upon upward
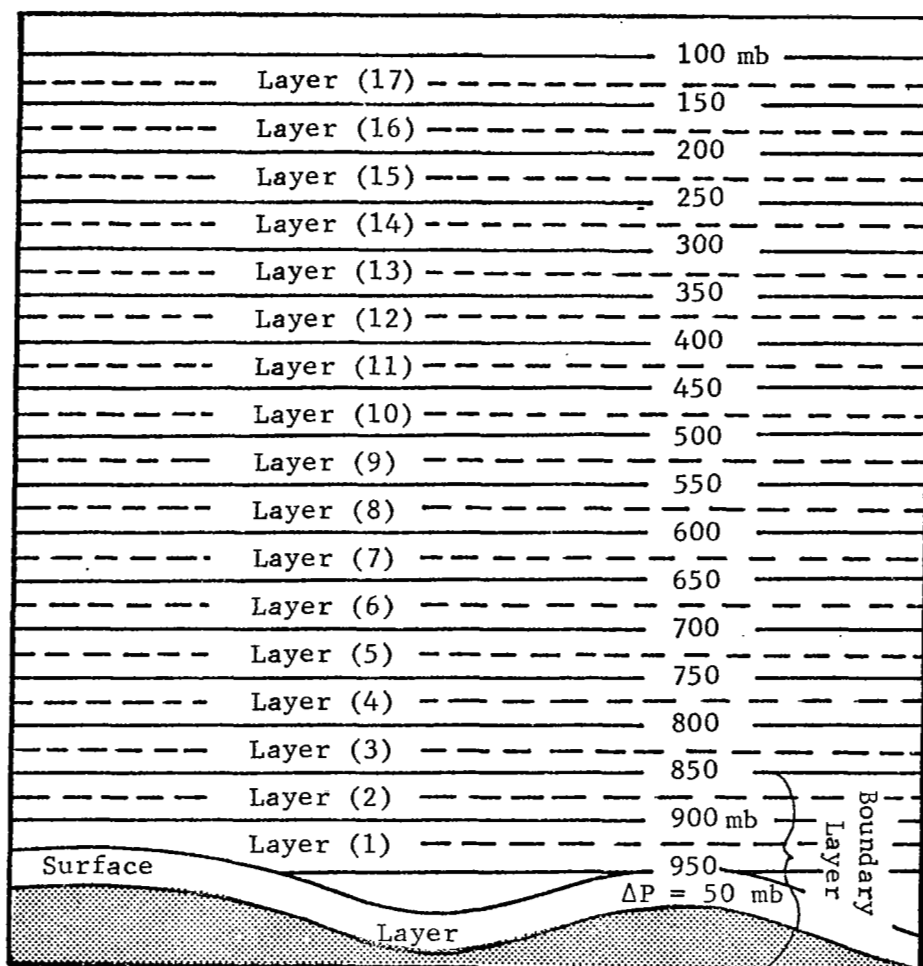
Fig. 8. Vertical structure of layers used in the objective analysis program.

vertical motion through a layer of potentially and convectively unstable air (Byers 1959). Since the vertical component of the wind is not a measured quantity, it must be calculated from other parameters. While all methods of computation of vertical motion have advantages and disadvantages, the kinematic method generally has been accepted as the best estimate of vertical motion in the lower troposphere since adiabatic assumptions are poor close to the ground. In addition, it is the vertical motion within the lower troposphere, and particularly within the boundary layer, that appears to relate best to the release of instability (Endlich and Mancuso, 1968).

The vertical motion calculations used in this study employ the kinematic scheme developed by O'Brien (1970). Since its development, this technique was examined by Smith (1971) who believes it to be one of the best kinematic methods for calculation of vertical motion in terms of obtaining the most physically realistic patterns and magnitudes relative to the observed synoptic conditions and existing weather. Fankhauser (1969) used this method successfully in calculations of mesoscale vertical motion fields associated with convective formation, and Chien and Smith (1973) and Kung (1973) also have reported that methods similar to the O'Brien technique produce the most realistic values and vertical profiles of kinematic vertical motion.

The derivation of the technique starts with the continuity equation in pressure coordinates:

$$\frac{\partial \omega}{\partial p} + \overline{(\vec{\nabla}_p \cdot \vec{V}_p)}_k = 0 \tag{14}$$

where the subscript k refers to the pressure layers discussed earlier. Integration of this equation with respect to pressure from the surface upward yields the vertical component of velocity, ω_p, at the top of any layer k. Integration gives:

$$\omega_{p_k} = \omega_{p_o} + \sum^k \overline{(\vec{\nabla}_p \cdot \vec{V}_p)}_k \, \Delta p \tag{15}$$

where $p_k < p_o$ and ω_{p_o} is the vertical motion at the bottom of the first layer (ie. 950 mb).

When k = 1, Δp varies at various grid points according to the

surface pressure variations so that

$$(\Delta p)_{k=1} = [(P_s - 50 \text{ mb}) - 900 \text{ mb}]$$

$$= [(P_s) - 950 \text{ mb}] \tag{16}$$

where $(P_s - 50 \text{ mb})$ is the pressure at which the resultant surface vertical motion is calculated, and 900 mb is the top of layer k=1. Therefore, the vertical motion at the top of layer k=1 is given by

$$(\omega_p)_{k=1} = \omega_R + \overline{(\vec{\nabla}_p \cdot \vec{V}_p)}_{k=1} (\Delta p)_{k=1} \tag{17}$$

where ω_R is the resultant surface vertical motion 50 mb above the ground computed from Eq. 4.

While results obtained using the previous relationships have been found realistic in the low and middle troposphere, the accuracy of the rawinsonde data decreases with altitude and elevation angle (Fuelberg, 1974). The accuracy of divergence calculations, therefore, decreases at upper levels and reduces the accuracy of the computed vertical motion. Moreover, vertical integration of the horizontal divergence allows for the accumulation of errors which further reduces the accuracy of the computed vertical motion.

A correction was made by O'Brien (1970) to the calculated vertical motion at all levels so that the value of vertical velocity at the top of the highest layer obtains some predetermined value, usually zero so that $\omega_k = 0$ when k = 17. The adjustment factor significantly affects vertical motion in the layers above about 500 mb.

The vertical motion calculations for all layers from Eq. 15 were adjusted using the relation

$$\omega'_p = \omega_p - (\omega_k - \omega_T) \frac{k}{2M} (k + 1) \tag{18}$$

where ω'_p is the adjusted vertical velocity for any pressure layer p, ω_p is the unadjusted vertical velocity from Eq. 15, ω_T is the vertical velocity at the top of the highest layer (100 mb), ω_k is the unadjusted vertical velocity at 100 mb, and k is the pressure layer number. The

value of M is calculated from

$$M = \sum_{k=1}^{K} k = \frac{1}{2} K (K + 1) \tag{19}$$

where K is the total number of pressure layers (ie. K = 17).

The choice of $\omega_T = 0$ is based upon essentially a zero net vertical motion computed over the entire grid network for unadjusted values. The large corrections to upper-level vertical motion values also seem justified since unadjusted values are sometimes an order of magnitude larger than those vertical velocities computed from adiabatic methods (Fankhauser, 1969).

5. <u>Moisture divergence in the boundary layer</u>

Endlich and Mancuso (1968) found that large negative values of moisture divergence in the boundary layer correlated well in space with severe convective activity. From Eq. 9, negative values of moisture divergence through the boundary layer imply that most or all of this layer contains positive vertical motion within an area of high moisture content and/or strong positive moisture advection.

Moisture divergence in the boundary layer (D_{MBL}) was computed using the equation

$$D_{MBL} = D_{MS} + \int_{P_1}^{P_2} \overline{(\vec{\nabla}_p \cdot T_D \vec{V}_p)} \, dp \tag{20}$$

where p_1 and p_2 extend over the first two rawinsonde pressure levels below 850 mb (Fig. 8), and $\overline{(\vec{\nabla}_p \cdot T_D \vec{V}_p)}$ is the average moisture divergence. Again, the depth of the first layer was variable depending upon the value of the surface pressure.

5. RESULTS

a. Atmospheric structure in areas of convective storms

Since convective systems develop and propagate within the large-scale synoptic field, knowledge of the structure of the atmosphere surrounding convective systems is essential to the understanding of the interrelationships between convective- and synoptic-scale systems. In addition, forecasts of convection are inferred from large-scale synoptic parameters. Knowledge of the interactions between convective- and synoptic-scale systems is therefore needed for improving the accuracy of present forecast models.

The structure of the atmosphere in areas of convection was studied by using analyzed fields of moisture, stability, and kinematic parameters calculated for each of the nine time periods for AVE II. Results for the two time periods, 1800 GMT on 11 May and 0600 GMT on 12 May, will be shown; they were representative of all nine times unless otherwise stated. Selected vertical cross sections will also be shown in order to present a three-dimensional picture of atmospheric structure in areas of convection.

The composite digital radar charts for 1800 and 0600 GMT are shown in Figs. 9 and 10, respectively. These charts were superimposed onto the analyzed fields for easy comparison between radar-observed convection and analyses of particular parameters. Thunderstorm areas (MDR values $\geq$ 4) are identified by dark shading and rainshowers (2 $\leq$ MDR values $\leq$ 3) by a solid hatched line.

1. Environmental moisture fields

Surface analyses of dew point temperature and the fields of average relative humidity are shown in Figs. 11 through 15 with the radar-observed convection and surface frontal positions shown in each chart.

Figure 11 shows that shower and thundershower activity occurred within the warm sector when the surface dew-point temperature exceeded 50°F, while some shower activity occurred behind the cold front with surface dew-point temperatures between 40 and 50°F. Miller (1967) has shown similar results with thunderstorm activity occurring more frequently with surface dew point temperatures greater than 55°F.
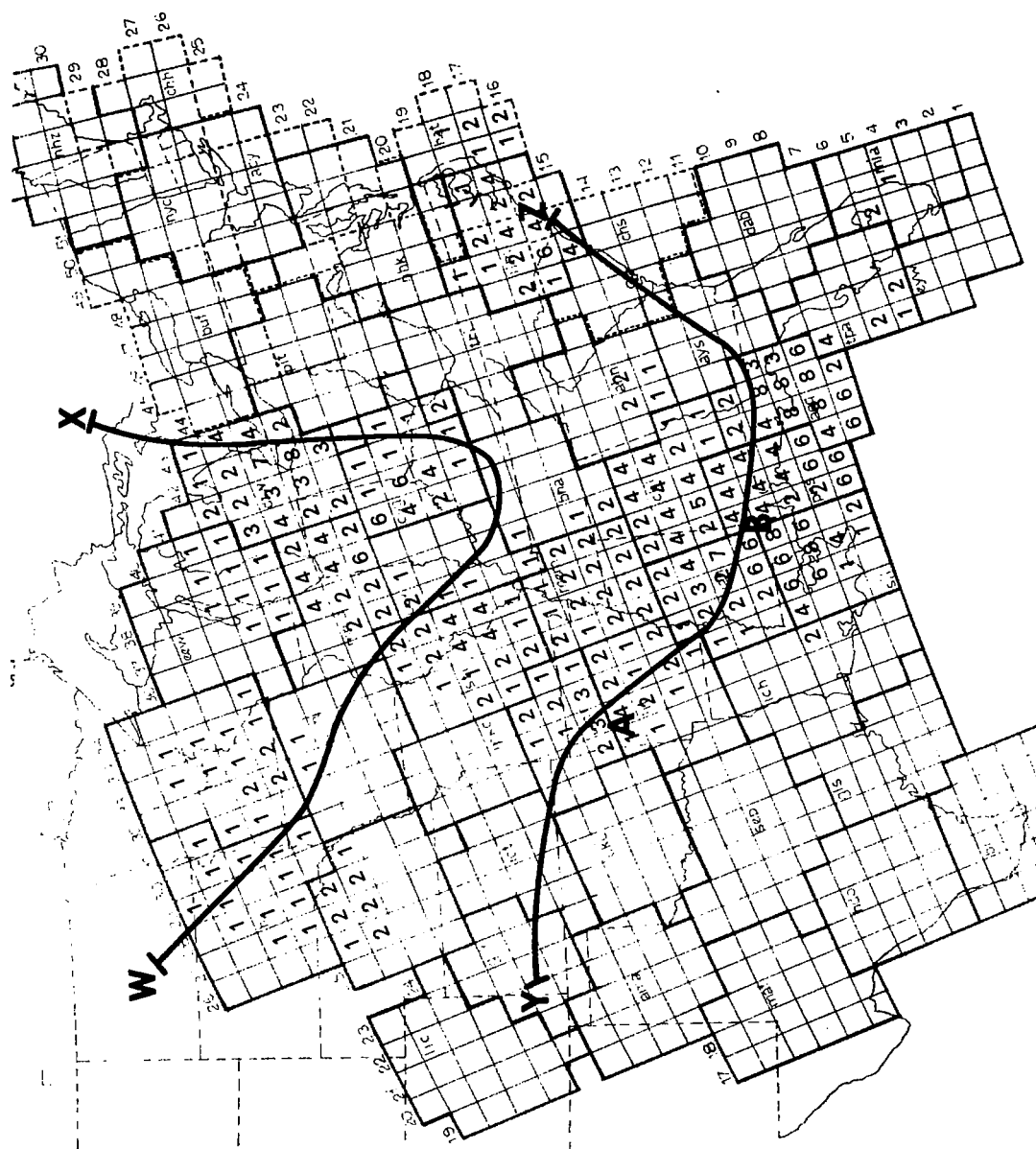
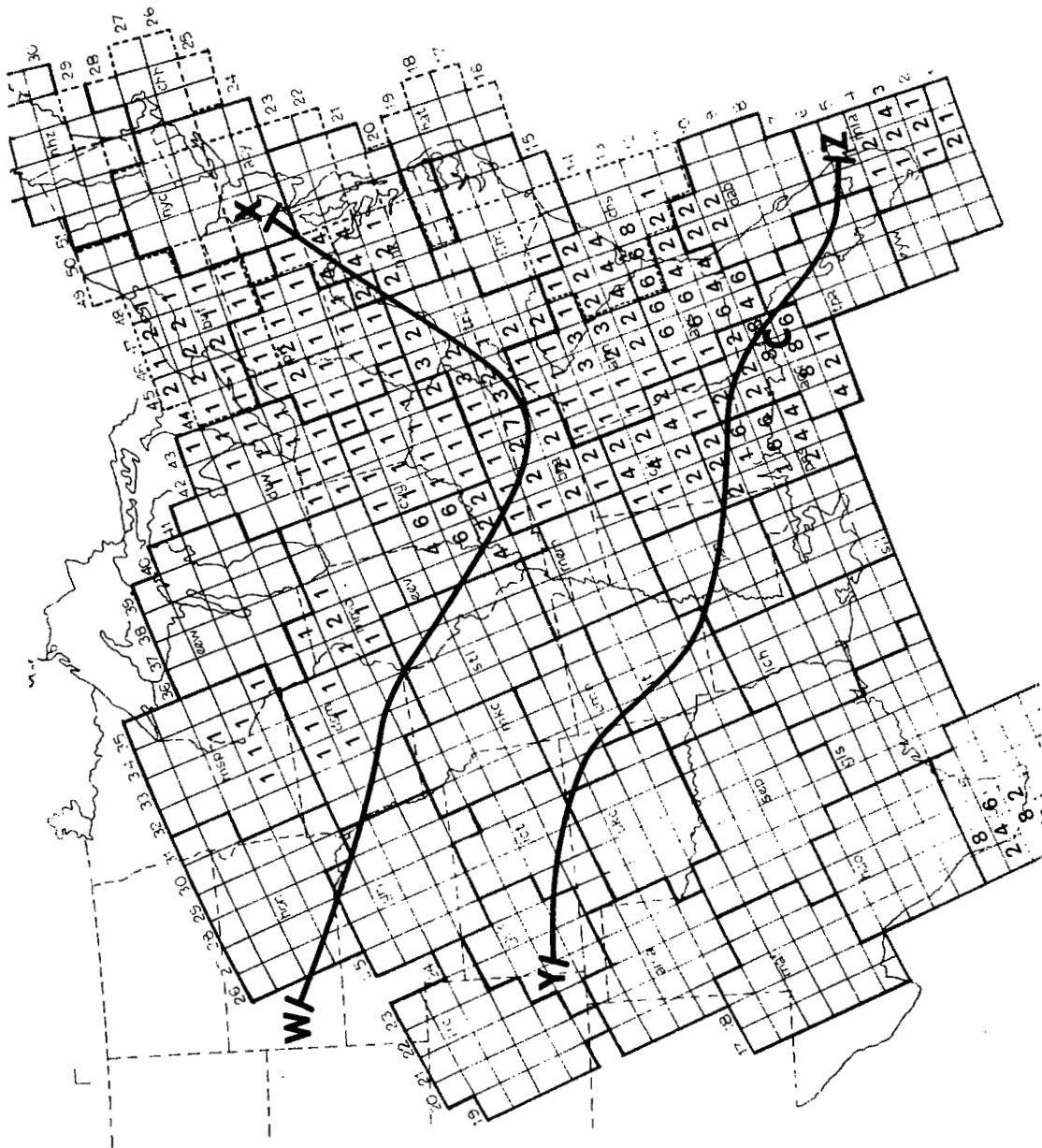Fig. 9. Composite digital radar chart for 1800 GMT on 11 May 1974.
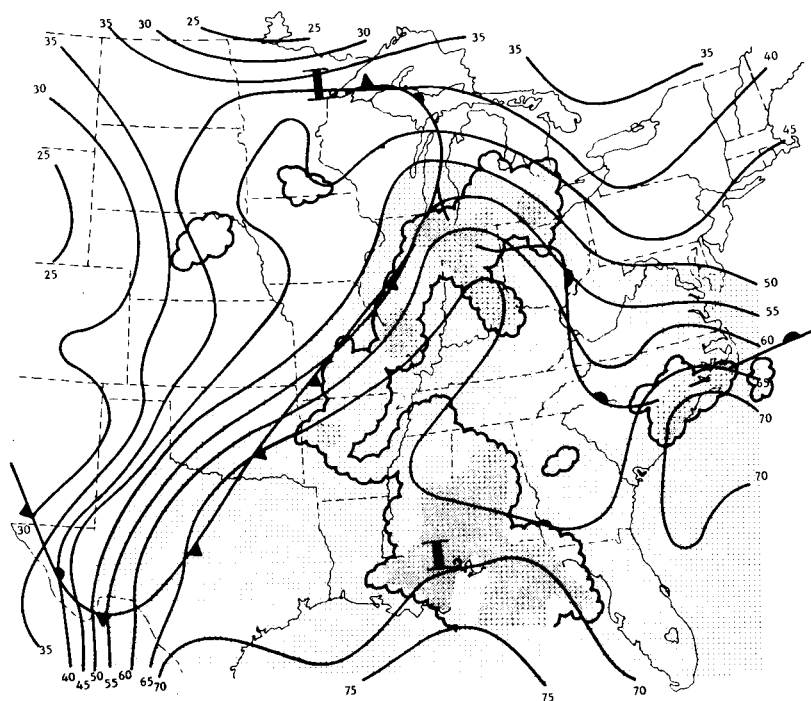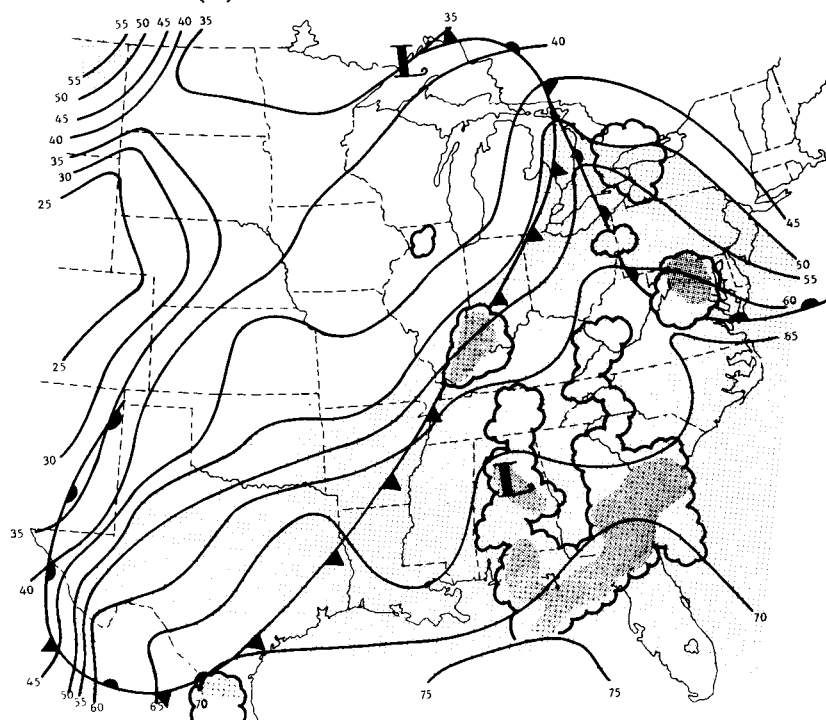
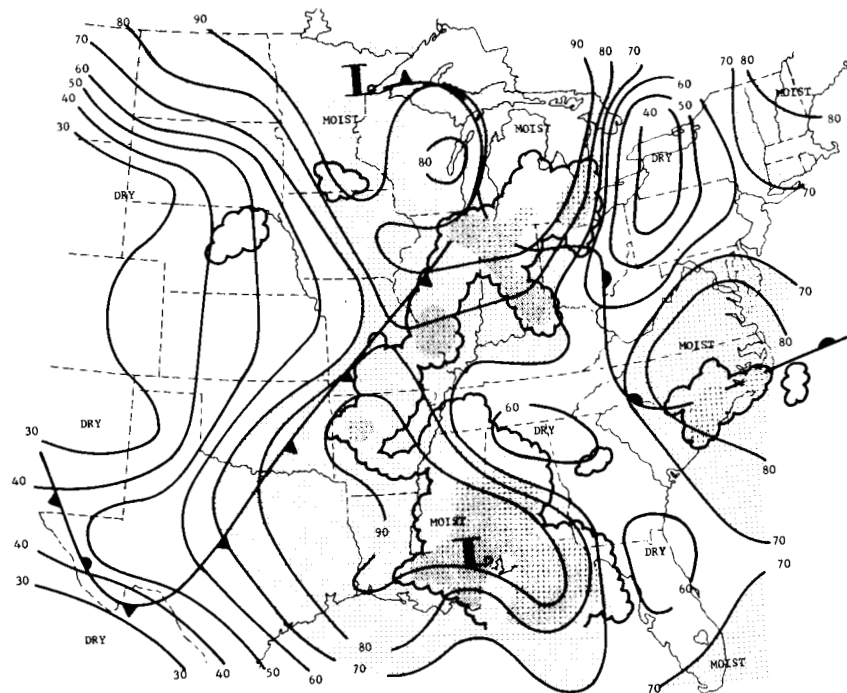Fig. 10. Composite digital radar chart for 0600 GMT on 12 May 1974.

(a) 1800 GMT, 11 May 1974.

(b) 0600 GMT, 12 May 1974.

Fig. 11. Surface analyses of dew point temperature (°F).
(Superimposed are surface frontal positions and
radar-observed convection, with dew point
temperatures > 50F lightly shaded).

34

(a) 1800 GMT, 11 May 1974.
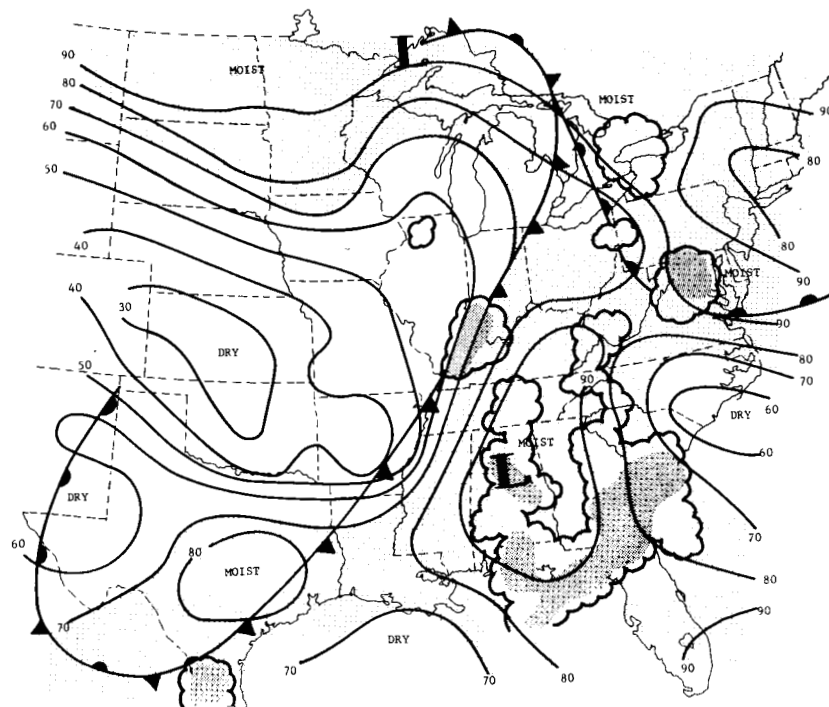
(b) 0600 GMT, 12 May 1974.

Fig. 12. Average relative humidity (SFC - 850 mb).
(Surface frontal positions and radar-observed
convection are superimposed with $\overline{RH}_{SFC-850}$
> 70% lightly shaded).

(a)   1800 GMT, 11 May 1974.

(b)   0600 GMT, 12 May 1974.

Fig. 13.   Average relative humidity (850 - 700 mb).
(Surface frontal positions and radar-observed
convection are superimposed with $\overline{RH}_{850-700}$
> 60% lightly shaded).

(a)   1800 GMT, 11 May 1974.

(b)   0600 GMT, 12 May 1974.

Fig. 14.   Average relative humidity (700 - 500 mb).
(Surface frontal positions and radar-
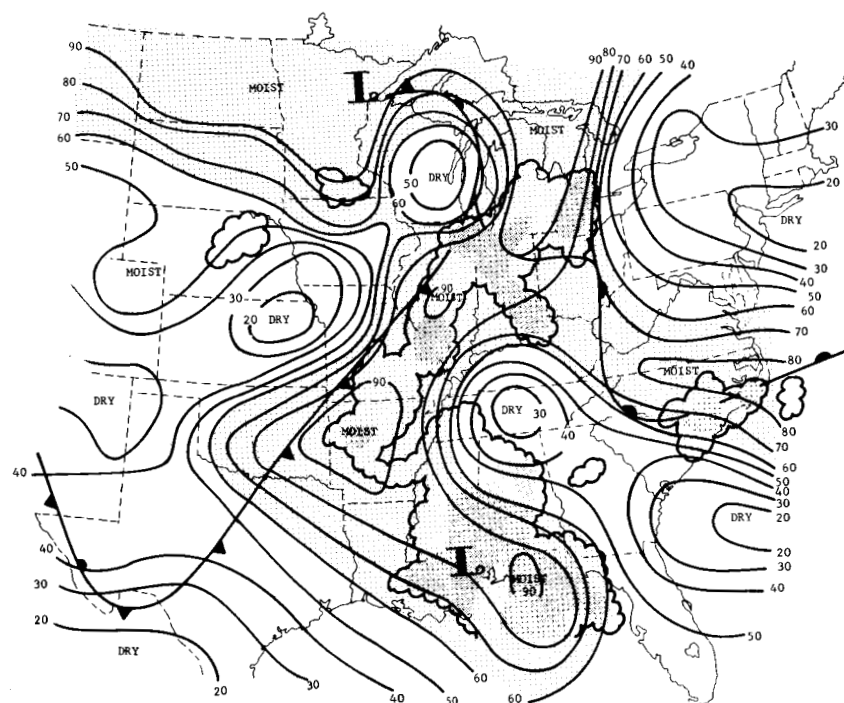observed convection are superimposed).
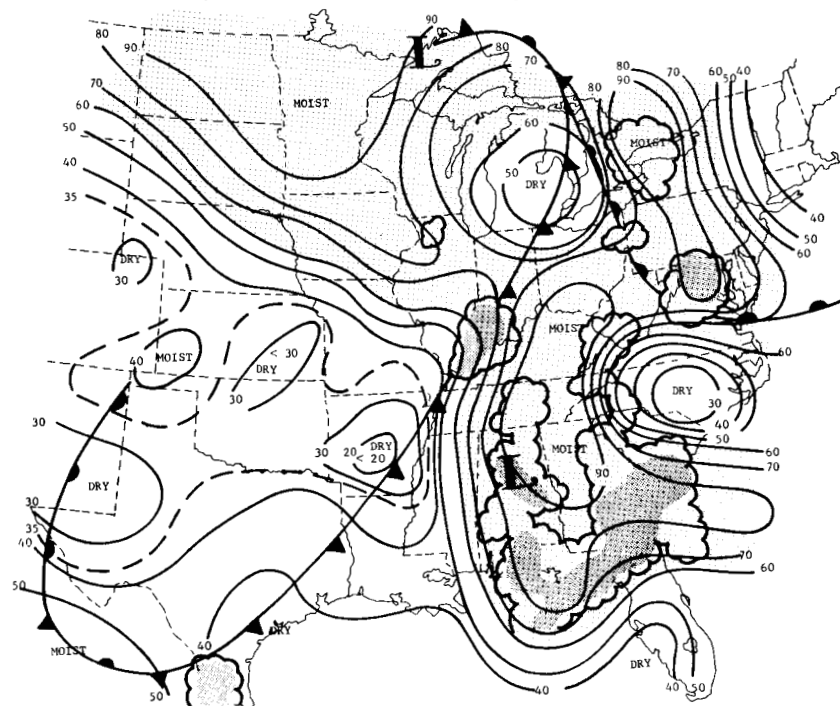
(a) 1800 GMT, 11 May 1974.

(b) 0600 GMT, 12 May 1974.

Fig. 15. Average relative humidity (SFC - 500 mb).
(Surface frontal positions and radar-observed
convection are superimposed with $\overline{RH}_{SFC-500}$
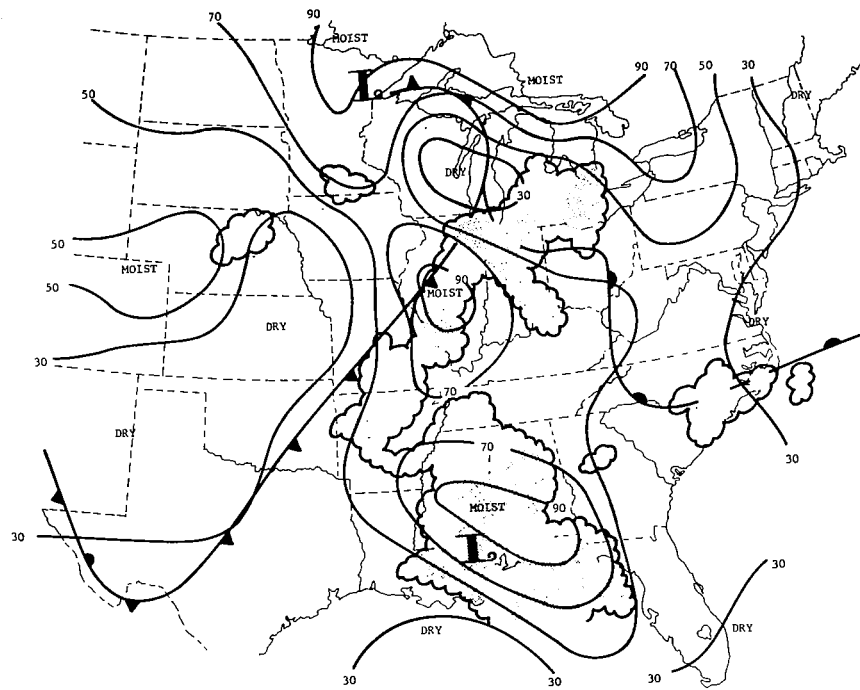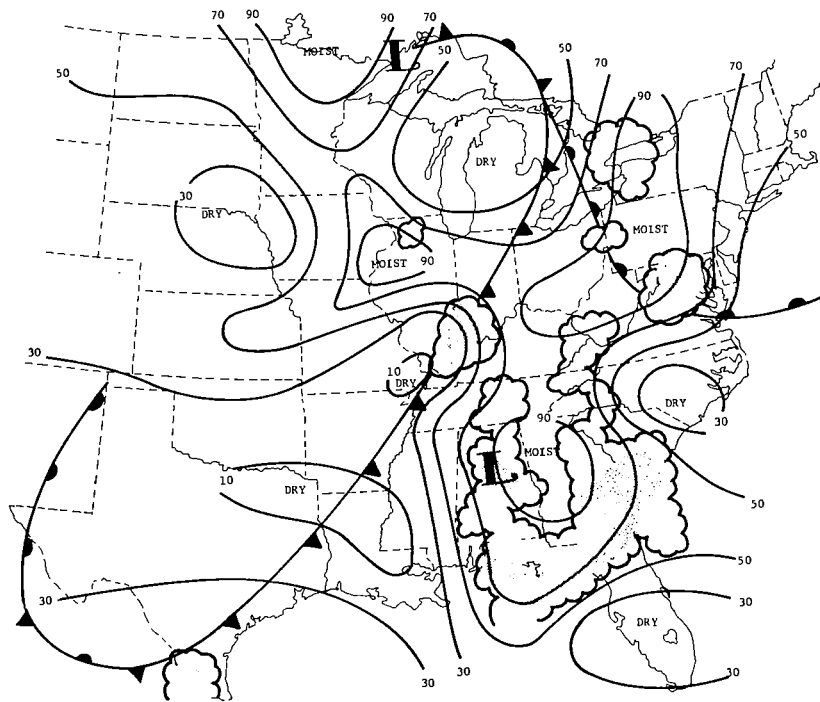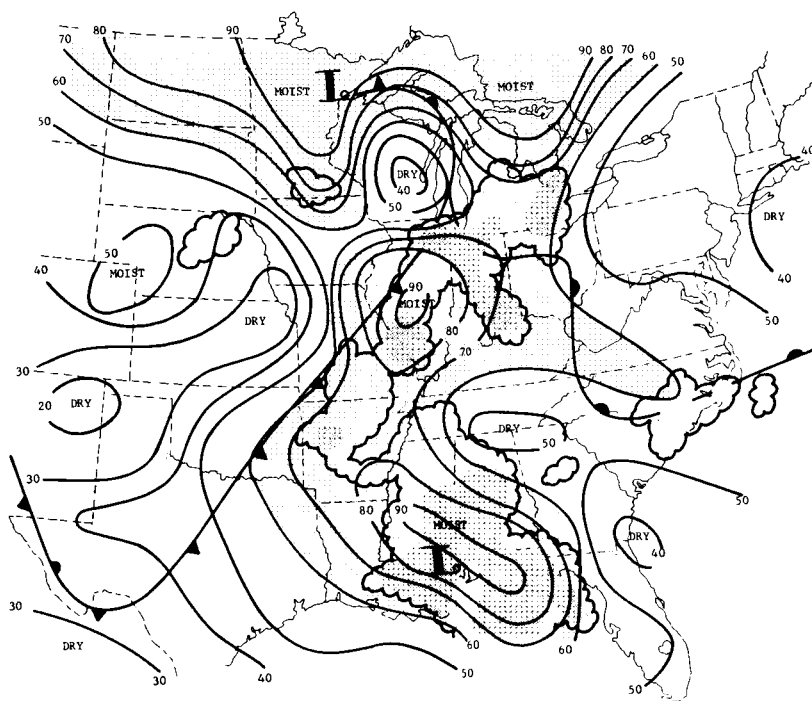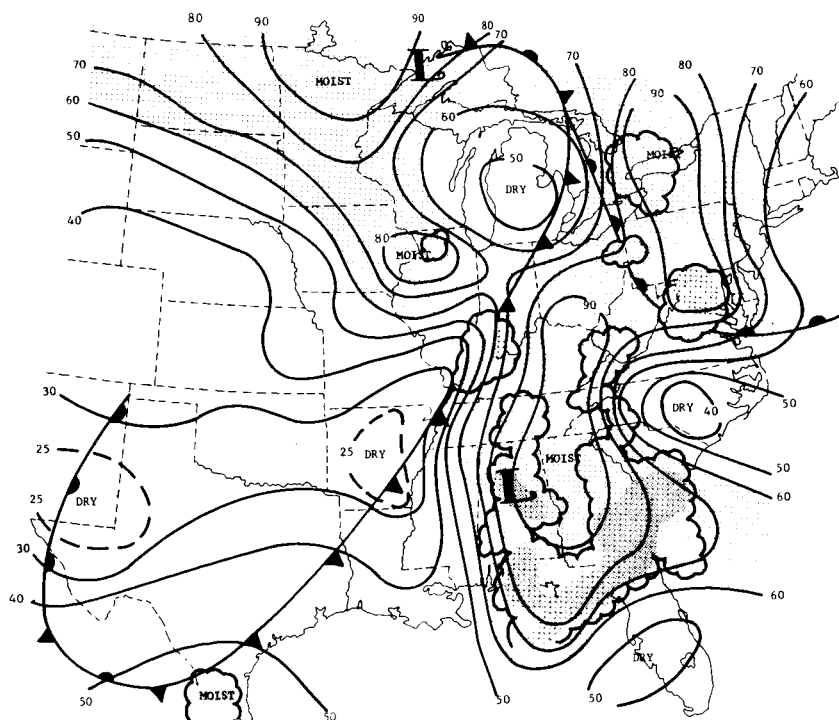> 60% lightly shaded).

High surface dew-point temperatures also mean high equivalent potential temperatures at the surface and suggest the importance of surface air in providing a source of high energy which could be a factor in the initiation and maintenance of convective activity.

Comparisons between average relative humidity and areas of convection show a definite tendency for the environmental air to be moist but not necessarily saturated. Figures 12 and 13 show high average relative humidity in the lower troposphere associated with the warm and cold frontal zones and southeast U.S. cyclone. Shower and thundershower activity was consistently located within these moist areas so that values of $\overline{RH}_{SFC -850\ mb}$ and $\overline{RH}_{850 - 700\ mb}$ > 70% and > 60%, respectively, were present in areas of convection. Dry areas in the northern and central Plains States behind the cold front, in the northeast U.S., and northeast of the cyclone in the southeast U.S. contained no convection. However, high average relative humidity in the lower troposphere does not imply that convection will be present. The area within and west of the major cyclone in Minnesota was almost saturated during the entire AVE II experiment but thunderstorms were never observed there.

The correlation between high average relative humidity and areas of convection is much weaker from 700 to 500 mb. Figure 14 shows that convection was sometimes located in areas where the middle troposphere was relatively dry. This occurred in Fig. 14a over the Carolinas and Michigan, while in Fig. 14b dry air was observed over southern Illinois and Indiana where convection was present. In contrast, the middle troposphere was moist and almost saturated over the southeast U.S. where convection was present.

The average relative humidity between the surface and 500 mb (Fig. 15) also shows a high correlation between moist environmental air in the low and middle troposphere and areas of convection. Moist air is present over the southeast U.S. and along the cold and warm frontal zones where convection is observed. In addition, a small center of moist air is associated with shower activity that moved from the northern Plains States at 1800 GMT on 11 May (Fig. 15a) eastward into northern Illinois at 0600 GMT on 12 May (Fig. 15b). Shower activity ($2 \le MDR \le 3$) always occurred where $\overline{RH}_{SFC - 500\ mb}$ > 50% while thunderstorms

(MDR values $\geq$ 4) generally occurred where $\overline{RH}_{SFC - 500\ mb} > 60\%$.

A high correlation between high average relative humidity in the lower troposphere (particularly in the boundary layer) and convective activity has been shown by Reap (1975), and Endlich and Mancuso (1968). Apparently, condensation and convective cloud formation occur within or slightly above the boundary layer where air with high equivalent potential temperature is brought to saturation.

2. Stability

The stability indexes discussed previously were analyzed objectively and compared to radar-observed convection at all times of the experiment to determine if any relationships existed between large-scale stability and convective activity. The index that correlated best in space with the convective activity was determined.

Fields of the Total Totals Index (TTI), the Lifted Index (LI), and the "K" Index (KI) are given for 1800 GMT, May 11 and 0600 GMT, May 12, 1974, in Figs. 16 through 18. Surface frontal positions and observed convection are shown on each chart with unstable areas shaded lightly.

Generally, the spatial distributions of stable and unstable regions is similar in all three stability fields. Figures 16, 17, and 18 all show the movement of stable air, containing no convection, over western Kansas and the Texas panhandle at 1800 GMT eastward into Arkansas and Missouri at 0600 GMT. An area of unstable air is also shown by all indexes over the Dakotas at 1800 GMT which moved southeastward into northern Illinois by 0600 GMT. Some shower activity was associated with this unstable area. Stable areas were shown by all indexes approximately 750 km north and east of the southeast U.S. cyclone and in the northeast U.S. at both time periods, but some convection was observed in these stable areas. Convection was generally found in the unstable air shown by all indexes ahead of the cold front and along the warm front at both times but very unstable air shown by the TTI and LI in central Texas contained no convection.

In summary, many unstable areas in Figs. 16, 17, and 18 do not contain convective activity and convection is sometimes observed where a stability index showed a stable environment. Therefore, the stability index alone was only a fair indicator of convective activity even
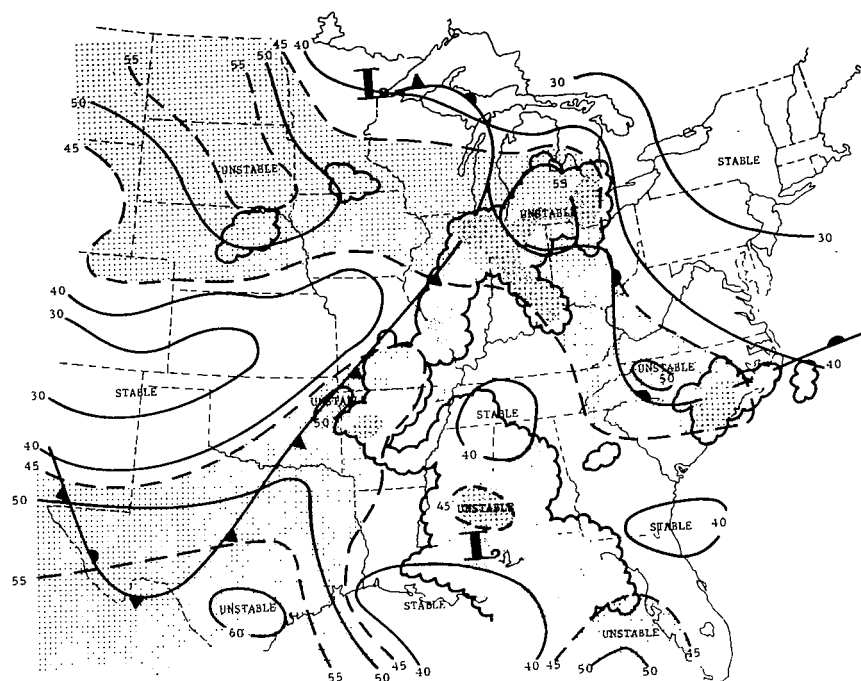
(a) 1800 GMT, 11 May 1974.
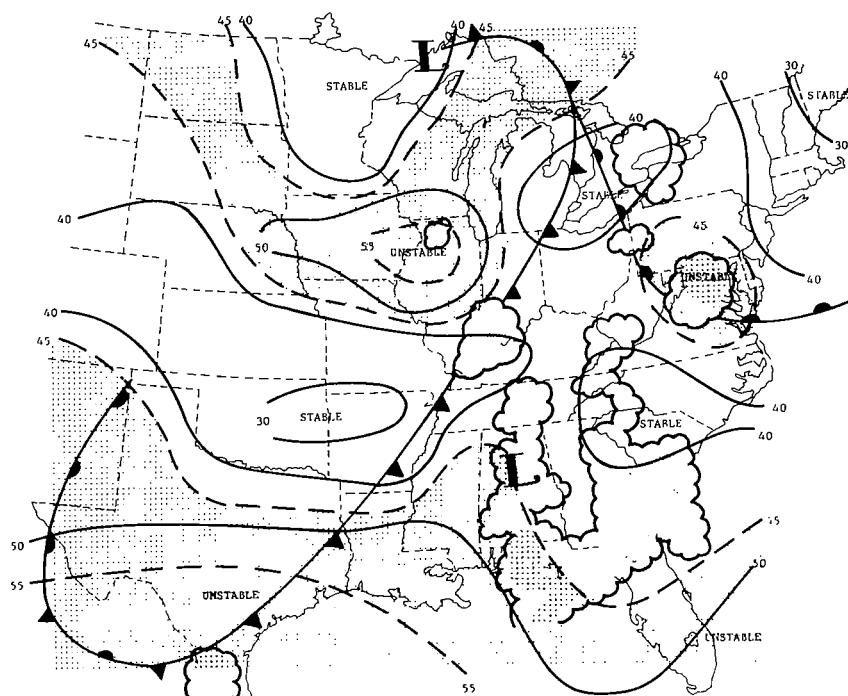
(b) 0600 GMT, 12 May 1974.

Fig. 16. Total Totals Index analyses. (Surface
frontal positions and radar-observed
convection are superimposed with TTI
values > 45 lightly shaded).

(a) 1800 GMT, 11 May 1974.

(b) 0600 GMT, 12 May 1974.

Fig. 17. Lifted Index analyses. (Surface frontal
positions and radar-observed convection
are superimposed with LI values < + 4
lightly shaded).
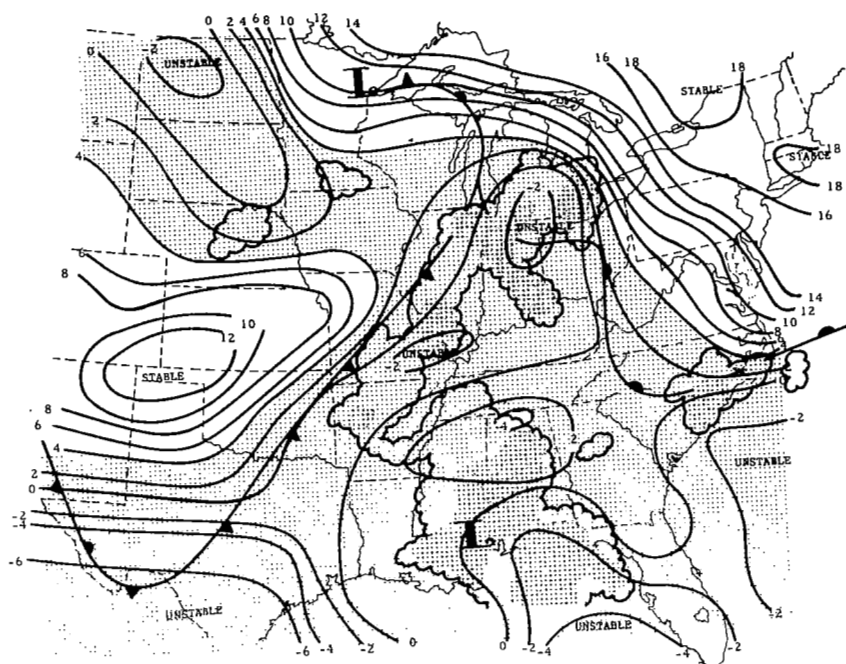
(a) 1800 GMT, 11 May 1974.
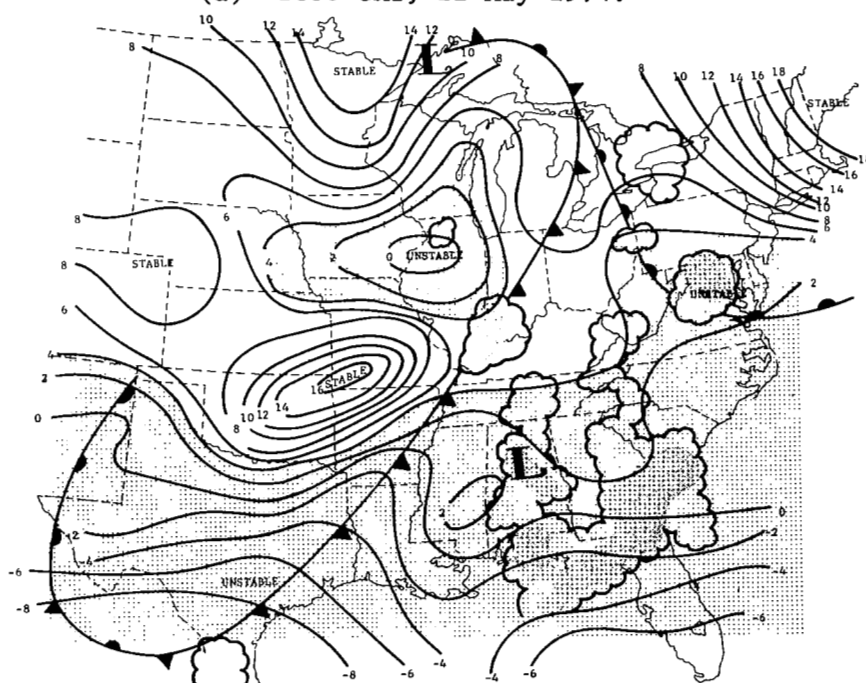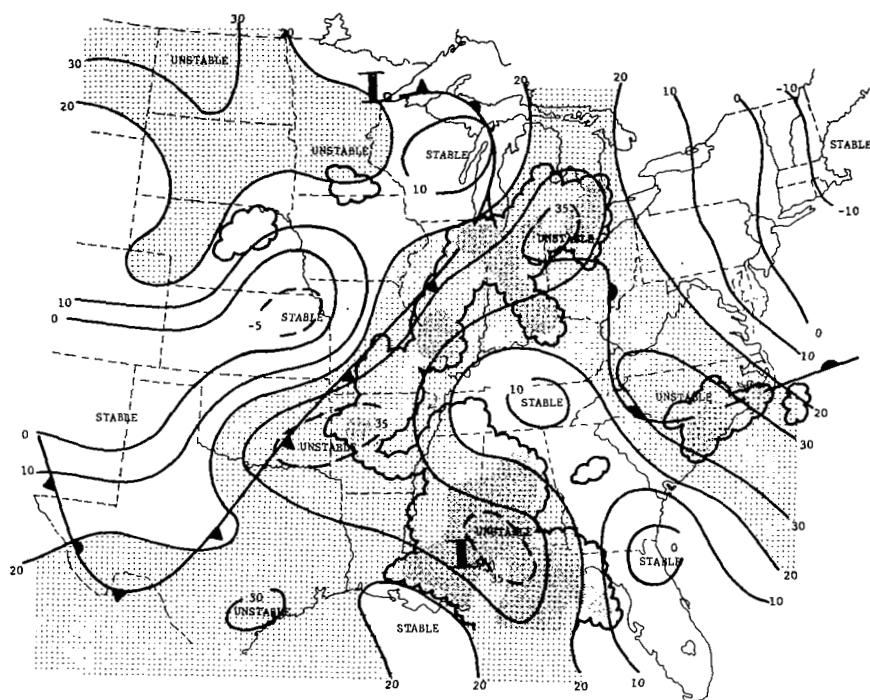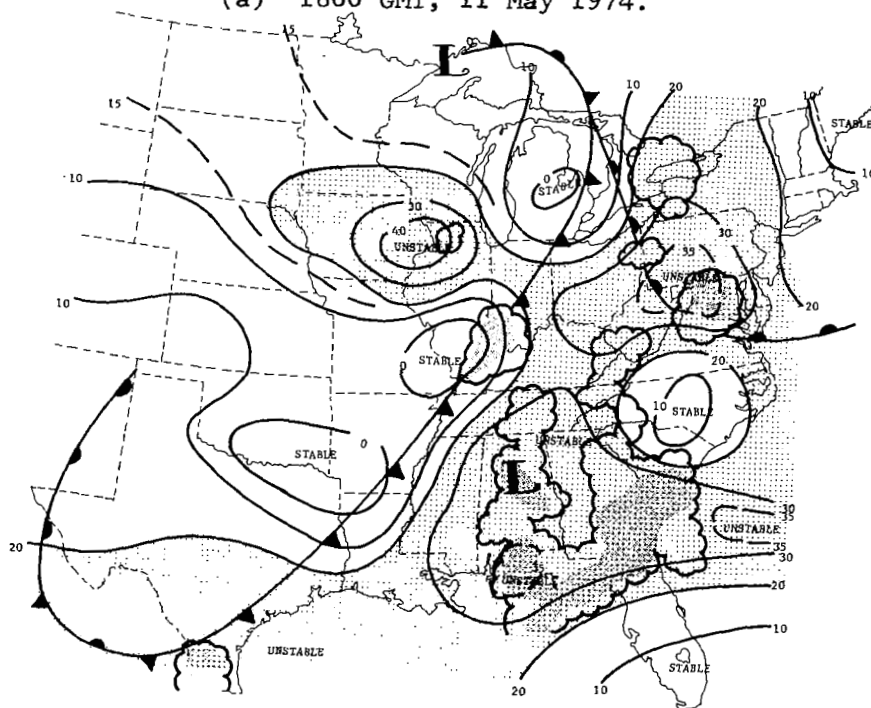
(b) 0600 GMT, 12 May 1974.

Fig. 18. "K" Index analyses. (Surface frontal
positions and radar-observed convection
are superimposed with KI values > 20
lightly shaded).

though a definite correlation does exist.

To determine which stability index correlated best with convective activity, two relative frequency distributions for each index were computed, one where convective activity was observed and the other when convective activity was not observed. The curves were computed from all nine times of the AVE II experiment by comparing areas of MDR $\geq$ 2 with the objectively analyzed stability fields. Convective activity was assumed to exist at a grid point if MDR $\geq$ 2 was within 1/2 grid point distance ($\sim$80 km) of the grid value.

Figures 19 through 21 show the distributions for the TTI, LI, and KI, respectively. Those stability index values that fall between the intersections of the two curves in each figure have a higher probability of occurring in a convection area. To compare the accuracy of the indexes in delineating areas of convection, the percent convective cases at grid points to the total number of grid point values of stability were compared using only those index values for which there was a greater
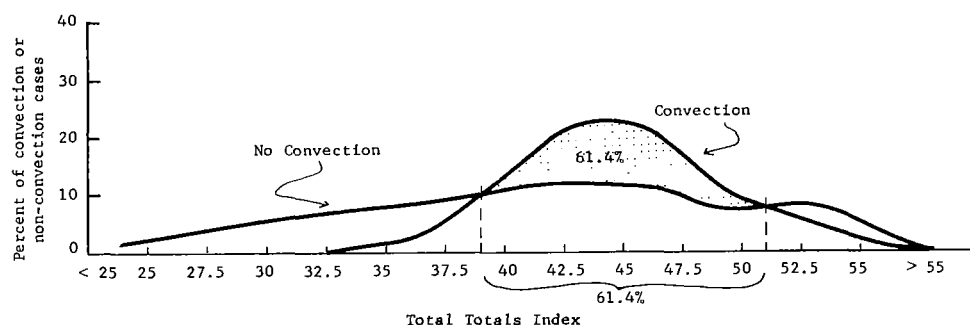
Fig. 19. Relative frequency distributions of TTI vs percent of convective cases and percent of non-convective cases.
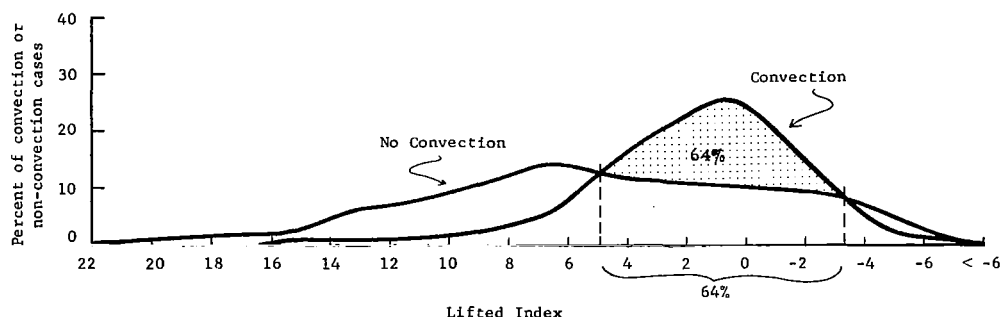
Fig. 20. Relative frequency distributions of Lifted Index vs percent of convective cases and percent of non-convective cases.
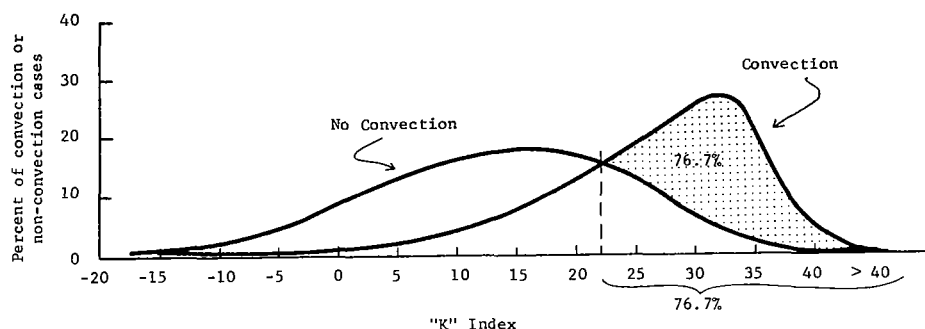
Fig. 21.   Relative frequency distributions of "K" Index vs percent of convective cases and percent of non-convective cases.

probability of convection. The results ranged from 61.4% for the TTI, to 64.0% for the LI, to 76.7% for the KI. The superior success of KI was apparently due to its consideration of moisture at 700 mb since the other two indexes consider only 500 mb and boundary layer parameters. The good correlation between high $\overline{RH}_{850 - 700 \text{ mb}}$ in Fig. 13 also suggests this. In addition, Reap (1975) found statistically the KI to be an accurate parameter for use in probability forecasting of thunderstorms that were not severe.

The measurement of convective instability is difficult because it requires detailed knowledge of the vertical moisture and temperature fields not normally available on an operational basis. In this study, the 25-mb data were used to measure the largest decrease in Θ_e over a 25-mb layer (in °C/25 mb) from the surface up to 700 mb. This value was the convective instability index. Figure 22 shows two examples of the CII at 1800 GMT, 11 May and 0600 GMT, 12 May 1974.

The CII fields indicate that Θ_e decreases with height in the lower troposphere almost everywhere within the AVE II area but decreases more slowly or increases slightly within the cold air behind the cold front or northeast of the warm front. This can be seen both in Figs. 22a and 22b. However, convection tends to occur in areas where Θ_e decreases rapidly with height as ahead of the cold front and over the Carolinas in Fig. 22a, and along the squall line in the southeast U.S. in Fig. 22b. Moreover, convective instability seems to be a necessary but not sufficient condition for convective activity as can be seen in Fig. 22b. A large area in northern Louisiana and southern Arkansas shows that Θ_e decreased 30°C in a 25-mb layer but no convection was present while
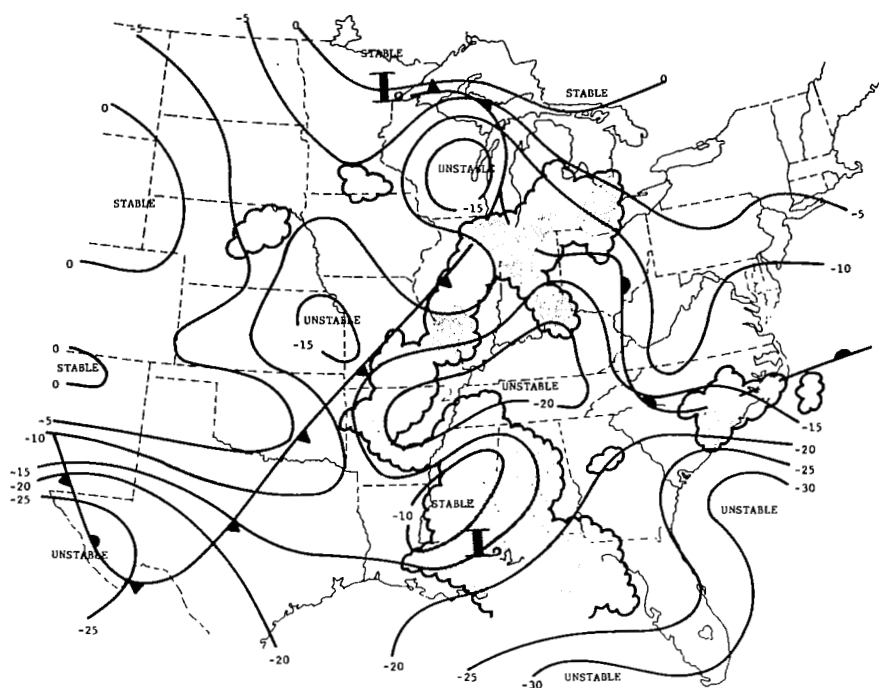
(a)   1800 GMT, 11 May 1974.
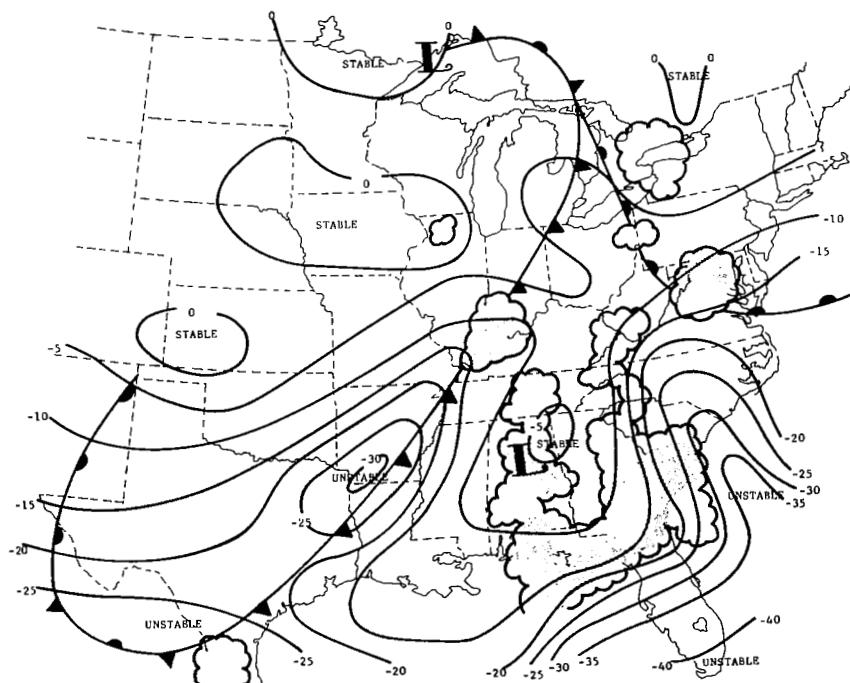
(b)   0600 GMT, 12 May 1974.

Fig. 22.   Convective instability index (CII) analyses. (Largest change in Θ_e over Δp = 25 mb between SFC and 700 mb, °C/25 mb, with surface frontal positions and radar-observed convection superimposed).

extreme convective instability existed very close to the squall line in southern Georgia. This suggests that heavy or severe thunderstorm activity may be associated with extreme convective instability.

However, extreme convection instability may exist within an area of strong subsidence in the lower troposphere that dries all layers of air except those near the surface. This was apparently the case in the Arkansas-Louisiana area in Fig. 22b.

The use of a critical value of CII in delineating convective activity met with only limited success in this study. No particular value of $-\Delta\Theta_e/\Delta P$ was found that consistently separated areas with and without convection. This suggests that perhaps there might be a relationship between the values of $-\Delta\Theta_e/\Delta P$ and the amount of vertical lifting required to produce convection since Θ_e did decrease with height almost everywhere.

3. Kinematic structure

Surface analyses at 1800 GMT, 11 May and 0600 GMT, 12 May 1974 of vector wind, terrain-induced vertical motion, surface wind divergence, and resultant vertical motion 50 mb above the surface are shown in Figs. 23 through 26 along with the surface frontal positions and observed convection at respective times.

The objectively analyzed wind fields in Fig. 23 show two well-defined cyclonic circulations associated with the two lows over the Great Lakes and the southeast U.S. Wind speeds exceeding 20 kts surround the low in the northern Plains States while speeds > 25 kts are located east and southeast of the cyclone in the southeast U.S.

In Fig. 24, the sign and magnitude of the terrain-induced vertical velocity showed a poor correlation with convective activity in general. Strong downward motion was associated with shower activity in the northern Plains States at 1800 GMT, while upward motion > 1 cm s^{-1} in the Texas panhandle was associated with a non-convective area at both time periods. However, the strong convection over the southeast U.S. was consistently occurring within an area of upward air motion at the surface throughout the experiment which suggests that, at least in some areas, the terrain-induced vertical velocity may be a factor in maintaining or producing the release of instability. This also may have
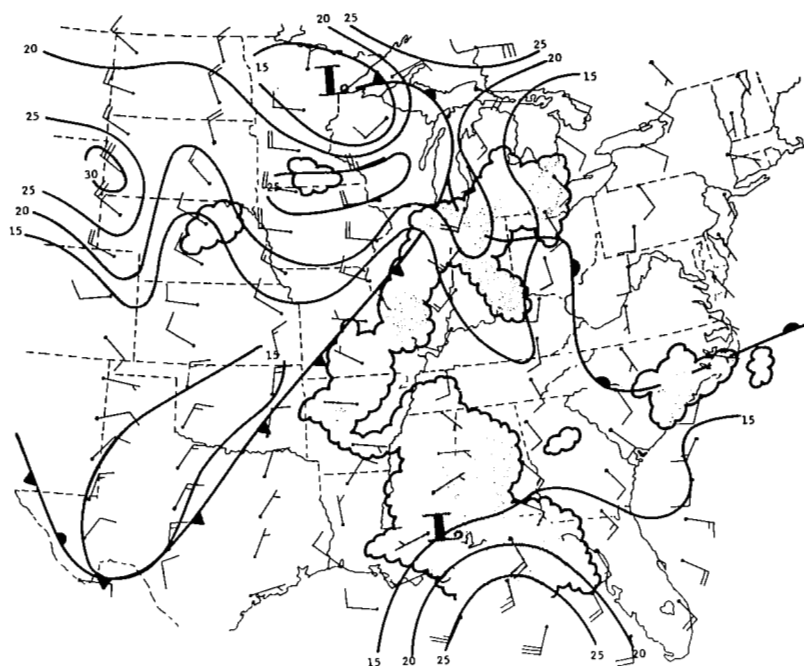
(a) 1800 GMT, 11 May 1974.
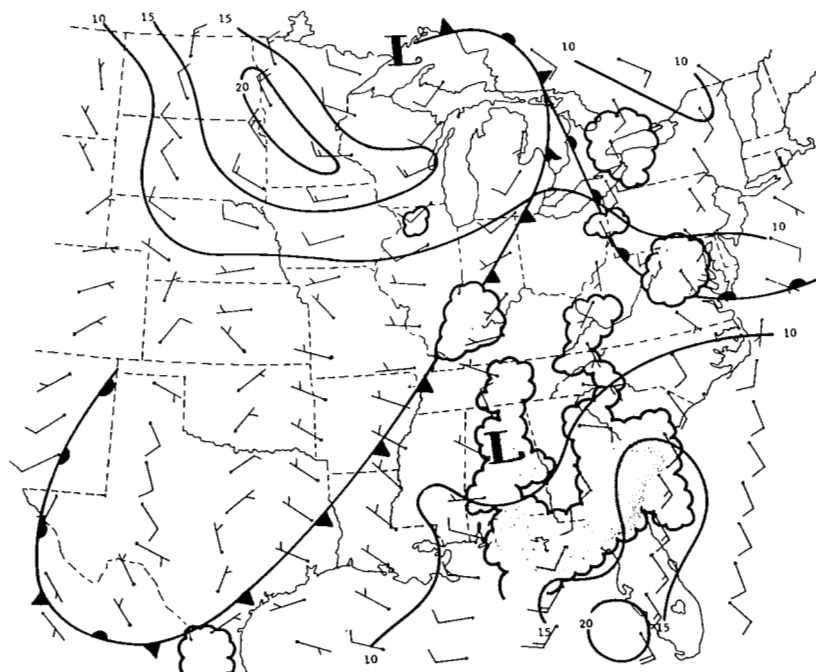
(b) 0600 GMT, 12 May 1974.

Fig. 23. Surface wind and isotach analyses (kts).
(Isotachs drawn from exact values; barbs
plotted to nearest 5 kts; superimposed are
surface frontal positions and radar-observed
convection).

48
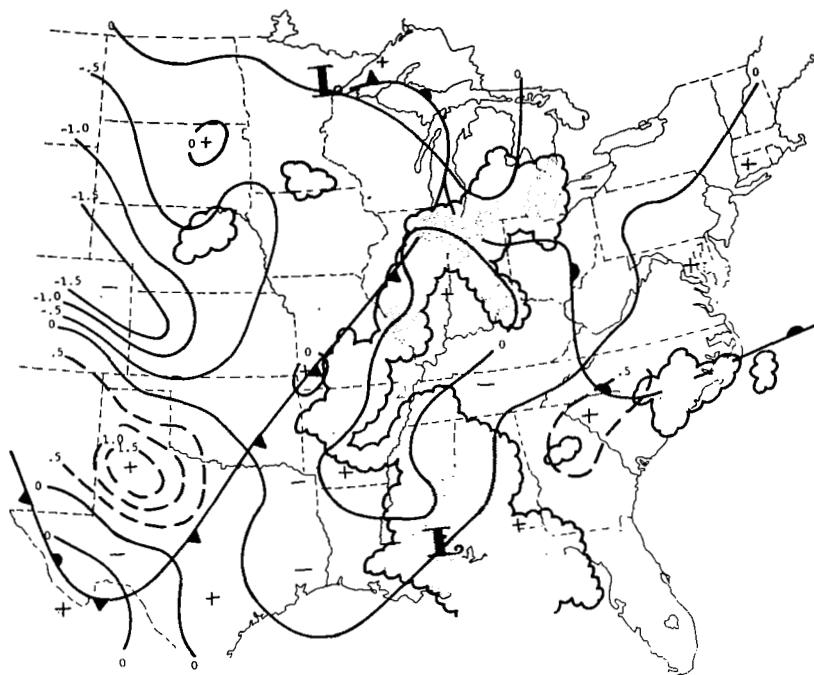
(a) 1800 GMT, 11 May 1974.
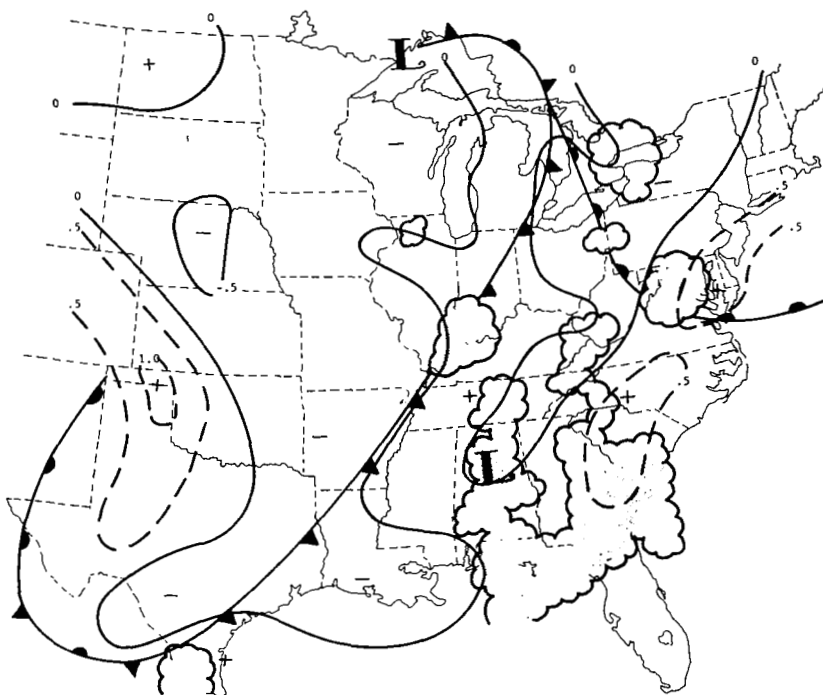
(b) 0600 GMT, 12 May 1974.

Fig. 24. Terrain-induced vertical velocity (cm s^{-1}).
(Superimposed are surface frontal positions
and radar-observed convection).
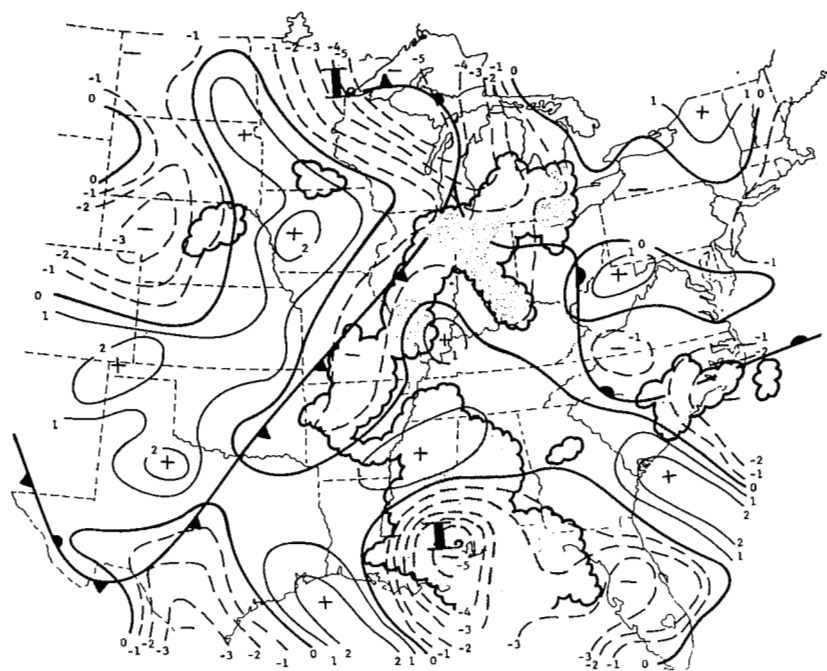
(a) 1800 GMT, 11 May 1974.
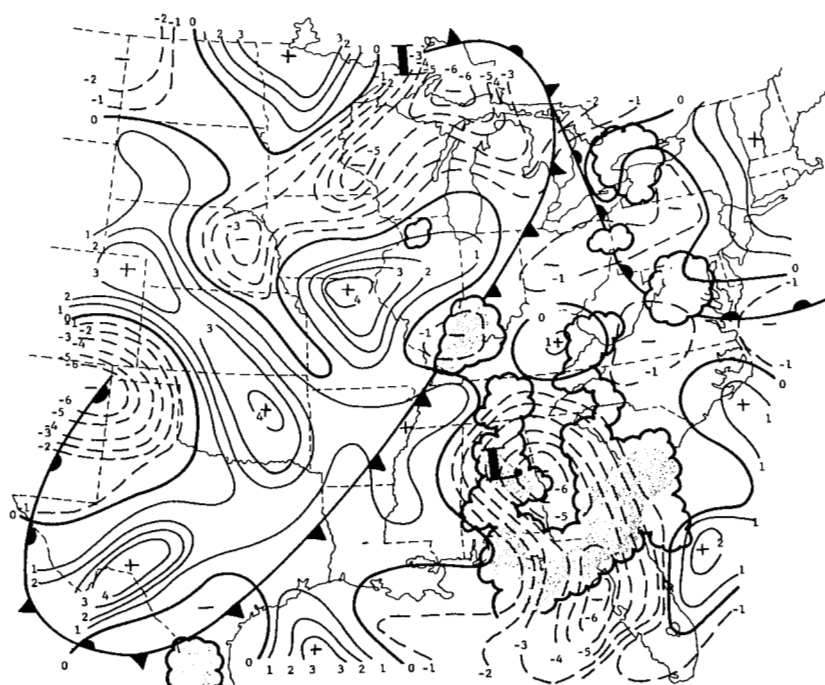
(b) 0600 GMT, 12 May 1974.

Fig. 25. Surface wind divergence analyses $(10^{-5} \ s^{-1})$.
(Superimposed are surface frontal positions
and radar-observed convection).

(a)   1800 GMT, 11 May 1974.

(b)   0600 GMT, 12 May 1974.

Fig. 26.   Resultant vertical velocity 50 mb above
the surface (μbar s^{-1}).   (Superimposed are
surface frontal positions and radar-observed
convection).

been the case ahead of the cold front in the upper Mississippi Valley
where convection was observed within upward vertical motion at both
1800 and 0600 GMT.

In contrast, the surface wind divergence fields in Fig. 25 showed
a strong correlation with convective activity. Strong velocity conver-
gence at both time periods was associated with convection found along
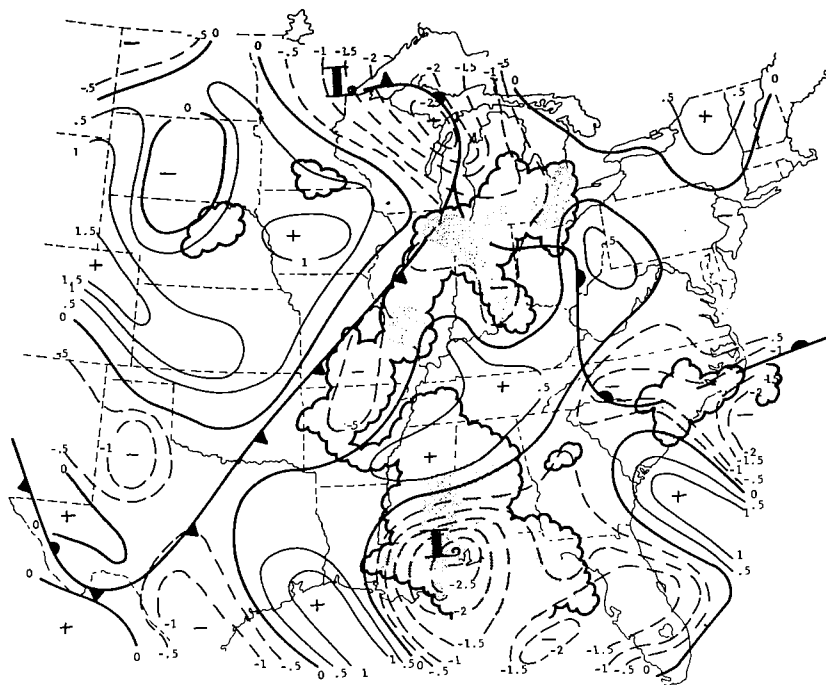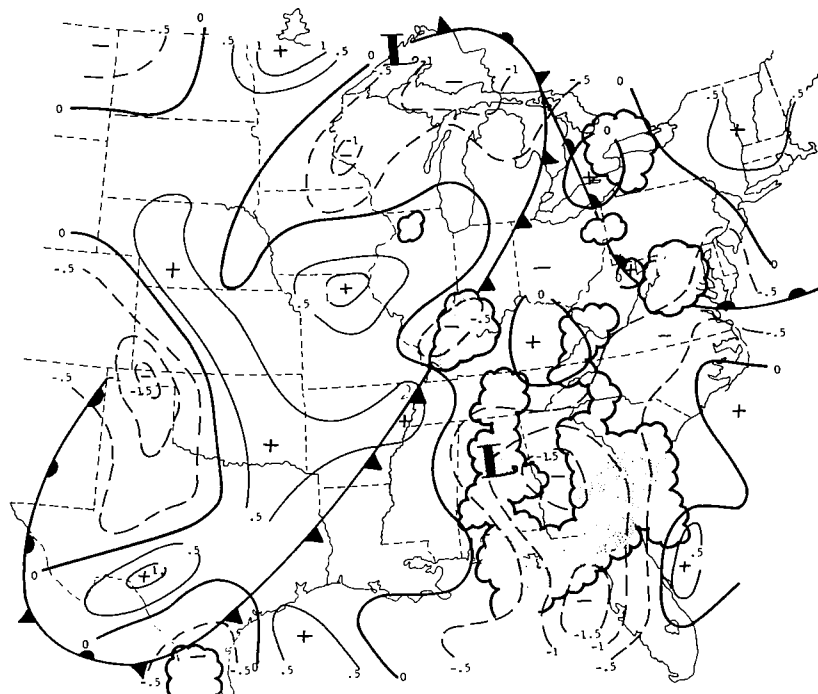the cold and warm frontal zones and within the southeast U.S. cyclone.
However, velocity convergence at the surface is not a sufficient condi-
tion for the formation of convection since thunderstorms were not found
within the strong convergence associated with the major cyclone in the
Great Lakes or within the convergence associated with the lee side low
found at 0600 GMT in the Texas panhandle (Fig. 25b). Convection was
seldom found in a divergent wind field at the surface which was consis-
tently located behind the cold front and west of the southeast U.S.
cyclone at both times.

The resultant field of vertical motion at the surface (Fig. 26),
calculated from Eq. 7, shows an almost perfect spatial correlation with
convective activity at all times of the experiment. Upward vertical
motion was associated with convection both along the frontal zones and
within the southeast U.S. low and small areas of strong upward motion
also were sometimes accompanied by stronger convection, especially
along the frontal zones and over the southeast U.S. where upward ver-
tical motion exceeded 2 μbar s^{-1}. Areas of thunderstorms (MDR $\geq$ 4)
seldom were located within subsidence close to the surface.

The combination of terrain-induced vertical motion and surface
wind divergence appeared to produce a vertical motion field that was
accurate in outlining areas where positive vertical motion produced
and maintained convection. The upward air motion close to the ground,
therefore, seems to be an essential ingredient for the release of
instability and convection. It appears that the combined effects of
both terrain-induced vertical motion and surface wind divergence must
be considered in producing accurate vertical motion.

Figure 27 shows the surface moisture divergence fields at 1800 GMT
and 0600 GMT calculated from Eq. 8. Physically, large negative values
represent areas where the surface wind field is convergent or positive
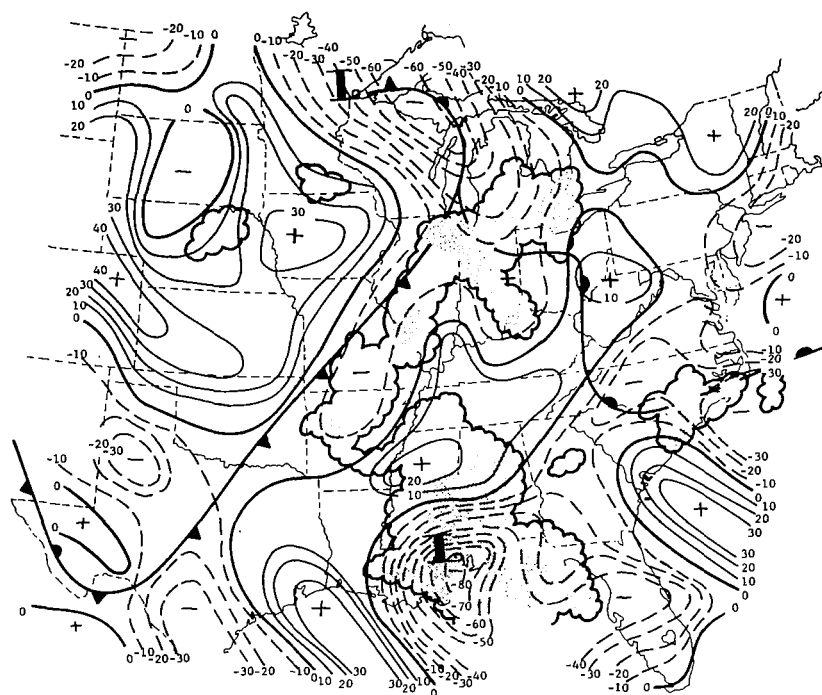
(a) 1800 GMT, 11 May 1974.
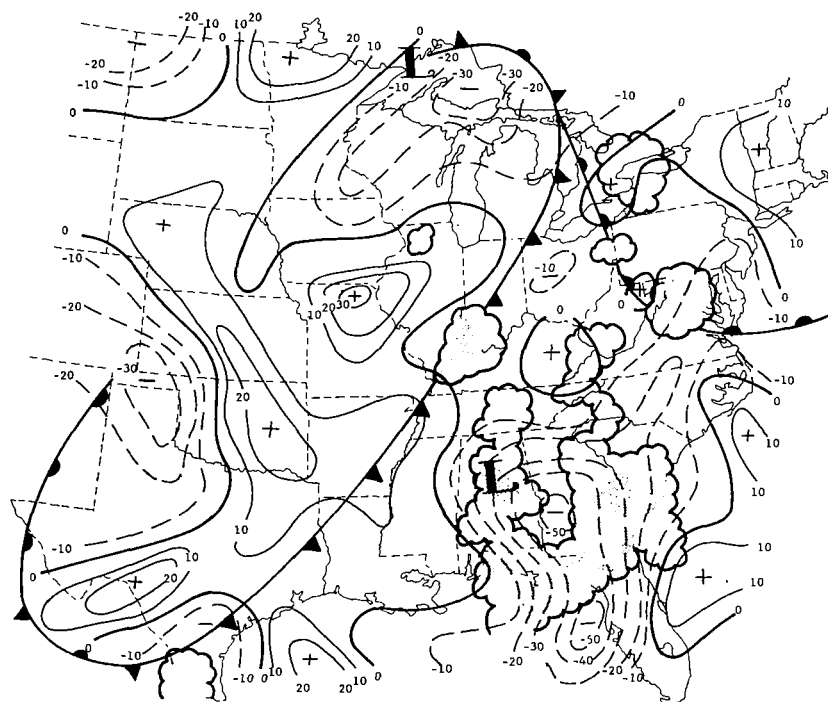
(b) 0600 GMT, 12 May 1974.

Fig. 27.   Surface moisture divergence (10^{-4} °K s^{-1}) analyses.
(Superimposed are surface frontal positions and
radar-observed convection).

moisture advection is occurring or both.

The fields of surface moisture divergence and surface wind divergence appear very similar indicating that the divergence term is dominant in most cases in the AVE II experiment over the advection term in Eq. 9. The spatial correlation between convection and moisture convergence is quite good, and shows that stronger moisture convergence results in stronger convective activity. This can be seen along both the cold and warm frontal zones, and within the low located over the southeast U.S. at both 1800 GMT and 0600 GMT. Both Ostby (1975) and Charba (1975) also found surface moisture divergence to be an excellent parameter for use in short-range forecasting of severe weather.

Figures 28 through 35 show the vector wind and divergence fields at 850, 700, 500, and 300 mb at 1800 GMT and 0600 GMT. In Fig. 28, winds at 850 mb > 40 kts were associated with the two cyclones at both times, and at 0600 GMT southerly winds > 40 kts were associated with the developing lee-side low. However, no consistent correlation seemed to exist between particular values of wind speed and convection at 850 mb since convective activity was located in both strong and weak wind speed areas. In contrast, convective activity and particularly thunderstorms consistently occurred in areas where the 850-mb wind field was convergent (Fig. 29), while stronger areas of convergence tended to be associated with stronger convective activity. This was particularly true ahead of the cold front in the Mississippi Valley and within the low over the southeast U.S. at both 1800 GMT and 0600 GMT.

At 700 mb, the wind and isotach analyses in Fig. 30 again showed poor correlation between particular values of wind speed and convective activity. Wind speeds > 40 kts were associated with two cyclones at 1800 and 0600 GMT but convection was located both within the strong wind areas, as in the cyclone over the southeast U.S., and in weak wind areas, as over Arkansas at 1800 GMT and in southern Illinois at 0600 GMT. The divergence analyses of the 700-mb wind (Fig. 31) showed no consistent correlation between convective activity and convergent or divergent wind fields. Even though strong convection tended to be located in areas where the 700-mb wind was convergent, as over the southeast U.S., convection was sometimes located in a divergent wind field as over Arkansas,
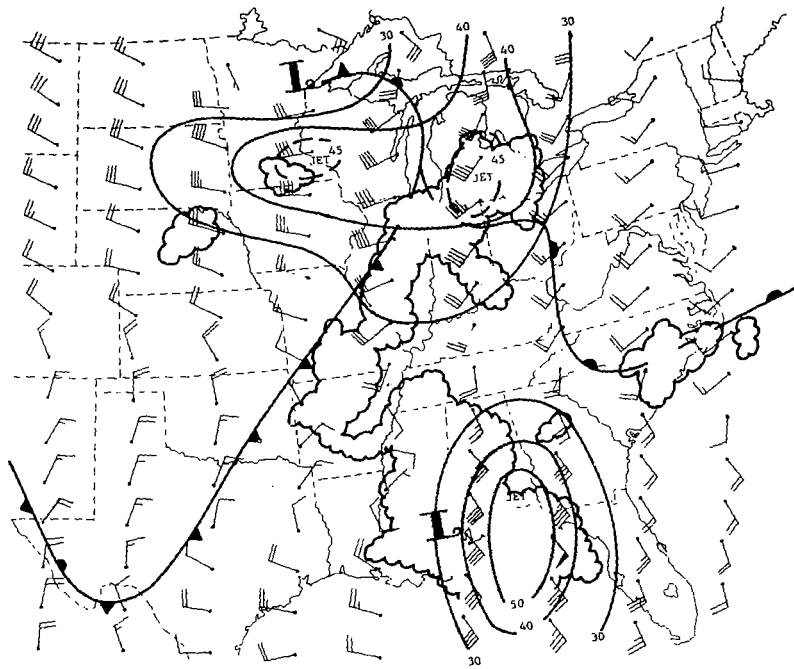
(a) 1800 GMT, 11 May 1974.
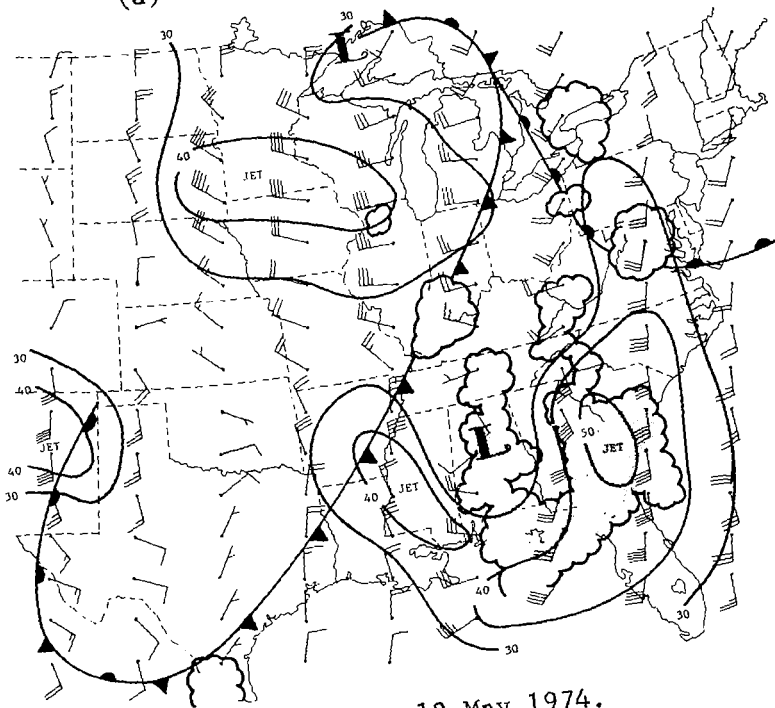
(b) 0600 GMT, 12 May 1974.

Fig. 28. Wind and isotach analyses (kts) at 850 mb.
(Superimposed are surface frontal positions
and radar-observed convection).

(a)   1800 GMT, 11 May 1974.

(b)   0600 GMT, 12 May 1974.

Fig. 29.   Wind divergence analyses (10^{-5} s^{-1}) at 850 mb.
(Superimposed are surface frontal positions
and radar-observed convection).

56

(a) 1800 GMT, 11 May 1974.

(b) 0600 GMT, 12 May 1974.

Fig. 30. Wind and isotach analyses (kts) at 700 mb.
(Superimposed are surface frontal positions
and radar-observed convection).

(a) 1800 GMT, 11 May 1974.

(b) 0600 GMT, 12 May 1974.

Fig. 31. Wind divergence analyses $(10^{-5}\ s^{-1})$ at 700 mb.
(Superimposed are surface frontal positions
and radar-observed convection).

58

(a) 1800 GMT, 11 May 1974.

(b) 0600 GMT, 12 May 1974.

Fig. 32. Wind and isotach analyses (kts) at 500 mb.
(Superimposed are surface frontal positions
and radar-observed convection).

(a)   1800 GMT, 11 May 1974.

(b)   0600 GMT, 12 May 1974.

Fig. 33.   Wind divergence analyses (10^{-5} s^{-1}) at 500 mb.
(Superimposed are surface frontal positions
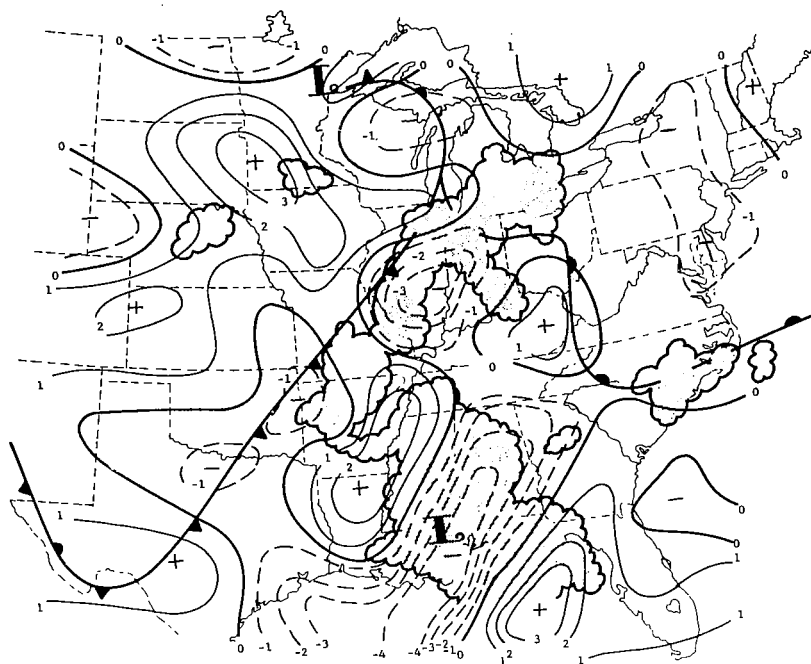and radar-observed convection).
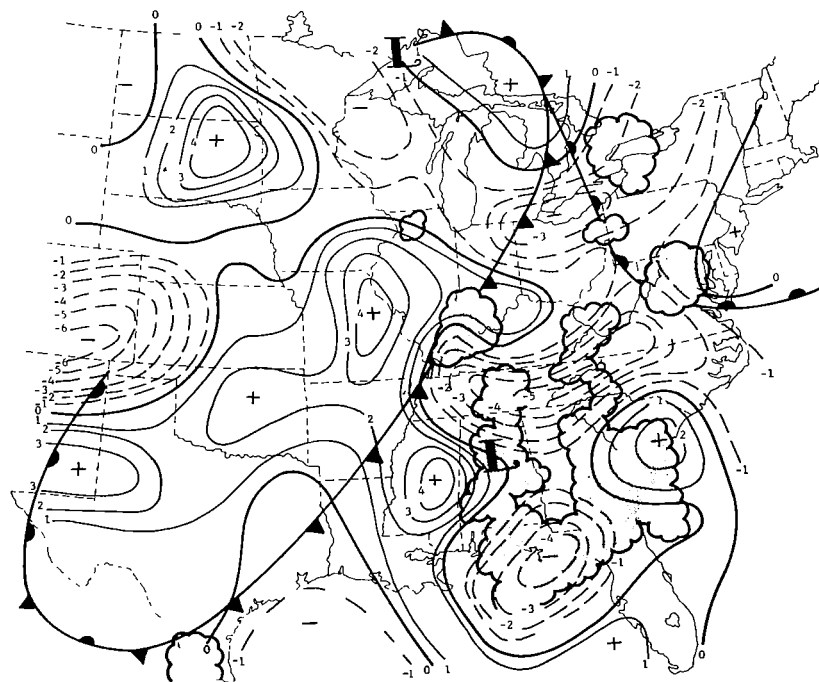
(a) 1800 GMT, 11 May 1974.

(b) 0600 GMT, 12 May 1974.

Fig. 34. Wind and isotach analyses (kts) at 300 mb.
(Superimposed are surface frontal positions
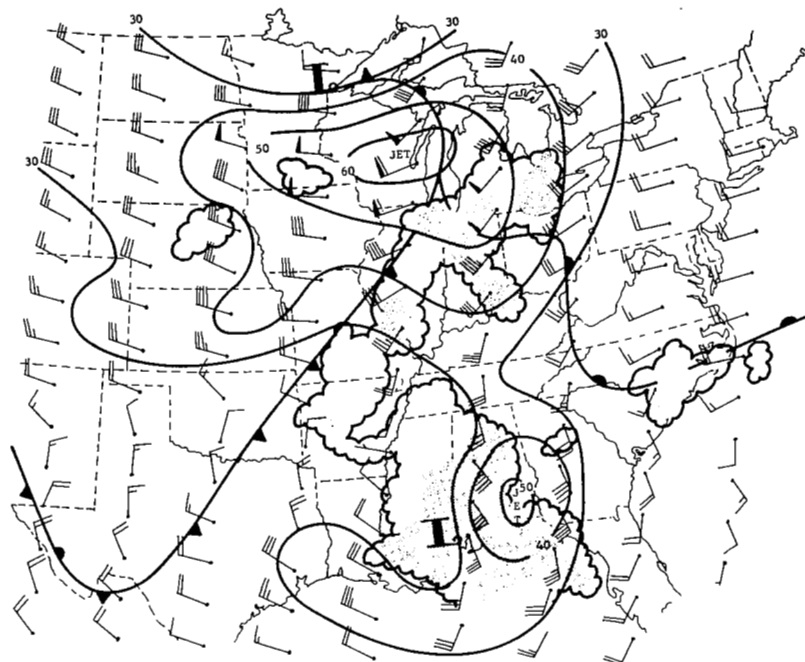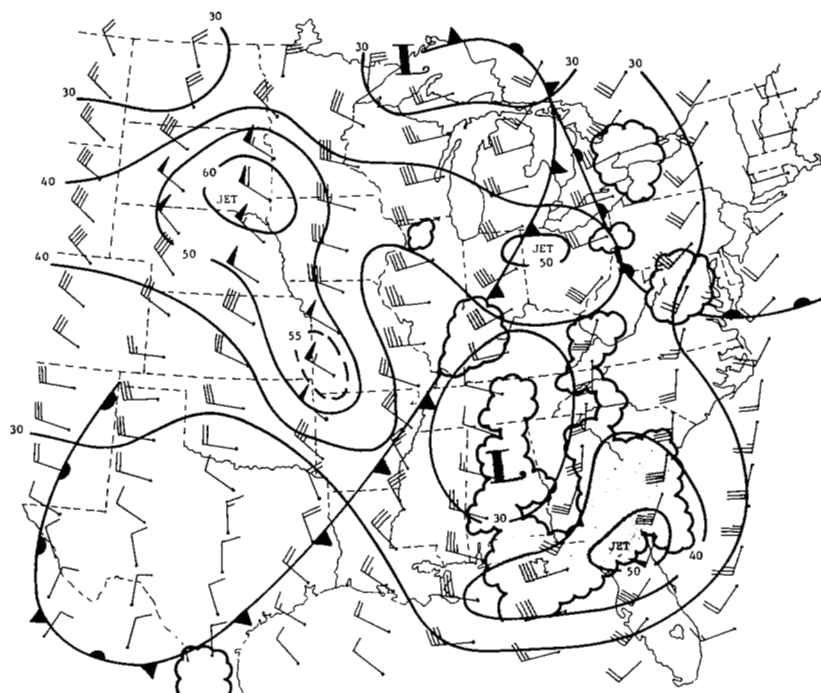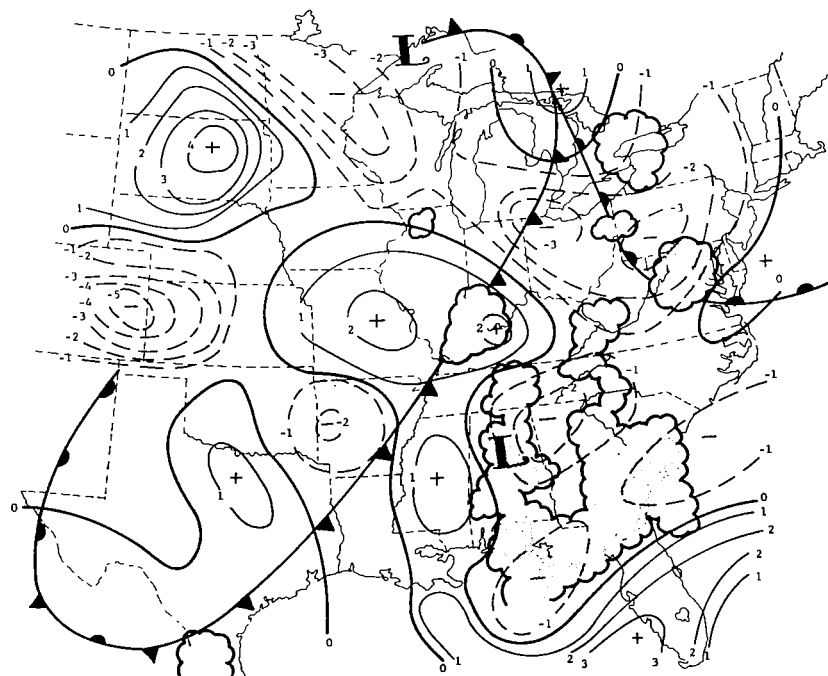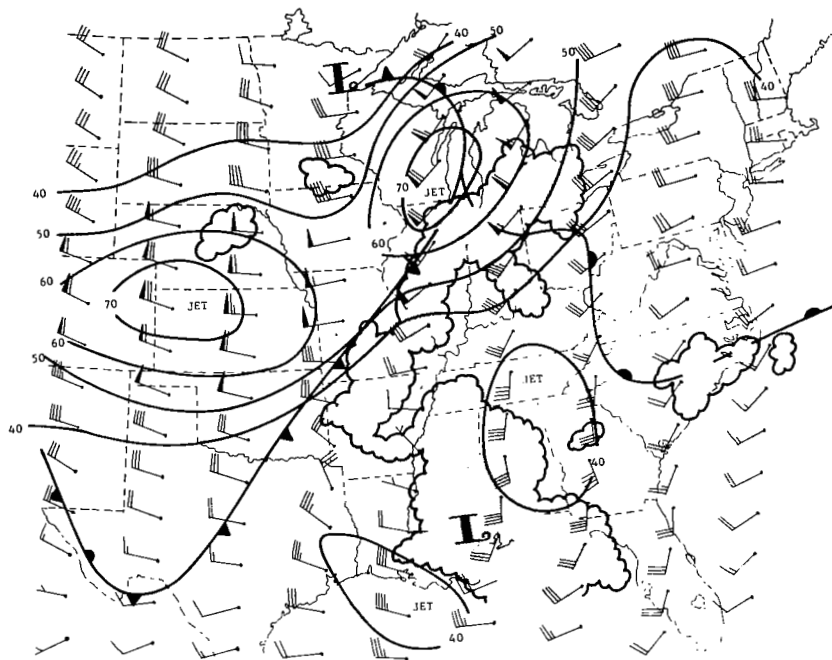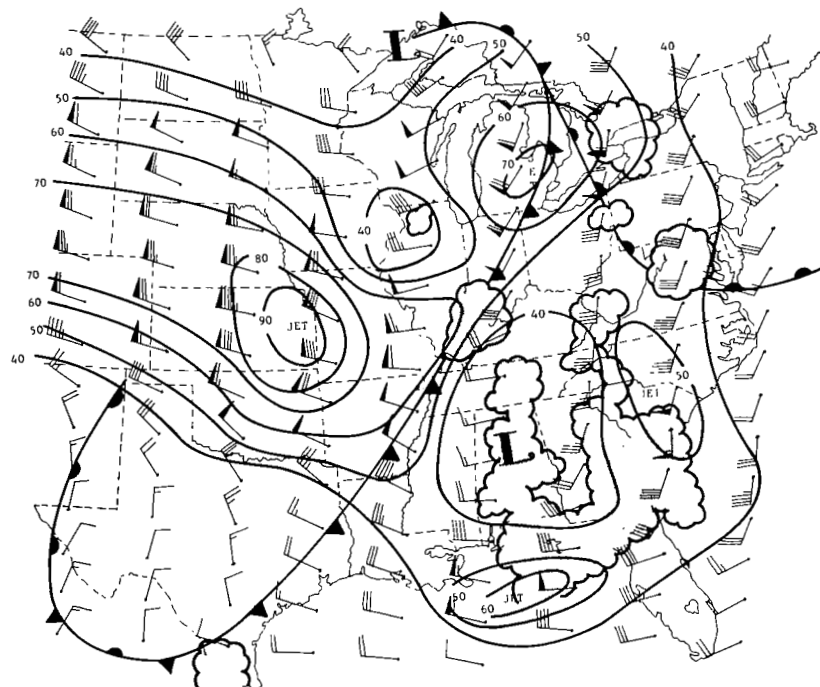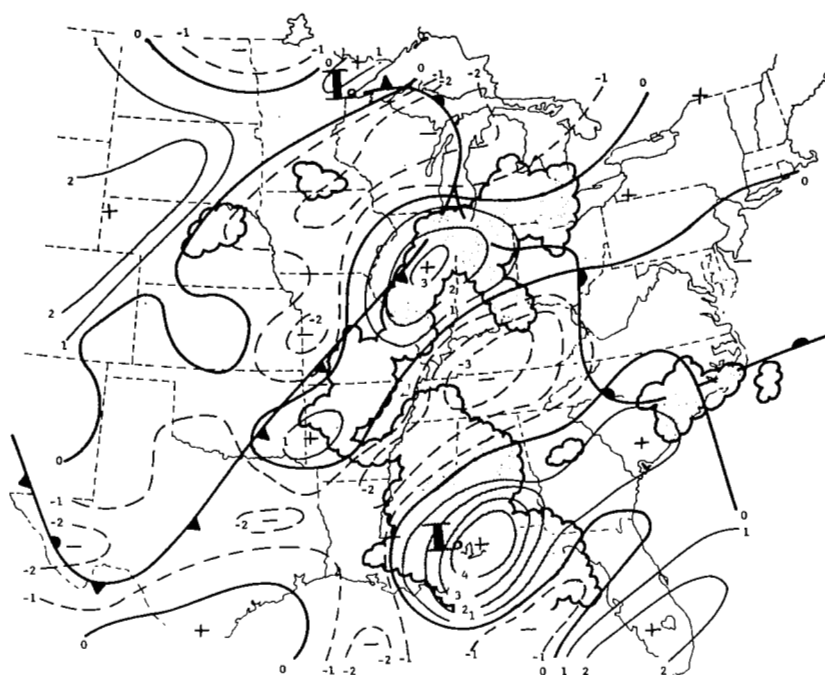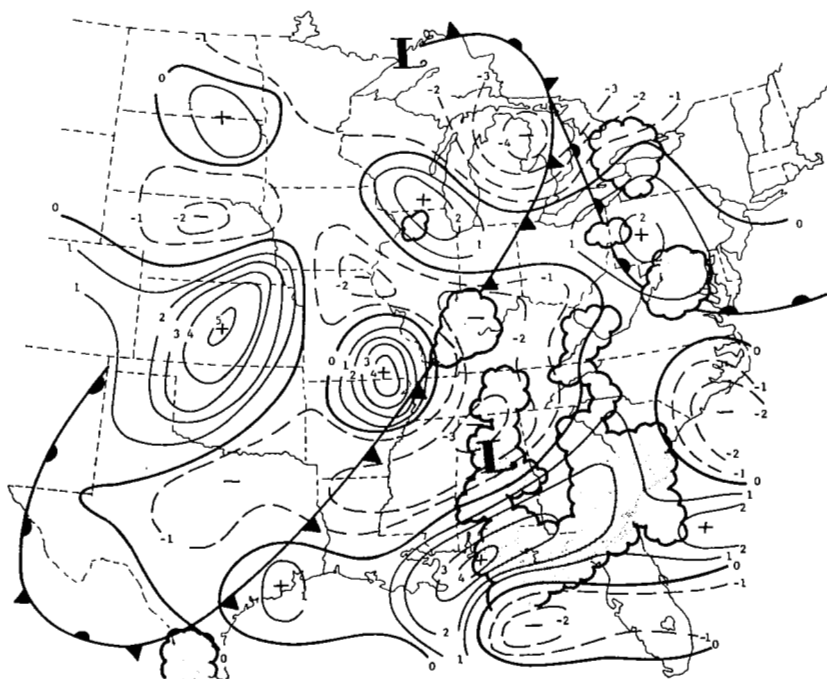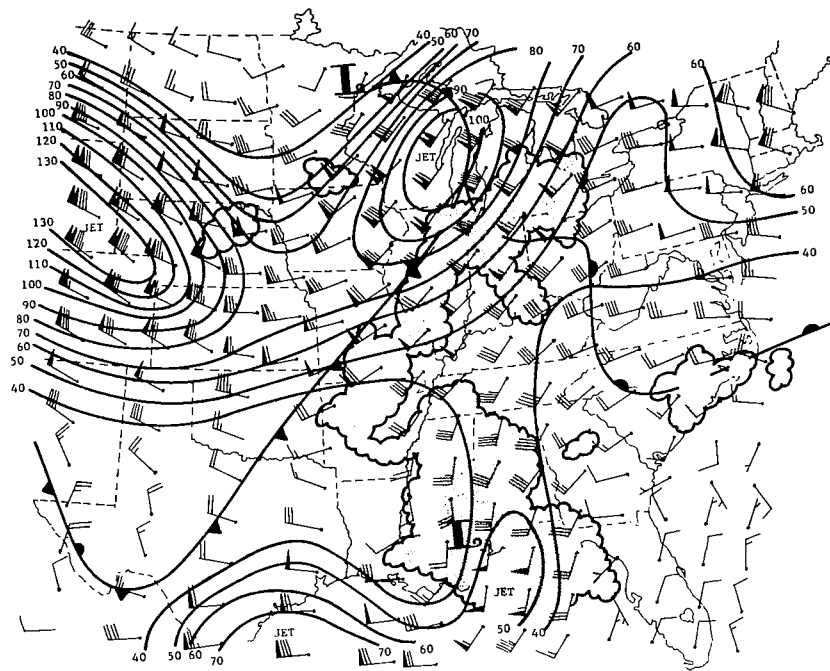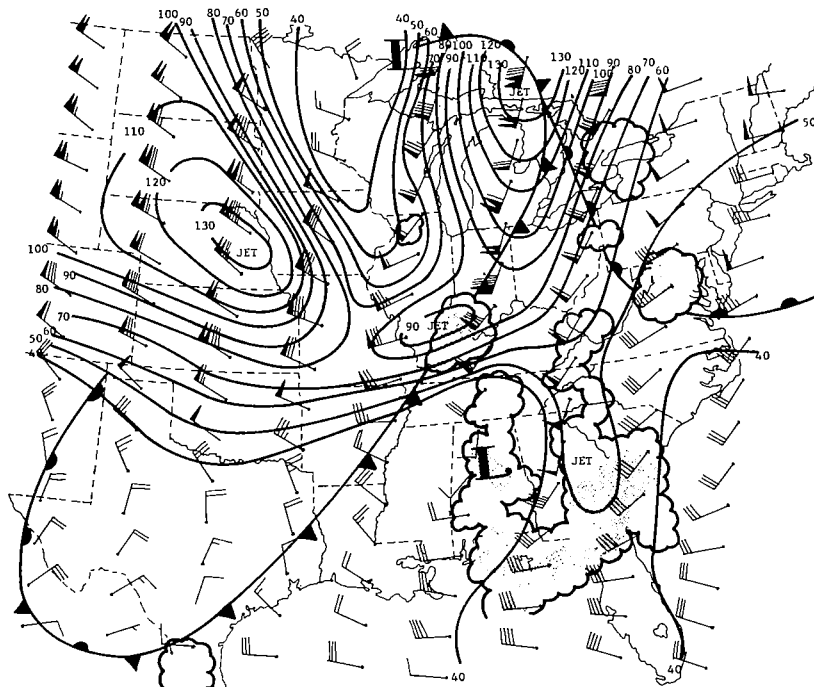and radar-observed convections).

(a) 1800 GMT, 11 May 1974.

(b) 0600 GMT, 12 May 1974.

Fig. 35. Wind divergence analyses (10^{-5} s^{-1}) at 300 mb. (Superimposed are surface frontal positions and radar-observed convection).

Florida, and the Carolinas at 1800 GMT and in southern Illinois at 0600 GMT.

The wind and isotach analyses at 500 mb and 300 mb in Fig. 32 and 34 show two well-defined jets at both times associated with the polar front in the Mississippi Valley and cyclone over the southeast U.S. Again, poor correlation exists between values of wind speed and areas of convection. However, the wind divergence analyses (Figs. 33 and 35) for the 500- and 300-mb levels show the wind field to generally be divergent over areas of convection. Well-defined divergent areas existed at both 300 and 500 mb along the cold frontal zone and over the southeast U.S. cyclone at 1800 GMT; thunderstorms were located in both of these areas. At 0600 GMT, the wind field became convergent at 500 mb along the cold frontal zone and only a small area of convection was located in southern Illinois, while strong divergence at both 500 and 300 mb was associated with the squall line over the southeast U.S.

In summary, convection occurred where velocity convergence was present in the lower troposphere and in the boundary layer and upper-tropospheric divergence was present. Stronger low-level convergence and upper-level divergence was associated with the stronger convection areas, particularly over the southeast U.S.

Vertical motion fields, calculated using Eq. 15, are shown in Figs. 36 through 38 for 850, 700 and 500 mb, respectively. In Fig. 36, convection was usually present in areas where upward vertical motion occurred at the top of the boundary layer (850 mb) although some shower activity existed in areas of subsidence at 850 mb within the cold air in the northern Plains States. Stronger areas of convection also correlated well in space with centers of upward vertical motion at both time periods both along the frontal zones and over the southeast U.S.

In Figs. 37 and 38, thunderstorms generally occurred in regions of upward vertical motion at 700 and 500 mb but in certain areas such as in central Arkansas at 1800 GMT, and in southeast Indiana at 0600 GMT, subsidence was calculated at both levels and thunderstorm activity was present. Therefore, it appears that upward vertical velocity at these levels is not a necessary condition for the formation and maintenance of convective activity. In contrast, strong convection consistently
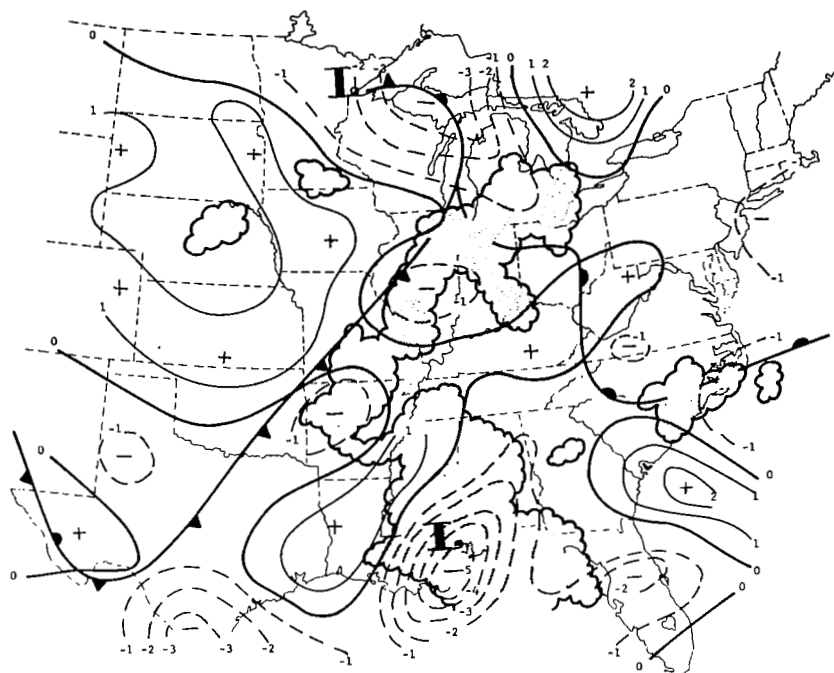
(a)   1800 GMT, 11 May 1974.

(b)   0600 GMT, 12 May 1974.

Fig. 36.   Vertical velocity (μbar s^{-1}) analyses at 850 mb.
(Superimposed are surface frontal positions
and radar-observed convection).

(a)   1800 GMT, 11 May 1974.

(b)   0600 GMT, 12 May 1974.

Fig. 37.   Vertical velocity (μbar s^{-1}) analyses at 700 mb.
(Superimposed are surface frontal positions
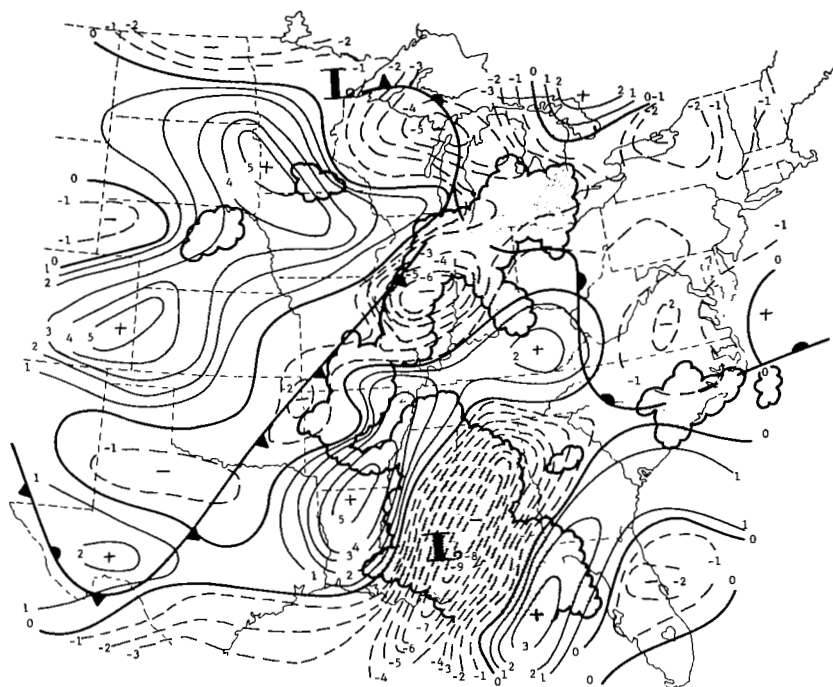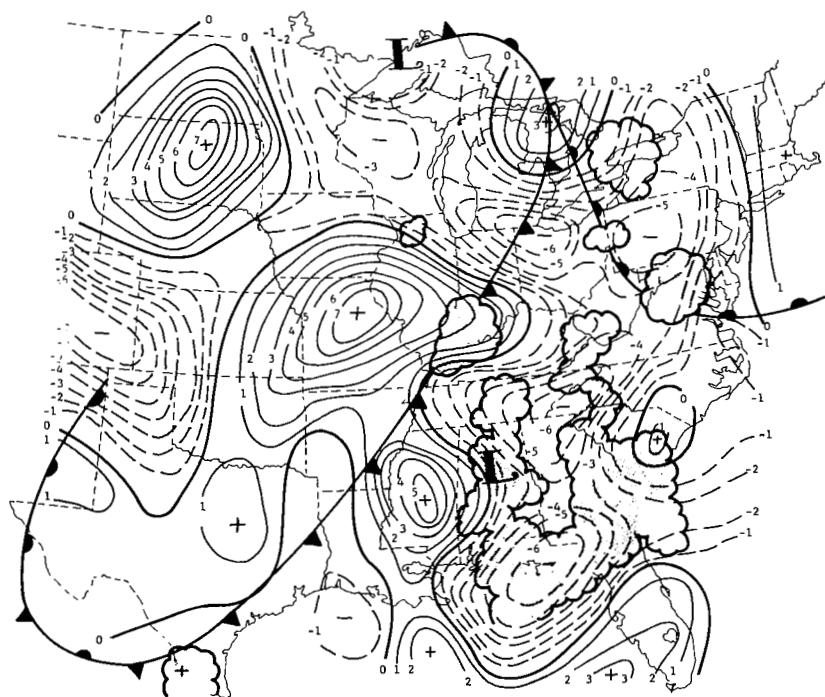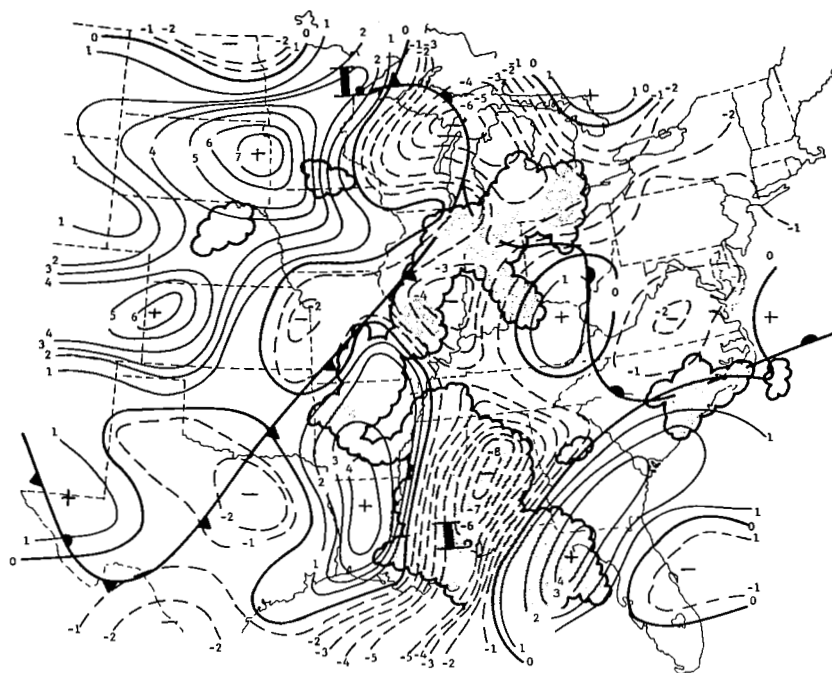and radar-observed convection).

(a)   1800 GMT, 11 May 1974.
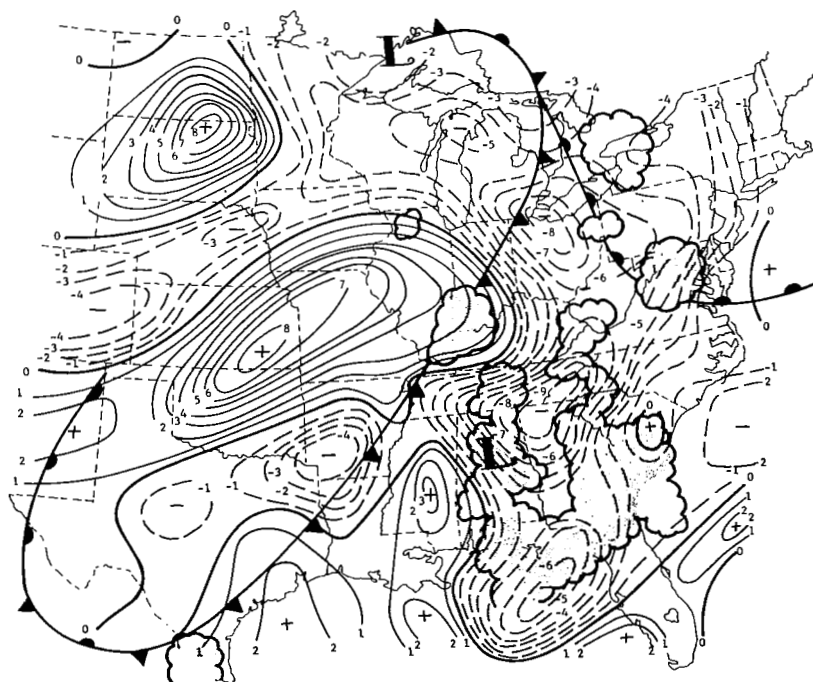

(b)   0600 GMT, 12 May 1974.

Fig. 38.   Vertical velocity (μbar s^{-1}) analyses at 500 mb.
(Superimposed are surface frontal positions
and radar-observed convection).

occurred in areas where strong upward vertical motion extended from the surface up through the entire lower and middle troposphere as was the case over the southeast U.S. throughout the AVE II experiment where upward vertical velocity exceeding 6 μbar s^{-1} was consistently occurring in the heavy convection area.

Figure 39 shows three vertical profiles of vertical motion in areas of convection computed for the center of four surrounding grid points by averaging the four vertical motion grid values at a given level. Profiles A and B were computed at 1800 GMT at the locations marked in Fig. 9, while profile C was taken at 0600 GMT at the location marked in Fig. 10. Profile A was associated with only moderate convective activity with maximum MDR = 4. Weak upward vertical motion not exceeding 1 μbar s^{-1} existed from the surface up to 700 mb with subsidence from 700 mb up to 100 mb reaching a maximum value of about 2 μbar s^{-1} at 500 mb.

Profile B was taken in an area of extensive areal coverage of heavy thunderstorm activity where average MDR = 6. This profile shows upward vertical velocity throughout the entire atmosphere with a very strong value exceeding -8 μbar s^{-1} in the middle troposphere, but a strong decrease in magnitude of the vertical motion occurs in the upper levels.

Profile C was taken in an area of very strong convection where maximum tops exceeded 55,000 ft and some MDR values were equal to 8. In this case strong upward vertical motion generally exceeding -4 μbar s^{-1} was computed from 900 mb up to 350 mb with a maximum value of -6 μbar s^{-1} found in the mid-troposphere.

These profiles suggest that upward vertical motion in the boundary layer seems to be a necessary condition for the formation of convection (Endlich and Mancuso, 1968). Moreover, strong upward vertical motion throughout the entire troposphere seems to be associated with heavy or severe convection.

Figure 40 shows the objective analyses of boundary layer moisture divergence at 1800 GMT and 0600 GMT. An even better spatial correlation existed between high negative values of this parameter and areas of convection than was observed between boundary layer vertical motion and convection. Subsynoptic scale centers of D$_{MBL}$ within the field tended to better delineate particular areas in which stronger negative values
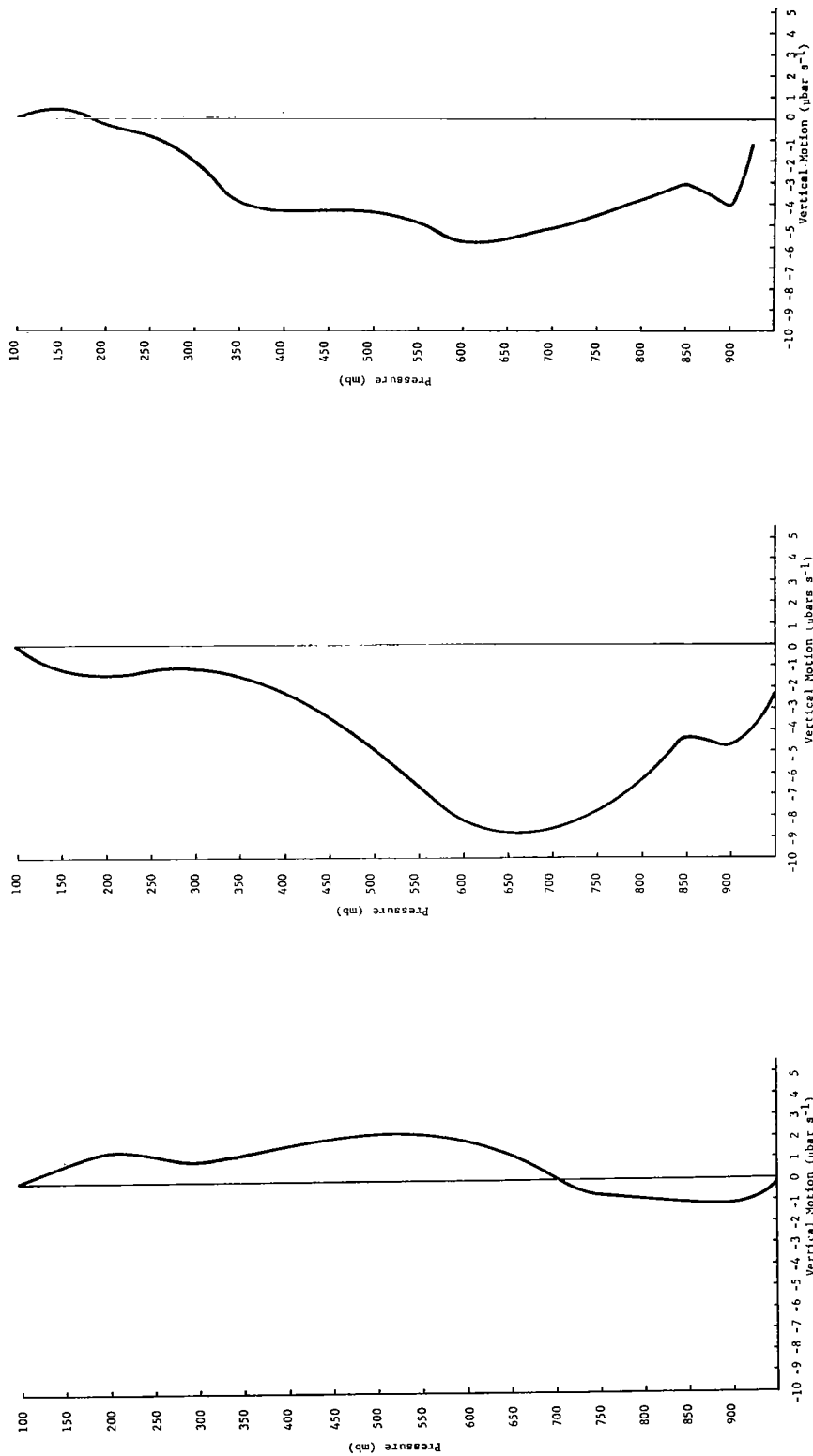
(a) Profile A
(Northwest Arkansas at
1800 GMT - maximum
MDR = 4)

(b) Profile B
(Southern border of
Mississippi and Alabama
at 1800 GMT - maximum
MDR = 6)

(c) Profile C
(Florida Panhandle at
0600 GMT over the
squall line - maximum
MDR = 8)

Fig. 39. Three vertical profiles of vertical velocity in thunderstorm areas.

68
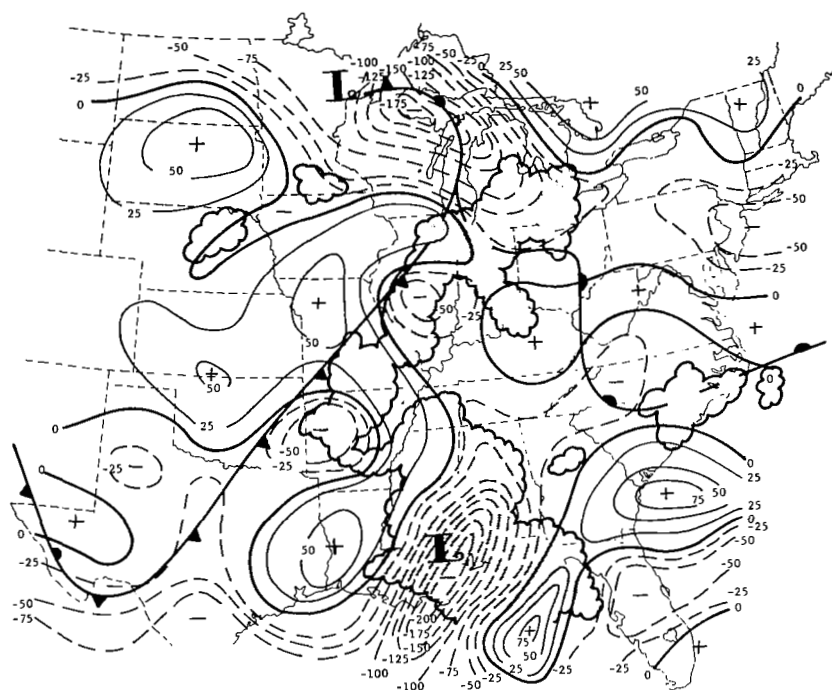
(a)   1800 GMT, 11 May 1974.
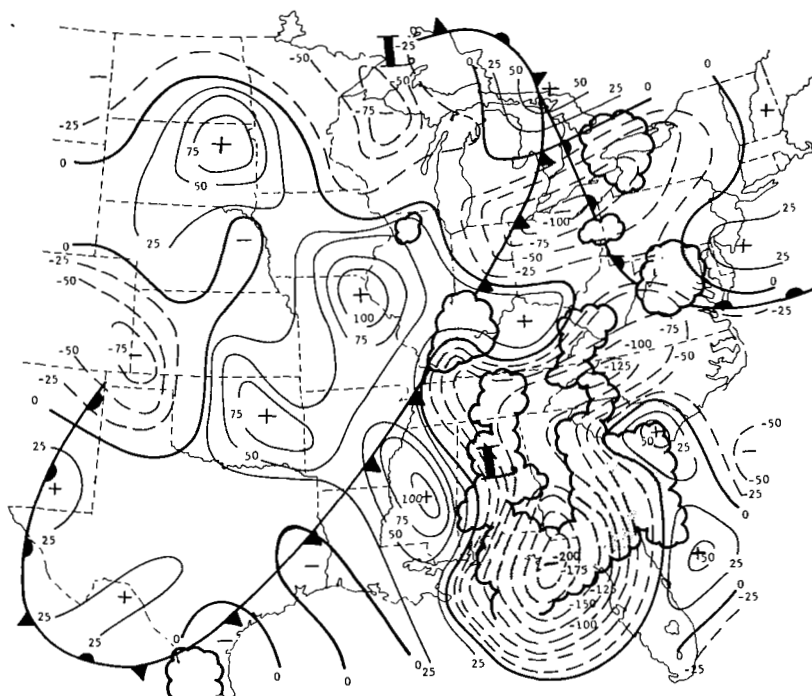
(b)   0600 GMT, 12 May 1974.

Fig. 40.   Boundary layer moisture divergence
$(10^{-4}$ °K s$^{-1})$ analyses. (Superimposed
are surface frontal positions and
radar-observed convection).

were associated with stronger thunderstorm activity and strong positive areas contained no convection. This was particularly true at both time periods along the frontal zones and over the southeast U.S. where convection was located within an area of extremely large D_{MBL} values. In addition, at 1800 GMT, the boundary layer vertical motion field showed subsidence associated with the shower activity in the northern Plains States while the D_{MBL} field showed a small tongue of negative values in the shower area.

Therefore, the combined effects of both wind convergence within a moist environment in the boundary layer and positive moisture advection within the boundary layer seem to relate extremely well to the spatial distribution of observed convection. Also larger negative values of D_{MBL} appear to be related to the stronger intensity of convection.

4. Space cross sections and soundings

Four vertical cross section at both 1800 GMT and 0600 GMT are shown in Figs. 41 through 48 along the lines marked WX and YZ in Figs. 9 and 10. Two cross sections were analyzed along each line, one containing the thermal field, frontal structure, and isotach analysis. The other contains the vertical velocity fields calculated from Eqs. 18 and 19 superimposed upon the frontal structures with the observed convection in each cross section marked along the bottom.

The WX cross sections at both times show strong, well defined cold and warm frontal zones, tropopause, and polar jet centers. These cross sections were constructed primarily to determine the relationships between the cold and warm frontal zones, the vertical motion fields, and the observed convection.

The vertical motion fields along the WX lines at both 1800 GMT and 0600 GMT show several similarities relative to the observed convection. Strong upward motion occurred just ahead or along the cold frontal zones over the northeast U.S. at both times and convection existed there also. No convection was observed within the subsidence computed behind the cold fronts or ahead of the cold front at 1800 GMT.

At 0600 GMT the presence of a subsynoptic-scale system was observed as it moved within the cold air behind the cold front in the northern Plains States. This weak system was associated with a lower

Fig. 41. Vertical cross section of wind (kts) and temperature (°C) along line WX of Fig. 9 at 1800 GMT, 11 May 1974.

Fig. 42. Vertical cross section of vertical motion ($\mu bar\ s^{-1}$) along line WX of Fig. 9 at 1800 GMT, 11 May 1974.

72

Fig. 43. Vertical cross section of wind (kts) and temperature (°C) along line WX of Fig. 10 at 0600 GMT, 12 May 1974.

Fig. 44. Vertical cross section of vertical motion (μbar s^{-1}) along line WX of Fig. 10 at 0600 GMT, 12 May 1974.

74

Fig. 45. Vertical cross section of wind (kts) and temperature (°C) along line YZ of Fig. 9 at 1800 GMT, 11 May 1974.
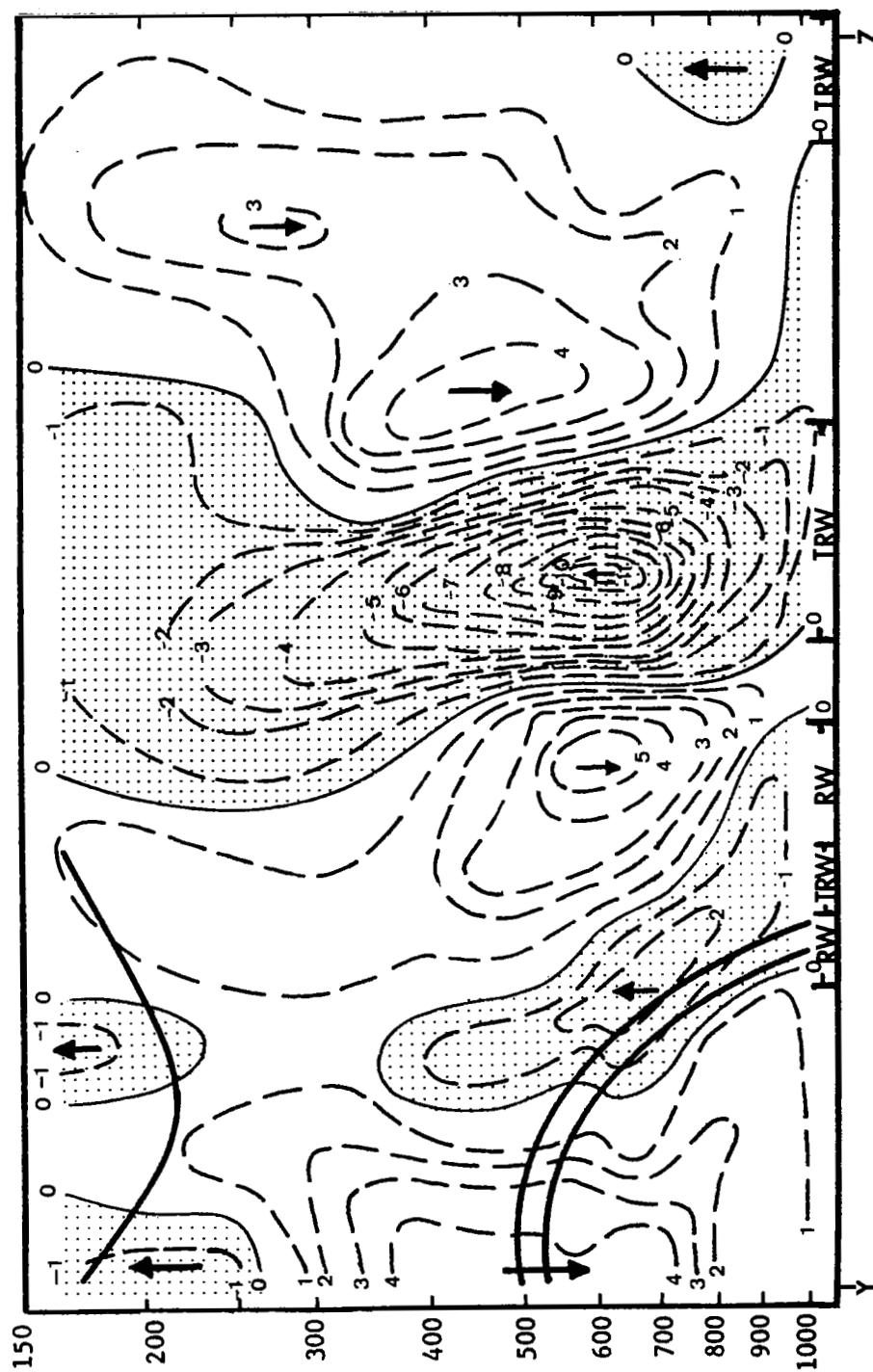
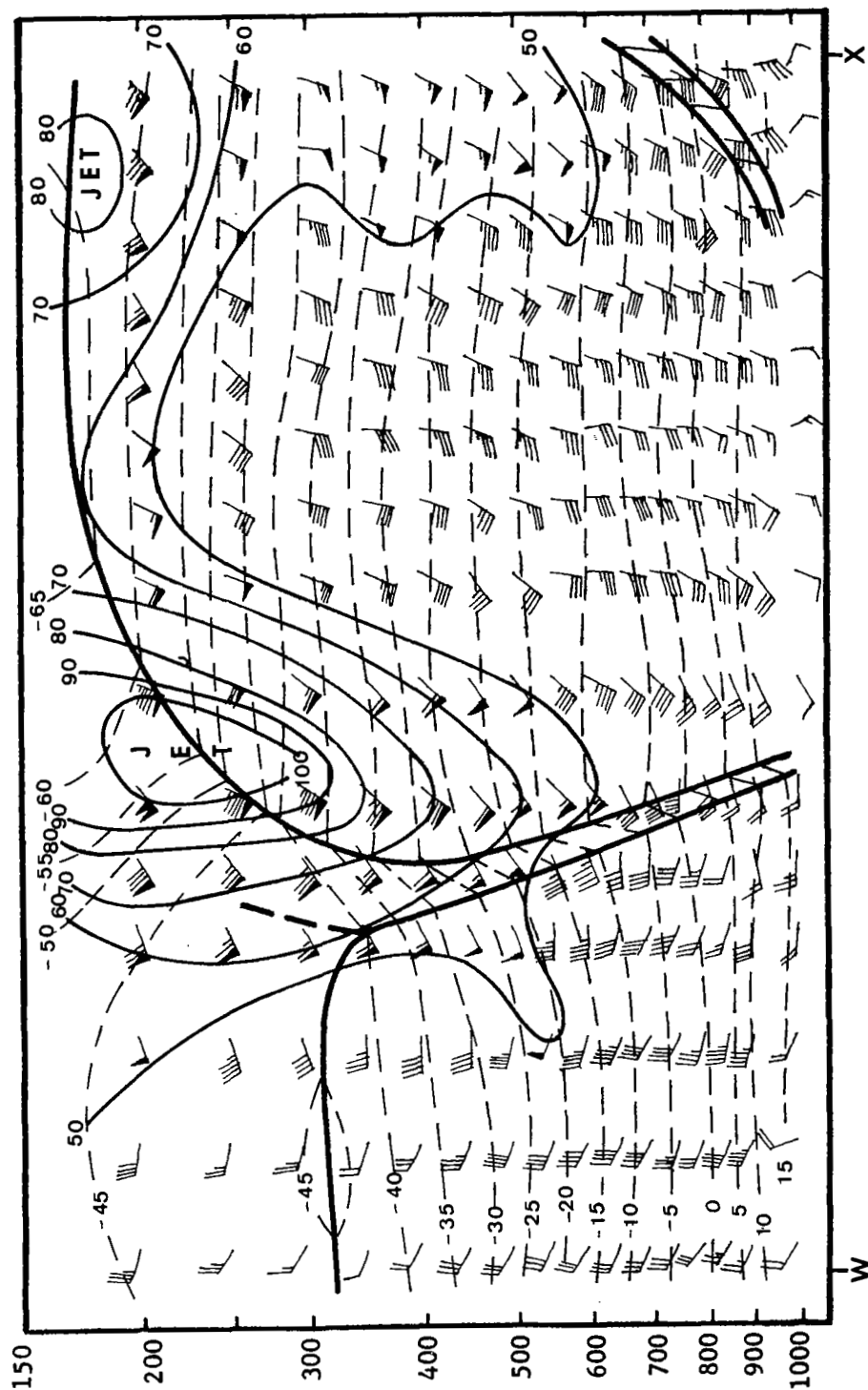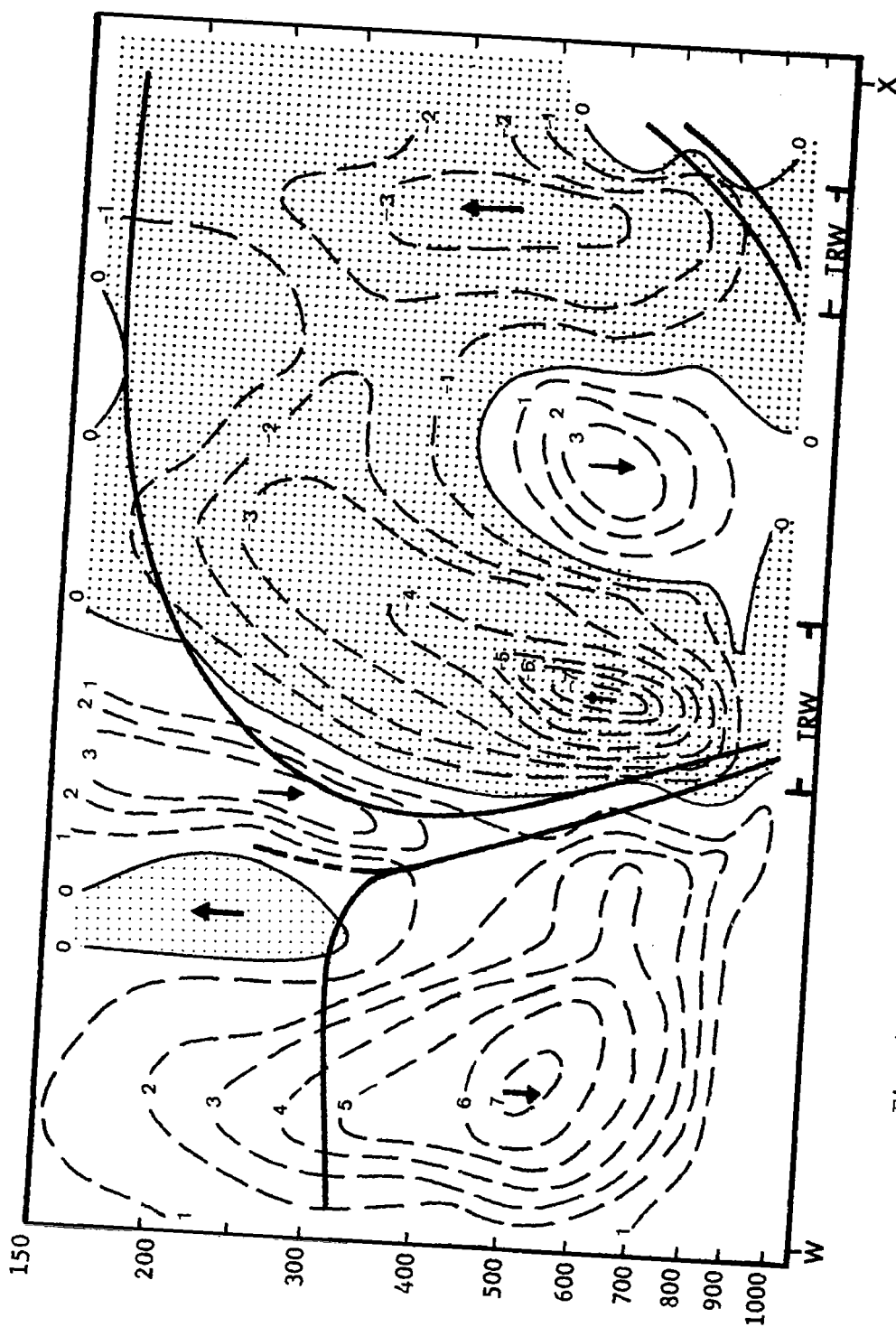Fig. 46. Vertical cross section of vertical motion (μbar s^{-1}) along line YZ of Fig. 9 at 1800 GMT, 11 May 1974.
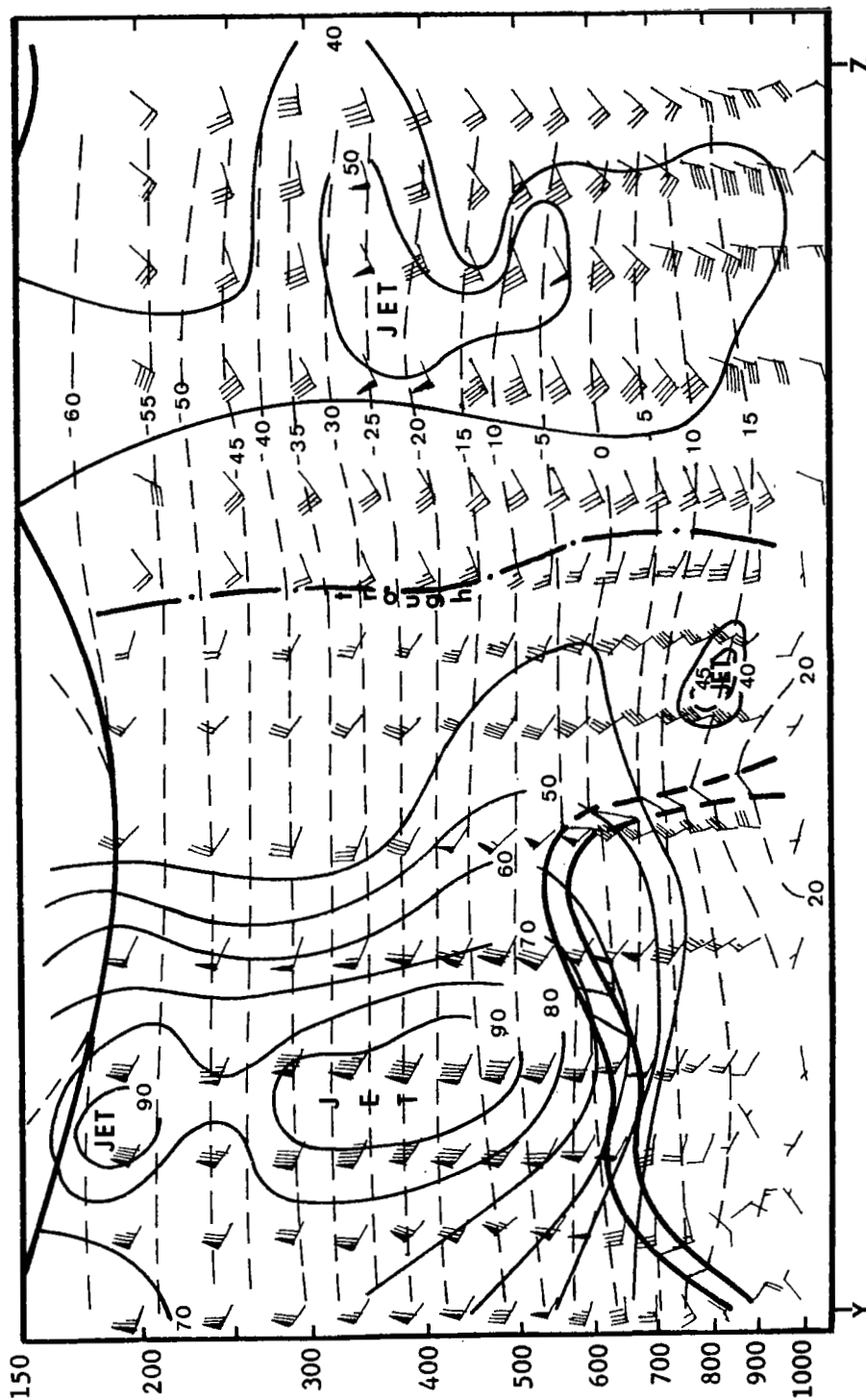
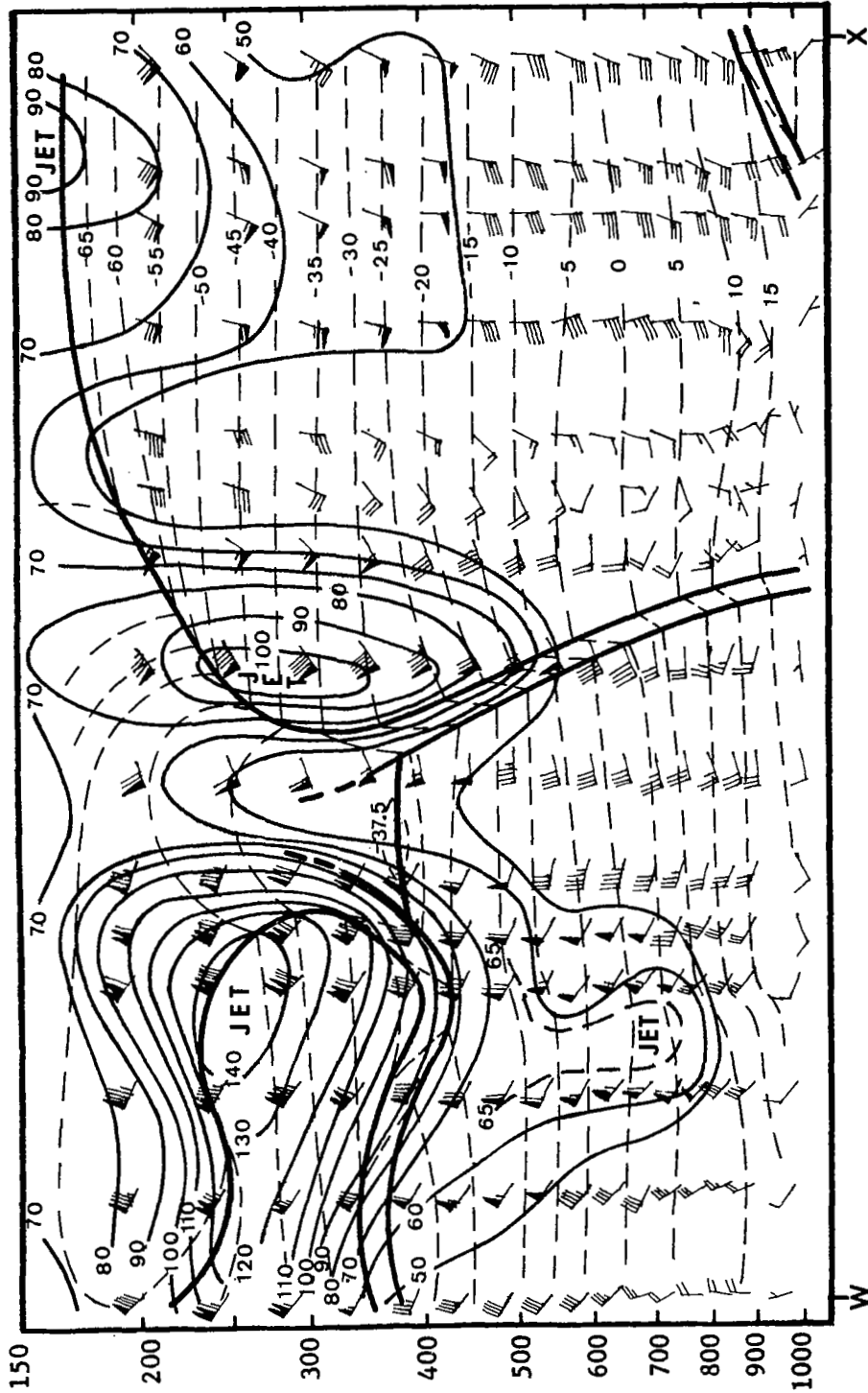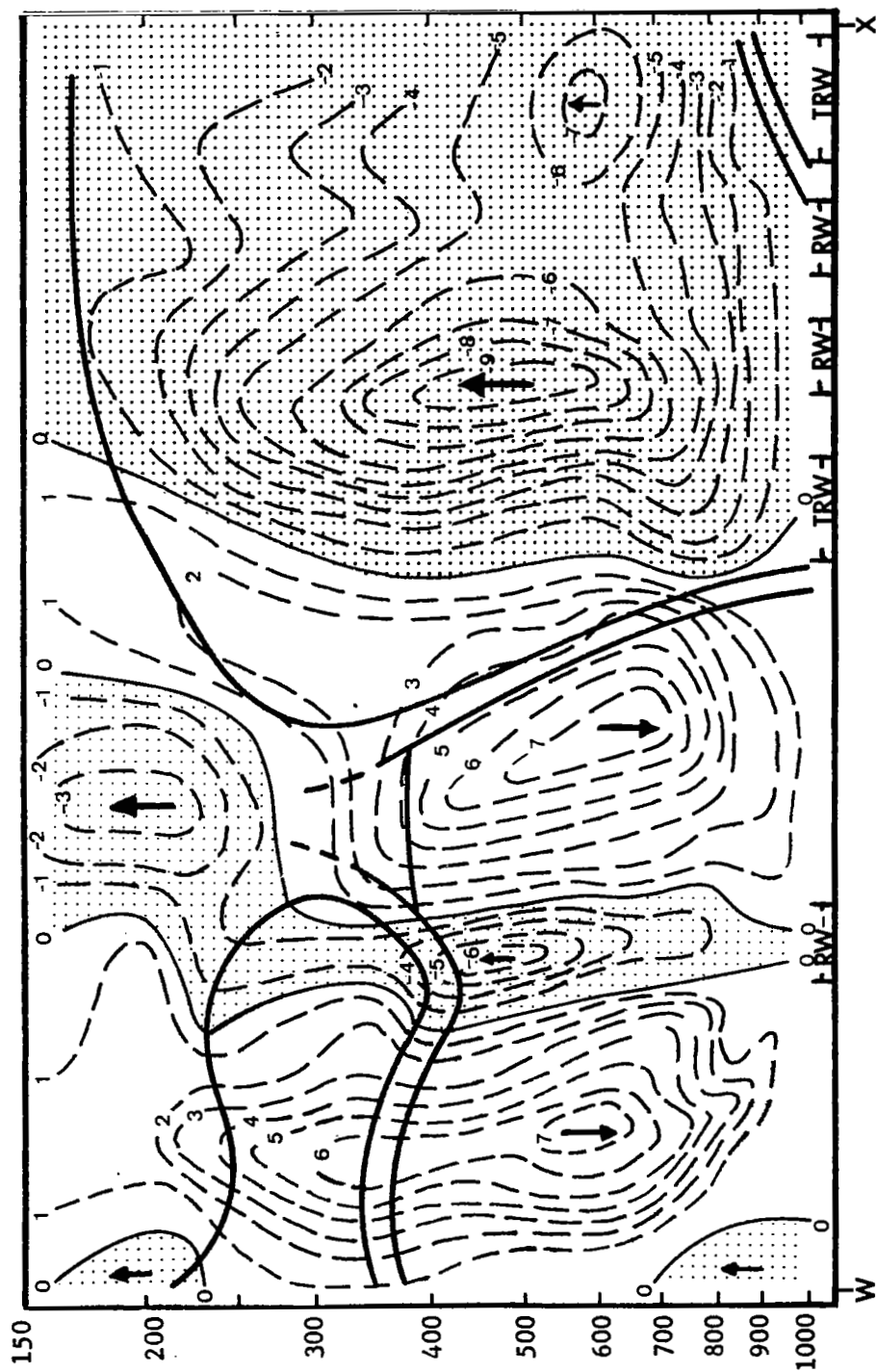Fig. 47. Vertical cross section of wind (kts) and temperature (°C) along line YZ of Fig. 10 at 0600 GMT, 12 May 1974.
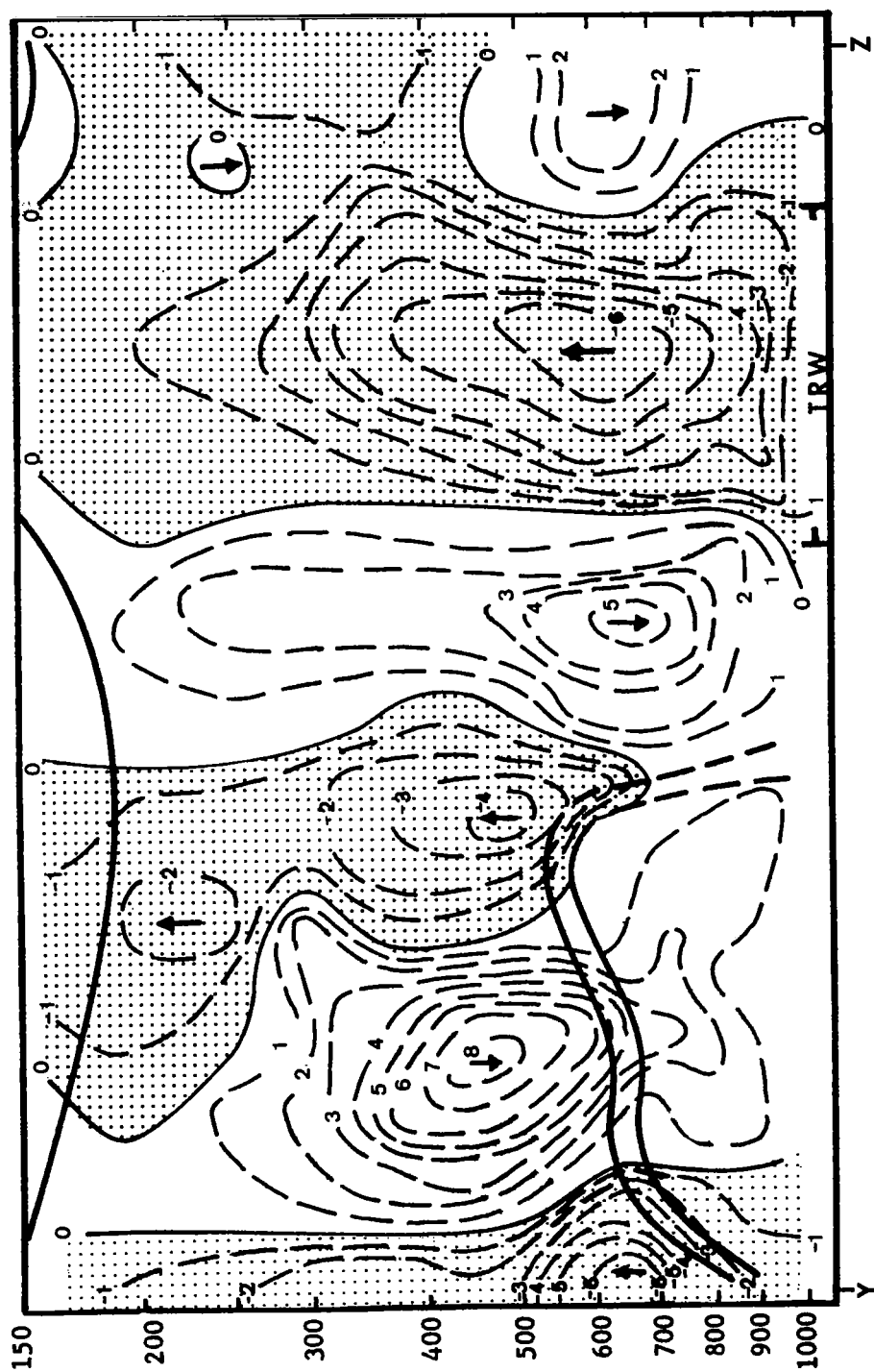
Fig. 48. Vertical cross section of vertical motion ($\mu bar\ s^{-1}$) along line YZ of Fig. 10 at 0600 GMT, 12 May 1974.
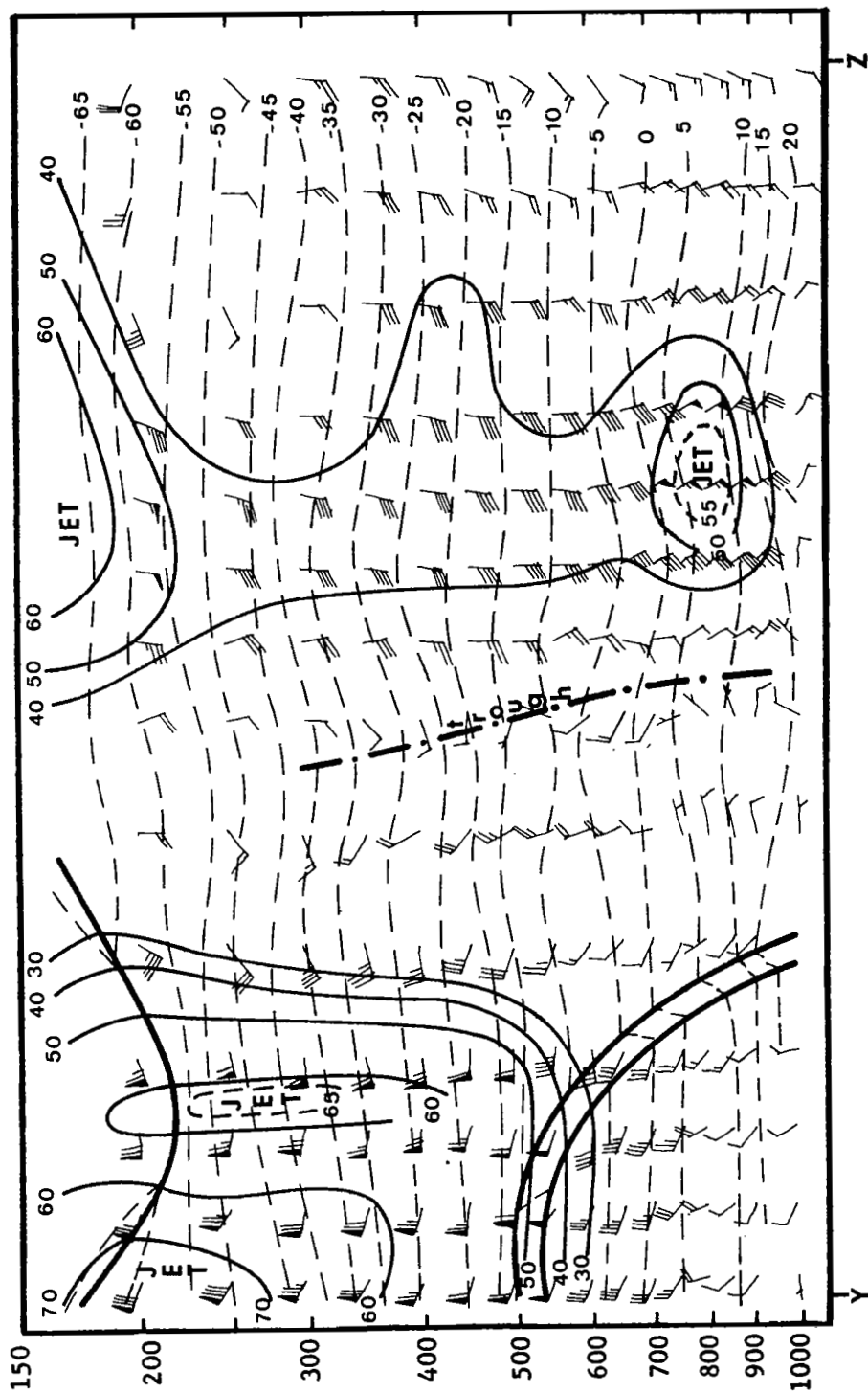
tropospheric jet maximum, a fairly strong cooling trend behind the
system, and a zone of upward vertical motion that was apparently only
able to produce weak stratiform-type precipitation and a few showers.

The cross sections along the YZ lines at both times were constructed
primarily to examine the vertical structure of the southeast U.S.
cyclone and its associated convection. The cold frontal zones at both
times are relatively shallow and at 0600 GMT the surface position of the
front is breaking up in the southeastern Arkansas area. Fairly strong
low- to middle-level jets were associated with the cyclone which had an
almost vertical structure throughout the experiment.

Very strong zones of upward vertical motion extending to the top of
the troposphere were computed to the east and northeast of the cyclone
and strong convection was observed within these zones. In addition,
strong subsidence occurred on both sides of the cyclone and behind the
cold fronts where no convection existed. Upward vertical motion was
computed from the surface up to 450 mb along the cold front at 1800 GMT
and convection was present. But at 0600 GMT, subsidence occurred from
the surface up to 700 mb where upward motion existed up to 100 mb but
convection was not present, indicating again the importance of upward
vertical motion in the boundary layer in the formation of convection.
Convection also was not present within the upward motion in the
developing lee side low in western Kansas where relatively dry air was
present.

The effects of vertical motion along the cold and warm fronts and
within the southeast U.S. cyclone upon the vertical soundings of tem-
perature and moisture were studied using 3-h consecutive soundings in
areas of convection.

Figure 49 shows the 3-h soundings at Monett, Missouri at 1200, 1500,
and 1800 GMT on 11 May 1974. The effects of the cold frontal passage at
1700 GMT upon the sounding at 1800 GMT can be seen by the zone of
saturation between 850 mb and 750 mb in which the temperature lapse rate
approaches the dry adiabatic lapse rate. The wind field also shifts
from west-southwest at 1200 and 1500 GMT to northwest at 1800 GMT
behind the front. Any lifted air parcel within the saturated zone at
1800 GMT would follow a saturated adiabatic and would be warmer than the
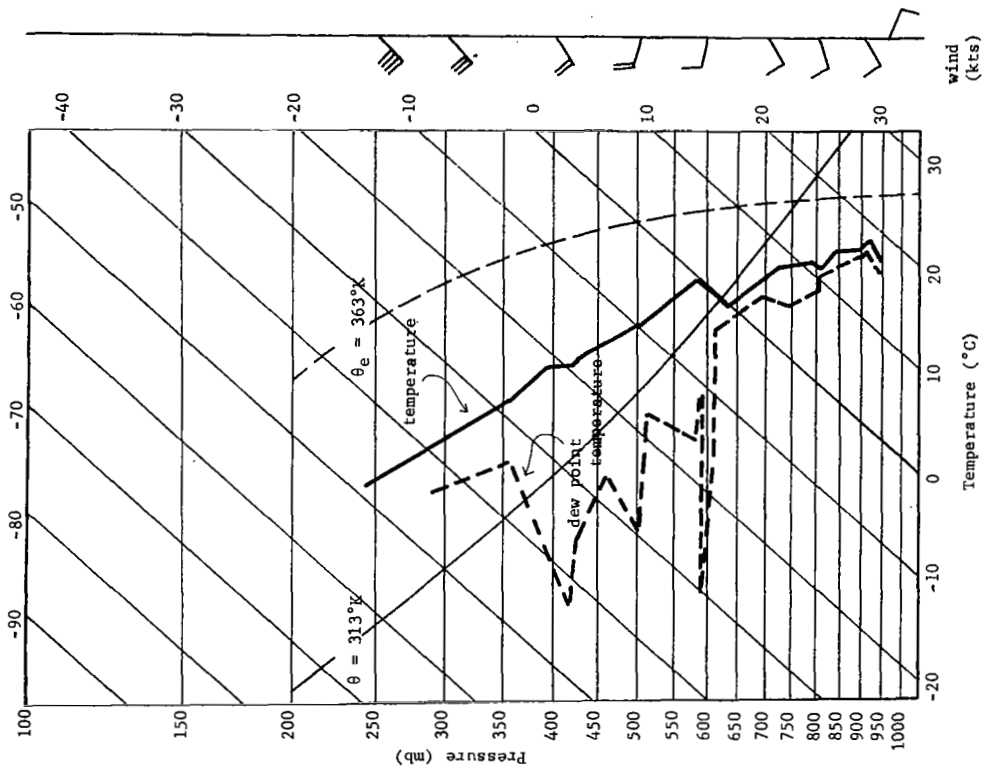
(b) 1500 GMT, 11 May 1974.
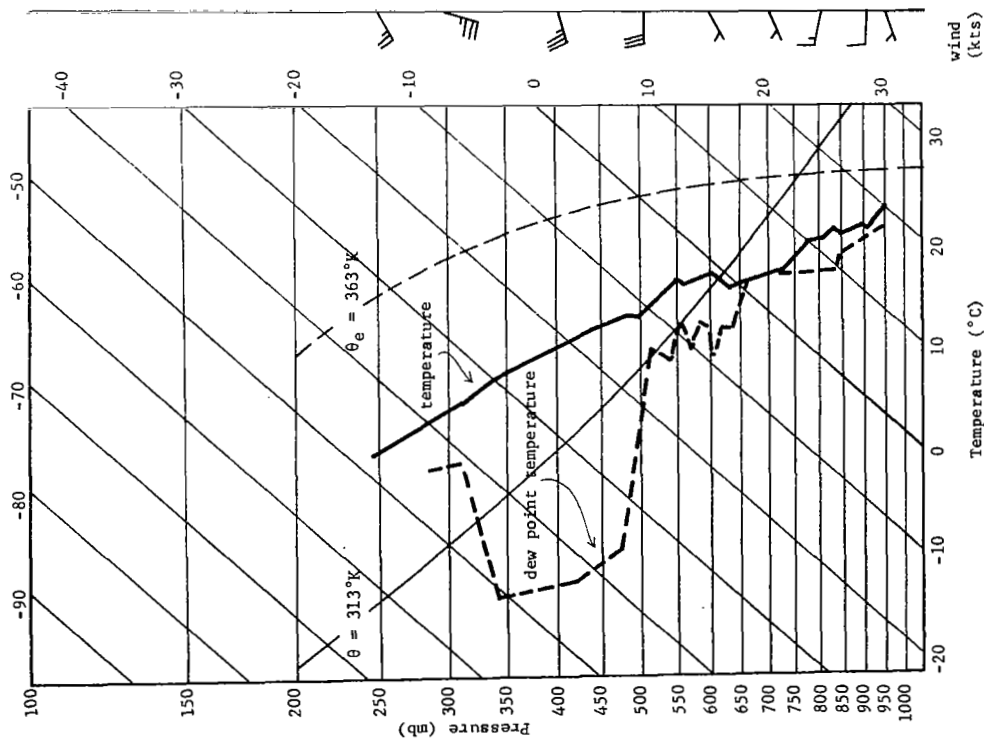
(a) 1200 GMT, 11 May 1974.

Fig. 49. Three consecutive soundings taken at intervals of three hours at Monett, Missouri.

(c) 1800 GMT, 11 May 1974.

Fig. 49. (Continued)

surrounding environment. As a result, towering cumulus and radar-observed convection with tops up to 29,000 ft were observed in the vicinity of Monett at 1800 GMT.

Strong convection at 0600 GMT at Washington, D.C. was apparently the result of strong upward vertical motion on top of the warm frontal surface within a highly convectively unstable layer. Figure 50 shows the 3-h consecutive soundings at 0000 GMT, 0300 GMT, and 0600 GMT on 12 May 1974 for Washington, D.C. The warm frontal surface was located around 900 mb at all three times where a frontal inversion was located; the southeast winds below the inversion support this position. A strong inversion, above which dry air was present, capped the release of instability from the saturated air below at 0000 GMT and 0300 GMT, but strong upward vertical motion was apparently responsible, in part, for the rapid removal of the inversion through adiabatic cooling by 0600 GMT. At this time, the entire sounding was nearly saturated and layers of air at 700 and 600 mb were completely unstable with respect to parcel displacement. As a result, a special surface observation at Washington D.C. at 0635 GMT reported a heavy thunderstorm at the station and maximum radar tops exceeded 40,000 ft over the Washington area at that time.

Finally, the consecutive 3-h soundings at Tampa, Florida, at 0600, 0900, and 1200 GMT on 12 May 1974 are shown in Fig. 51. A line of heavy thunderstorms with tops up to 58,000 ft was observed just north-west of Tampa during this time period and which had moved to about 100 km northwest of the station at 1200 GMT. In this system, no fronts were detectable so that vertical motion here was purely the result of strong low-level convergence ahead and within the Southeast U.S. cyclone.

The three soundings at Tampa resemble closely the Type I Tornado sounding described by Miller (1967) in which low-level, high-energy air near saturation is capped by an inversion between 800 and 700 mb. By 1200 GMT the inversion had apparently been lifted from the 850-mb level at 0600 GMT to about 750 mb and the underlying air was very near saturation. Continued lifting of the inversion and the resulting dry-adiabatic cooling of the air above it would result in the removal of the inversion so that saturation in the air below would release the large

(a) 0000 GMT, 12 May 1974.

(b) 0300 GMT, 12 May 1974.

Fig. 50. Three consecutive soundings taken at intervals of three hours at Washington, D.C.
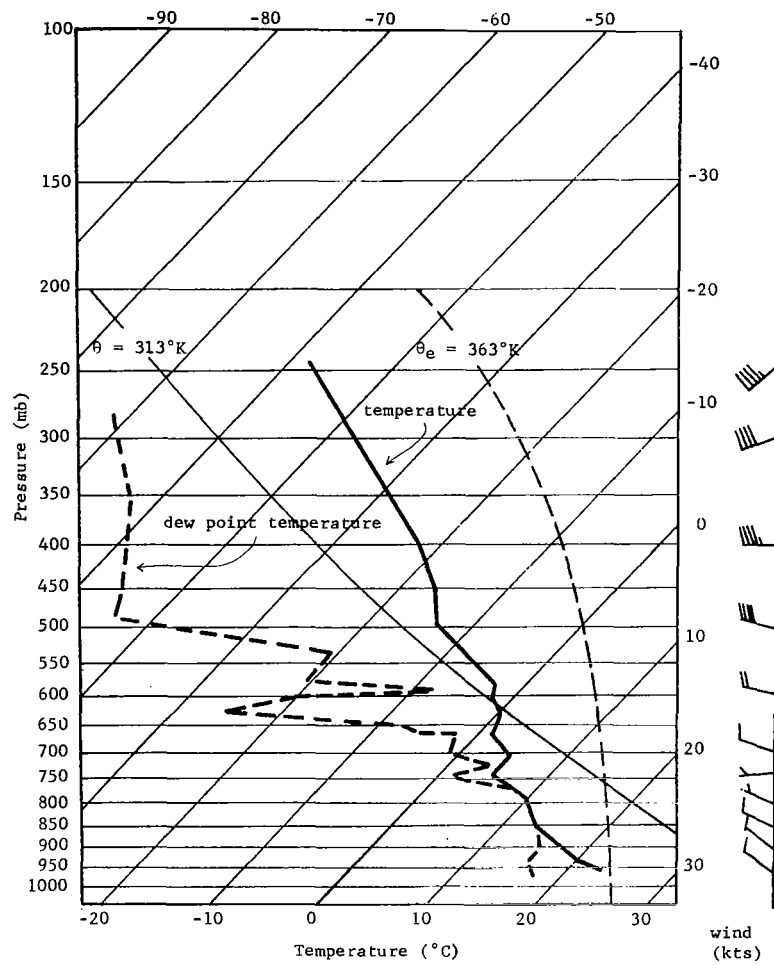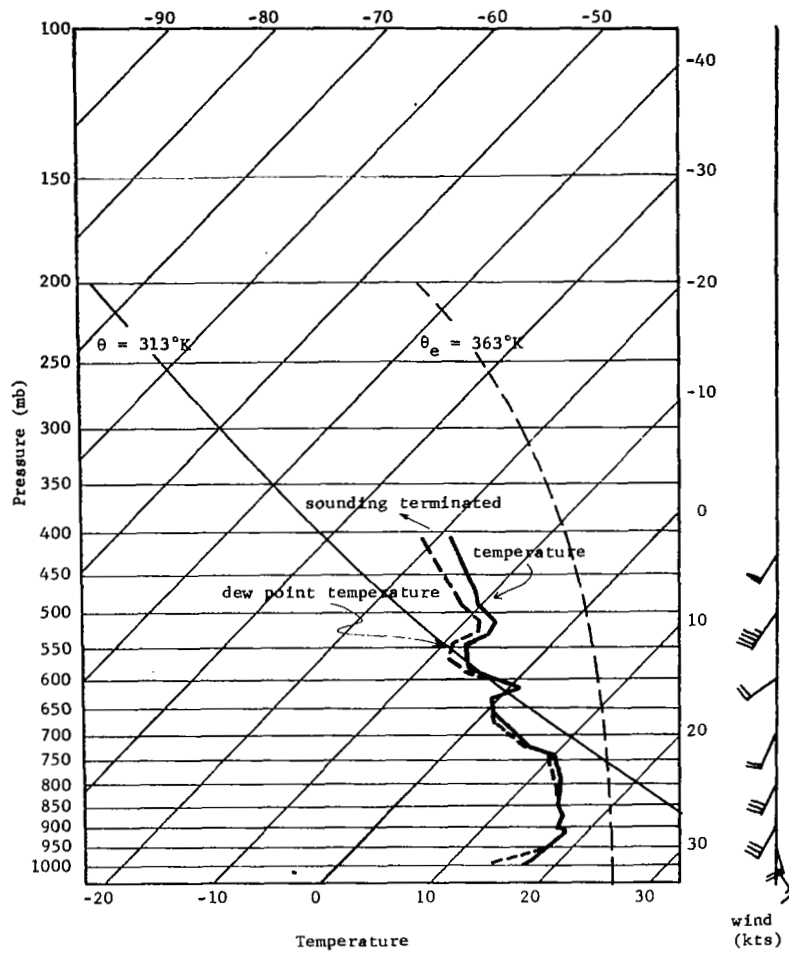
(c) 0600 GMT, 12 May 1974.

Fig. 50. (Continued)

(b) 0900 GMT, 12 May 1974.

(a) 0600 GMT, 12 May 1974.
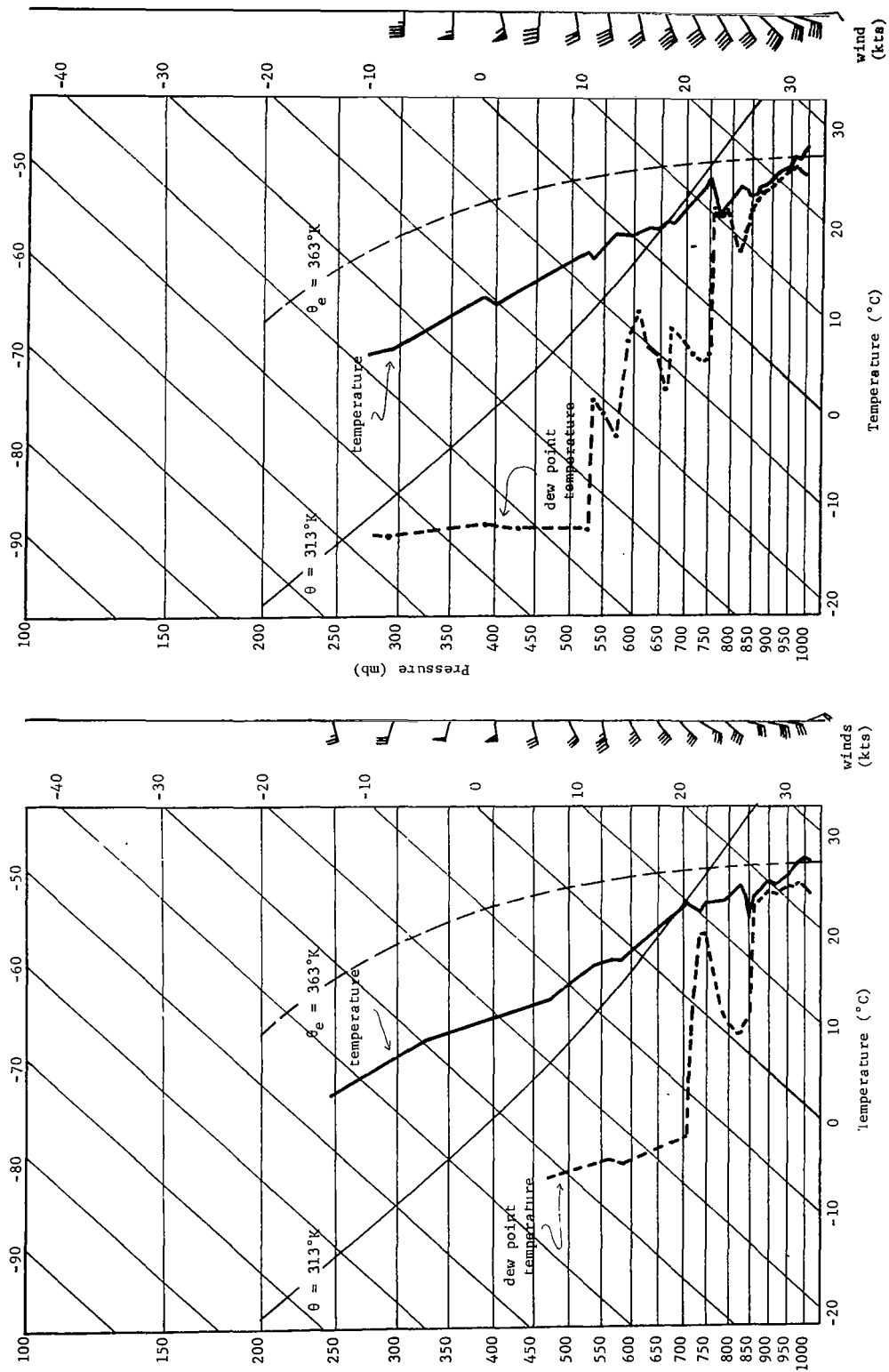
Fig. 51. Three consecutive soundings taken at intervals of three hours at Tampa, Florida.
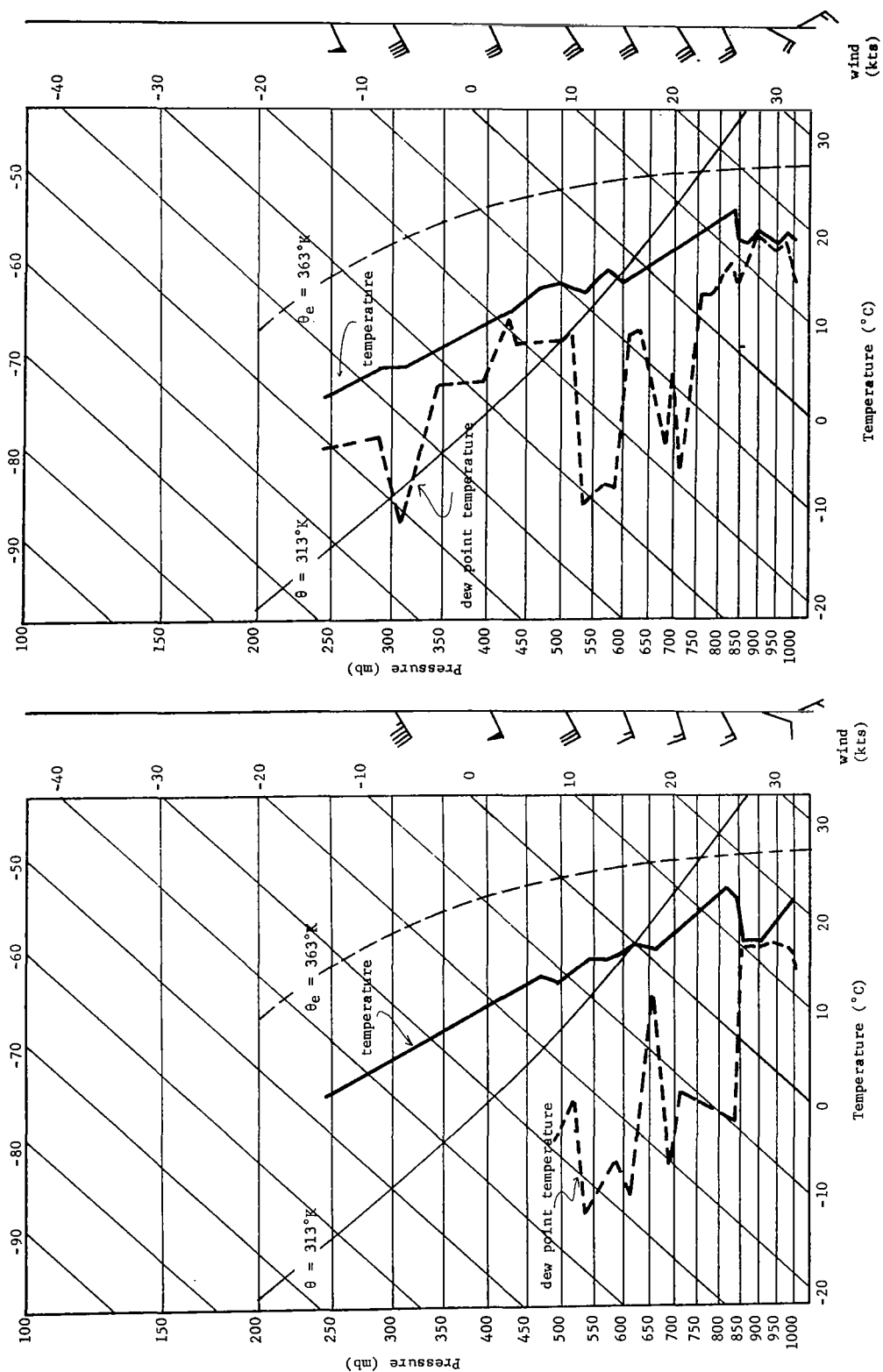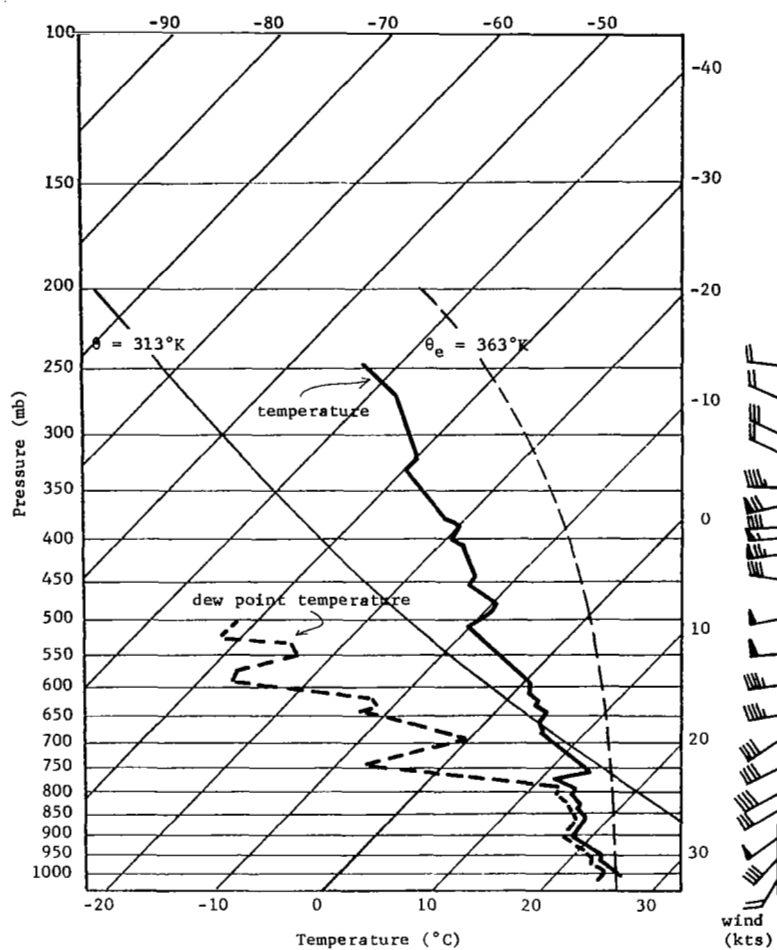
(c)   1200 GMT, 12 May 1974.

Fig. 51.   (Continued)

potential instability and result in severe convection.

b. Interrelationships between selected parameters and convective storms

From the relationships between synoptic-scale parameters and observed convection previously determined, it was clear that the spatial distribution of one particular parameter was not completely accurate in outlining all areas of convection.

1. Potential instability and vertical motion

Physically, an accurate measurement of potential instability in combination with the releasing mechanism (upward vertical motion), should accurately delineate areas of convection. As stated earlier, other authors also have found upward vertical motion in the lower troposphere and potential instability as important parameters in the formation of convection.

To examine the relationship between these two parameters and convection, the TTI was used as an indicator of air mass stability. Vertical motion in the lower troposphere (below 600 mb) was calculated on the 308°K isentropic surface by considering the average movement of the surface over a 3-h period as well as the air motion up or down the surface (Overall and Scoggins, 1975). For all nine time periods of the experiment, radar areas of convection were compared with the TTI and vertical motion fields and the results are shown in Fig. 52. Since the vertical motion and TTI fields were objectively calculated on a grid with spacing of about 160 km, radar observations of convection were associated with grid points if an echo was observed within 80 km of the grid point.

Figure 52 shows that the probability of convection increases with TTI values up to about 50, then decreases for higher values. Also, the probability of convection is greater by a factor of 4 when vertical motion is positive rather than negative. Moreover, when vertical motion < -2 cm s^{-1} the probability of convection is very small, regardless of stability.

The limited usefulness of stability indexes, when used alone to determine the presence of convection, is illustrated in Fig. 52. When conditions are most favorable for convection, use of the TTI
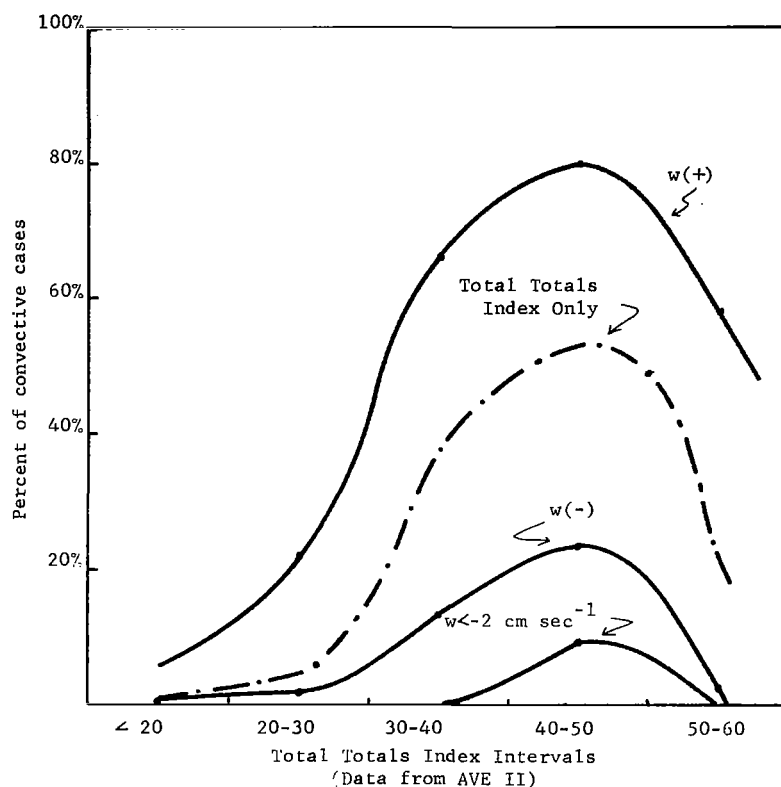
Fig. 52. Relationship between TTI and vertical motion
on 308°K potential temperature surface and
radar-observed convective activity.

alone correctly indicates the presence of convection in only about 50%
of the cases. But, this percentage varies between 20 and 80 by consider-
ation of only the sign of vertical motion, and this range is further
increased when the magnitude of vertical motion is considered.

The decrease in the probability of convection with increasing TTI
> 50, regardless of the sign and magnitude of vertical motion, is most
likely due to the interaction of systems of different scale and the
rapidity and extent of vertical mixing when the atmosphere is highly
potentially unstable. A typical sounding in a high TTI area was similar
to the Type I tornado sounding (Miller, 1967) with a strong subsidence
inversion between 850 and 700 mb capping the moist, potentially unstable
air below the inversion, and a nearly dry-adiabatic lapse rate above to
about 500 mb creating the large difference in temperature between 850 and
500 mb. While only the presence of convection and not its intensity was

considered here, observations in AVE II indicate that generally the heights of the tops of convective clouds and their severity continue to increase with higher TTI values but the areal coverage is reduced.

2. Potential instability, average boundary layer relative humidity, and combined surface and boundary layer moisture convergence

By combining particular values of synoptic-scale parameters that correlated best in space with observed convection, it was possible to graphically outline areas which contained convective activity.

Previously it was shown that convection tended to occur where $\overline{\overline{RH}}_{SFC - 850 mb} \geq 70\%$. Also, KI ≥ 22 were shown to have a better correlation with convection than critical values of LI and TTI. Moreover, negative values of both surface and boundary layer moisture divergence correlated well with convective activity.

Figure 53 shows the relation between graphically determined areas of the above parameters and convective activity at 1800 GMT and 0600 GMT. The light shaded regions are the areas where KI ≥ 22, $\overline{\overline{RH}}_{SFC - 850 mb}$ $\geq 70\%$, and either surface or boundary layer moisture divergence was negative.

This technique was particularly successful in outlining areas where MDR ≥ 4 and thunderstorms were likely while some small areas of shower activity, especially behind the cold front, were not accurately delineated. Therefore, it appears that thunderstorms form within the large scale synoptic field in areas where the boundary layer is moist, the low and middle troposphere is potentially and convectively unstable, and wind convergence and positive moisture advection is occurring within the boundary layer.

c. Variability of parameters associated with convective activity

Previous sections have established the parameters or combinations of parameters that correlated best with areas of convection. The three-dimensional distribution of the parameters then constitutes the atmospheric structure in convective storm areas. Since normal rawinsonde measurements are made at 12-h intervals, forecasts of convection are based upon expected changes in the synoptic-scale structure. Therefore, knowledge
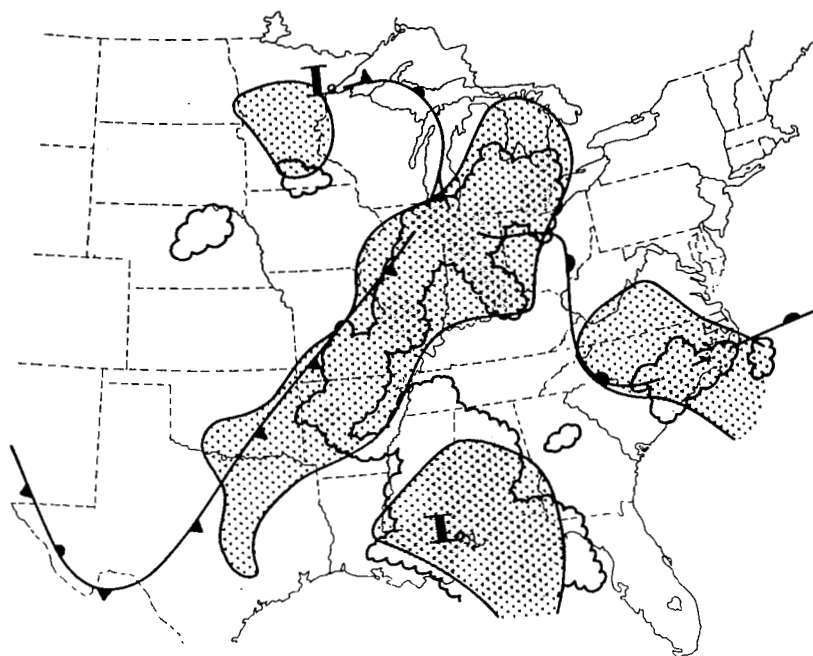
(a)   1800 GMT, 11 May 1974.
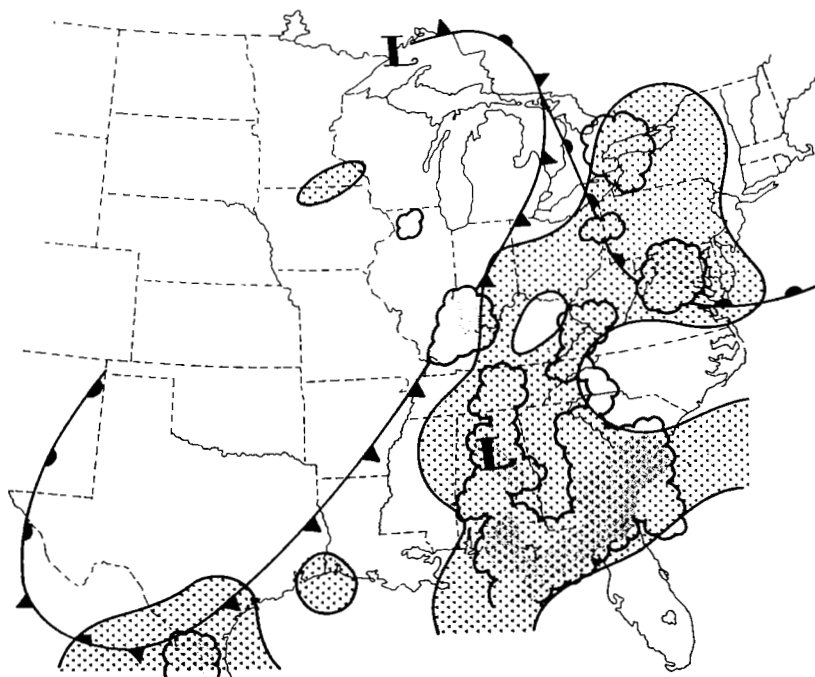
(b)   0600 GMT, 12 May 1974.

Fig. 53.   Graphically determined fields (shaded areas) of
$\overline{RH}_{SFC-850\ mb} > 70\%$, KI > 22, and negative moisture
divergence either at the surface or in the boundary
layer.   (Superimposed are surface frontal positions
and radar-observed convection).

of the variability of parameters associated with atmospheric structure in areas of convection over periods shorter than 12 h is essential for good forecasting. Both the variability of the large-scale synoptic structure and subsynoptic-scale features were examined in this study.

1. **Charts at 3-h intervals**

The previous relationship between synoptic-scale parameters and convection was established using two time periods, 1800 GMT and 0600 GMT, which are separated by the normal 12-h time interval. In comparing the movements of both the large-scale synoptic structure (lows, highs, and frontal zones) and the subsynoptic-scale features, it is clear that large changes in parameters associated with convection occurred during the 12-h period. The AVE II 3-h rawinsonde data was used to establish the variability and structure of particular synoptic-scale parameters between the two times of 1800 GMT and 0600 GMT.

Figures 54 through 57 show the fields of $\overline{RH}_{850 - 700 \text{ mb}}$, KI, D_{MBL}, and vertical motion at 700 mb at 3-h intervals for 2100 GMT, 11 May 1974, and 0000 GMT and 0300 GMT, 12 May 1974. These charts give a qualitative estimate of the variability of parameters that correlated well with convection over periods from 3 to 12 h. In particular, the 3-h charts show the consistent movement of many subsynoptic-scale features of high humidity, potential instability, negative D_{MBL} and upward vertical motion at 700 mb that correlated well with the observed convection. The development and movement of these smaller features help explain the very different patterns and locations of convection that were observed at 1800 GMT and 0600 GMT. This is especially true along the frontal zones where convection had almost disappeared by 0600 GMT, and over the southeast U.S. where a strong line of thunderstorms developed at 0600 GMT. In addition, the time and space continuity of many of the subsynoptic-scale features or centers from one 3-h period to the next gives credibility to the theory that these features are important in the delineation and forecasting of convective systems.

2. **3-h and 12-h changes in TTI**

Objectively analyzed fields of the TTI at 1200 GMT and 1500 GMT on 11 May, and 0000 GMT on 12 May 1974 are presented in Fig. 58. Areas of convection at these times are indicated by the darker shading on each
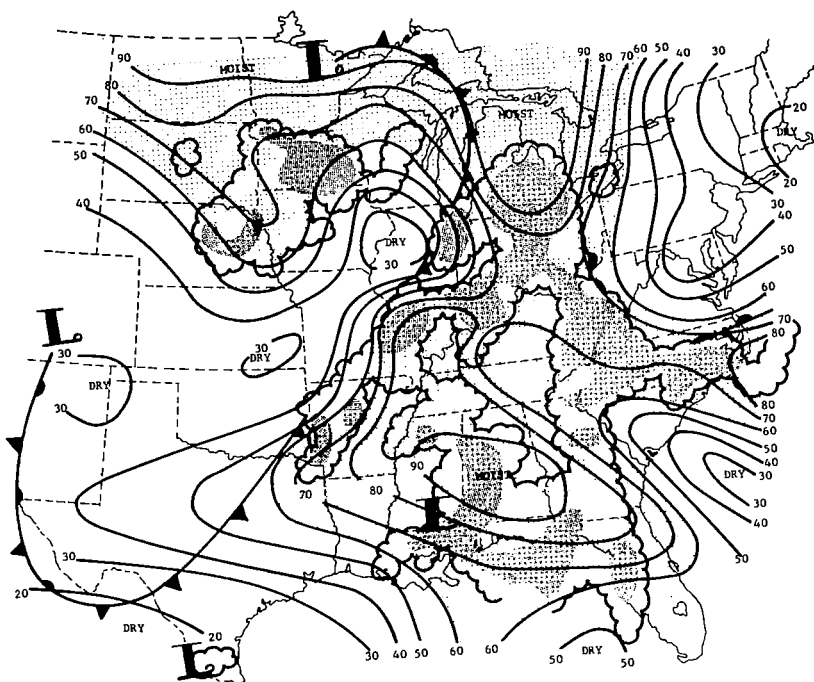
(a) 2100 GMT, 11 May 1974.

Fig. 54. Analyses of average relative humidity between 850 mb and 700 mb at consecutive 3-h intervals. (Superimposed are surface frontal positions and radar-observed convection with $\overline{RH}_{850-700} > 60\%$ lightly shaded).
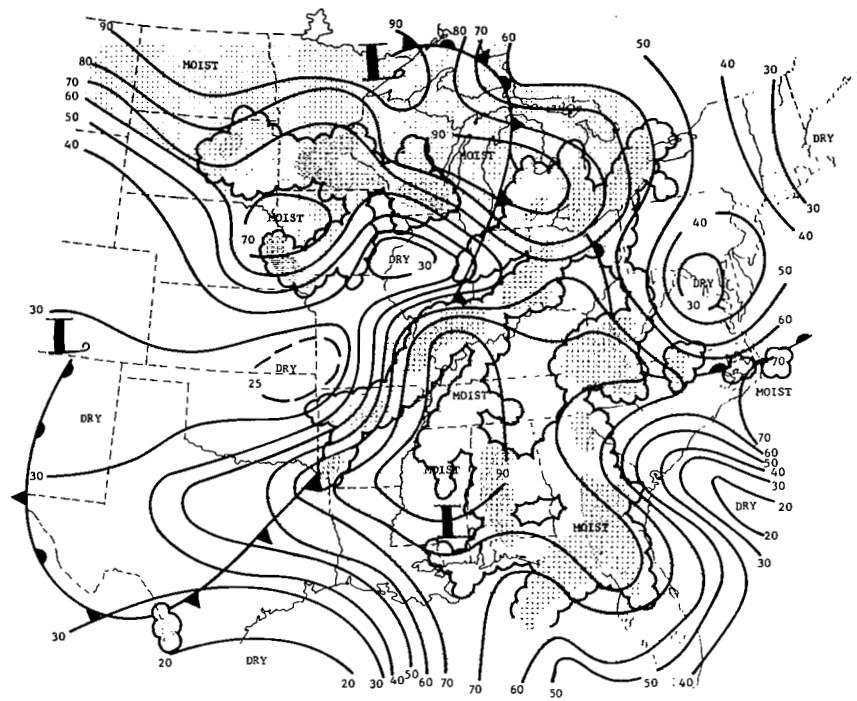
(b) 0000 GMT, 12 May 1974.
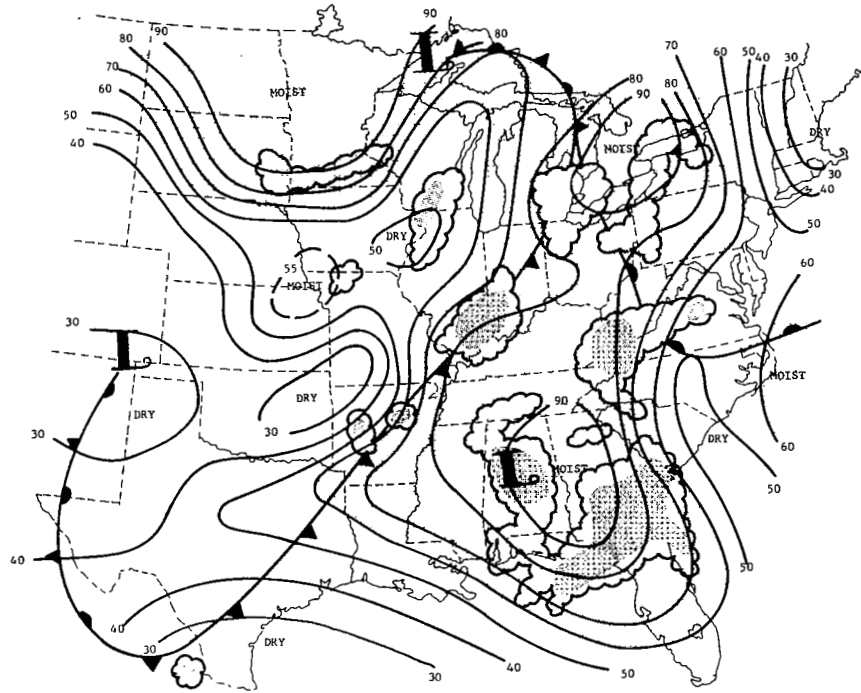
(c) 0300 GMT, 12 May 1974.

Fig. 54. (Continued)
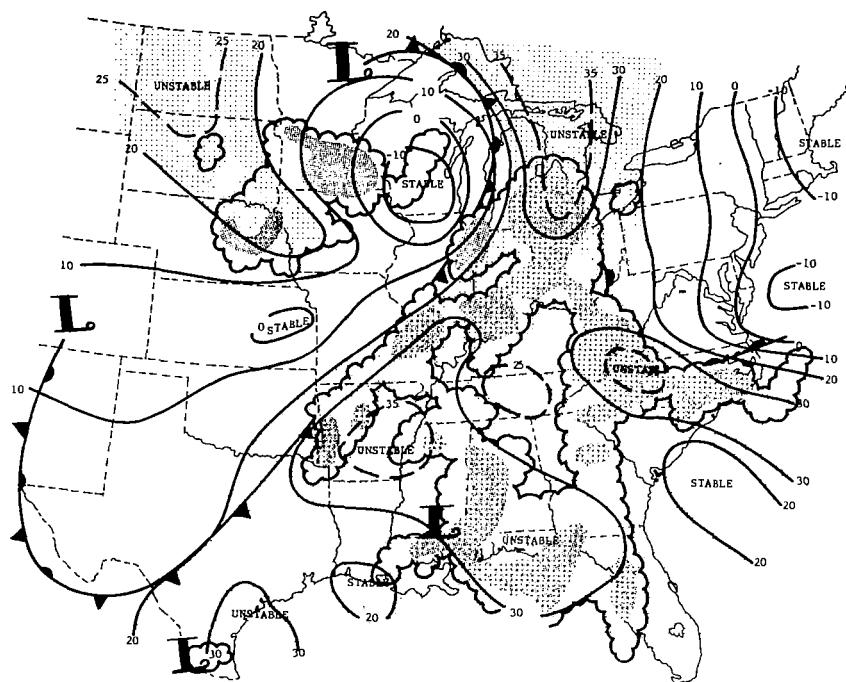
(a)   2100 GMT, 11 May 1974.

Fig. 55.   Analyses of the KI at consecutive
3-h intervals. (Superimposed are
surface frontal positions and radar-
observed convection with KI values
> 20 lightly shaded).

94
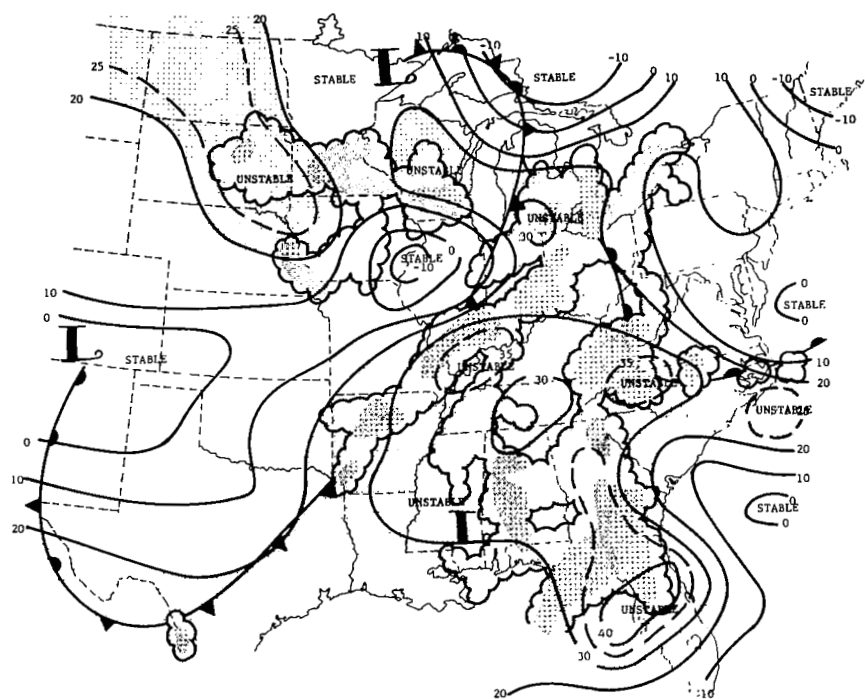
(b)   0000 GMT, 12 May 1974.
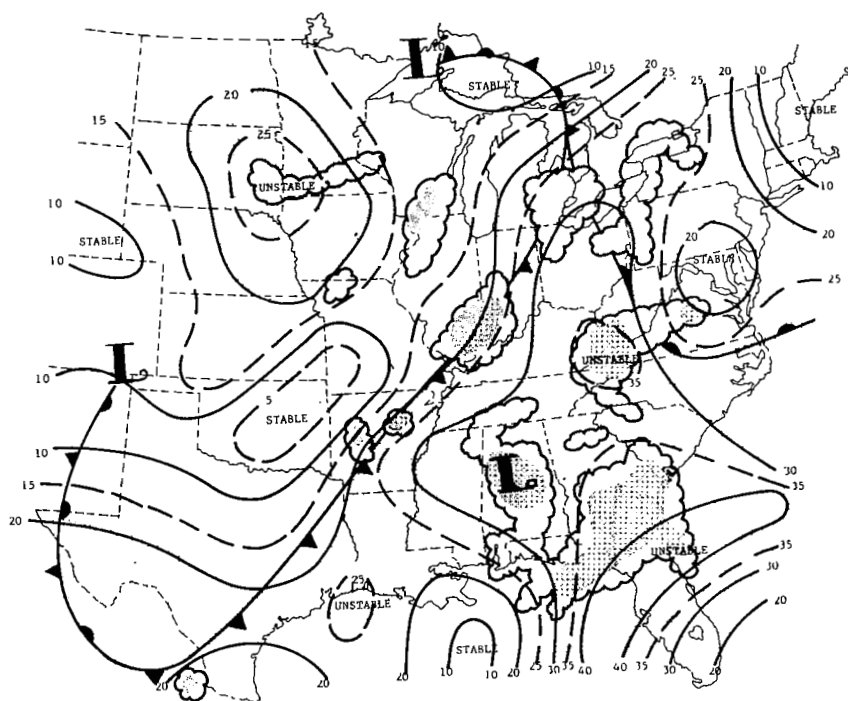
(c)   0300 GMT, 12 May 1974.

Fig. 55.   (Continued)
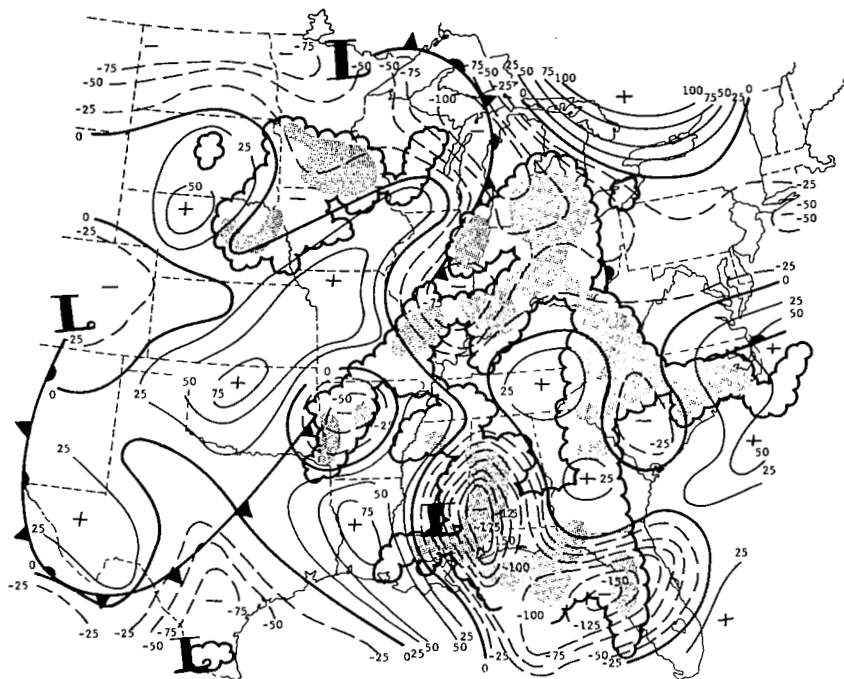
(a)   2100 GMT, 11 May 1974.

Fig. 56.   Analyses of boundary layer moisture
divergence (10^{-4} °K s^{-1}) at consecutive
3-h intervals.   (Superimposed are
surface frontal positions and radar-
observed convection).

96
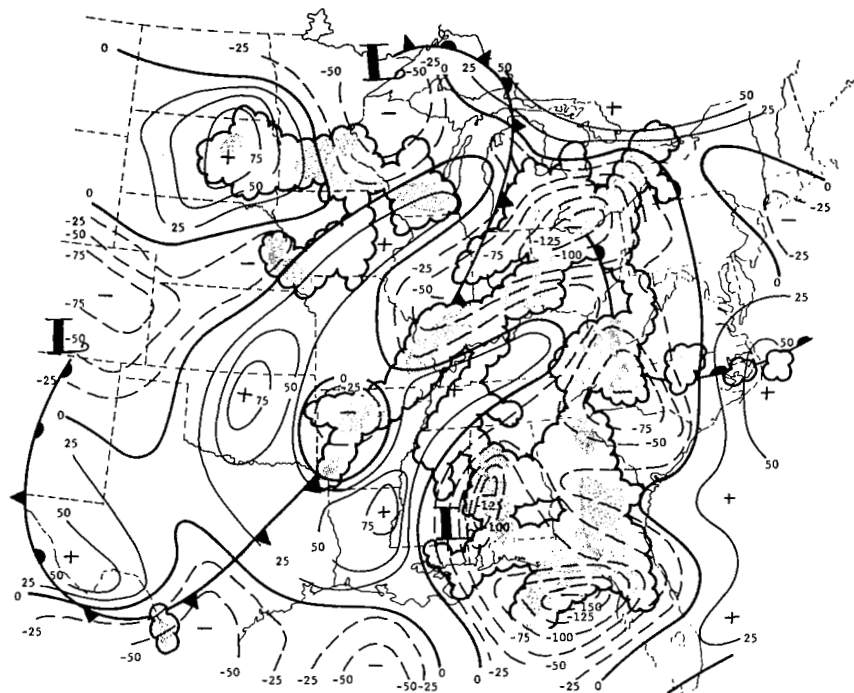
(b)   0000 GMT, 12 May 1974.

(c)   0300 GMT, 12 May 1974.

Fig. 56.   (Continued)
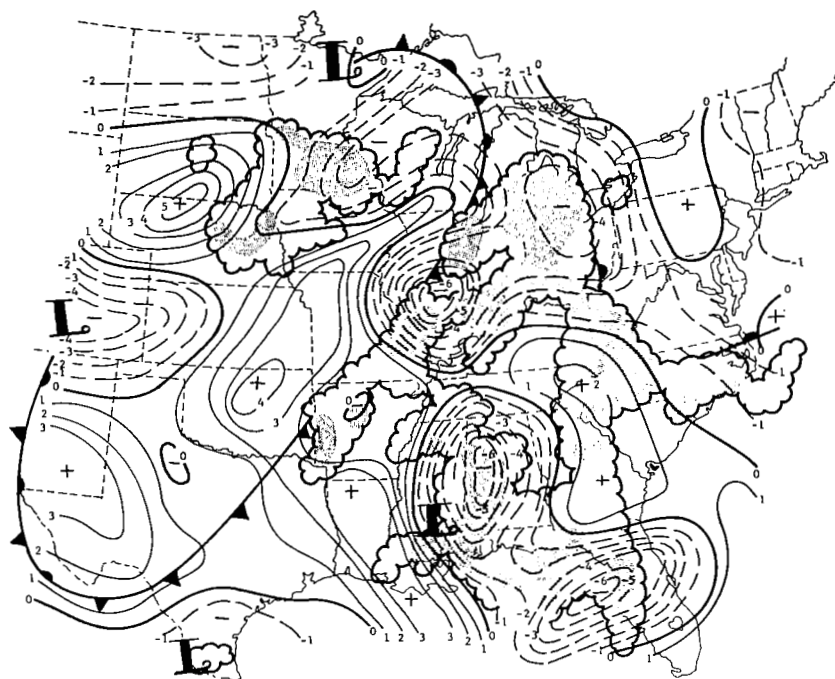
(a)   2100 GMT, 11 May 1974.

Fig. 57.   Analyses of vertical velocity (μbar s^{-1}) at
consecutive 3-h intervals at 700 mb.
(Superimposed are surface frontal positions
and radar-observed convection).
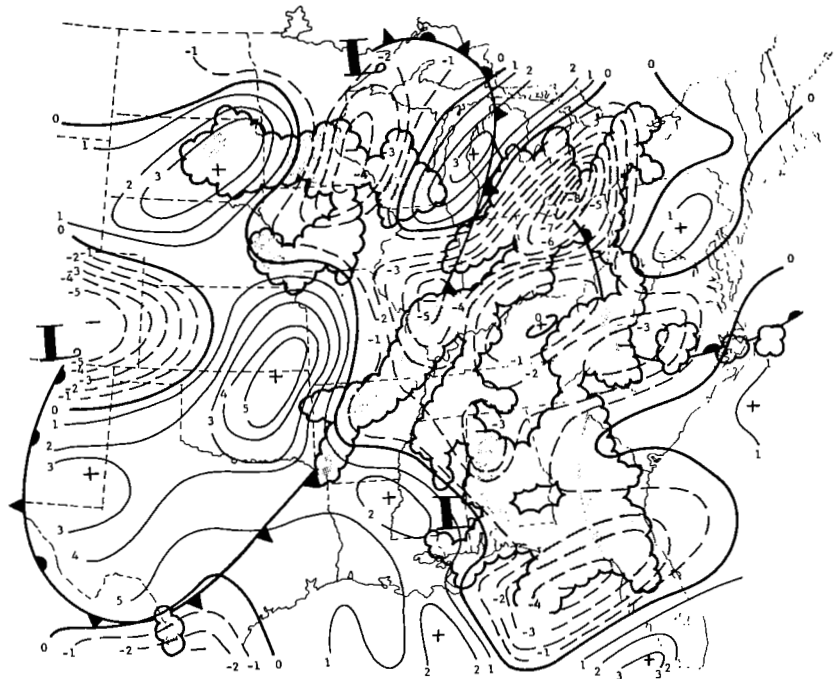
(b) 0000 GMT, 12 May 1974.
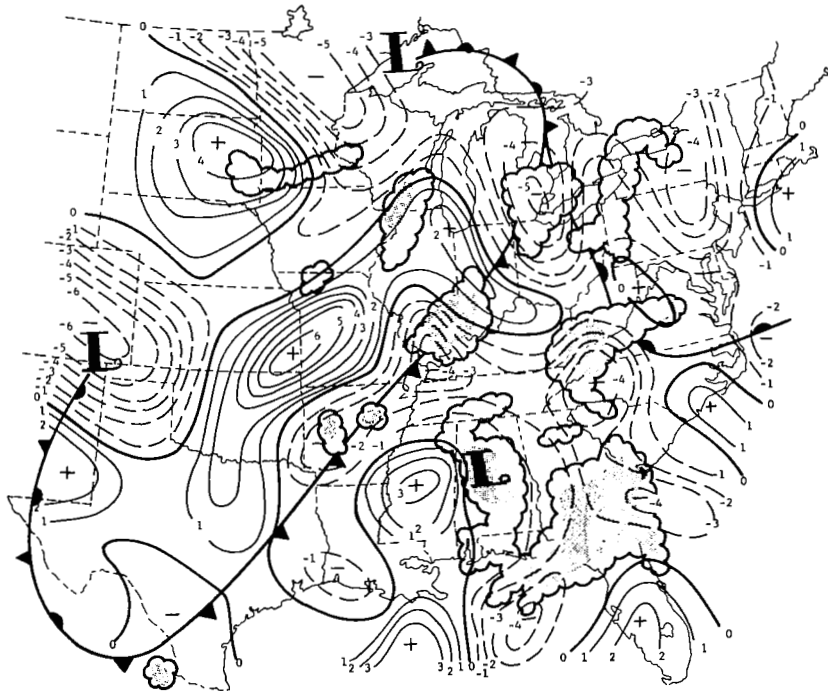
(c) 0300 GMT, 12 May 1974.

Fig. 57. (Continued)
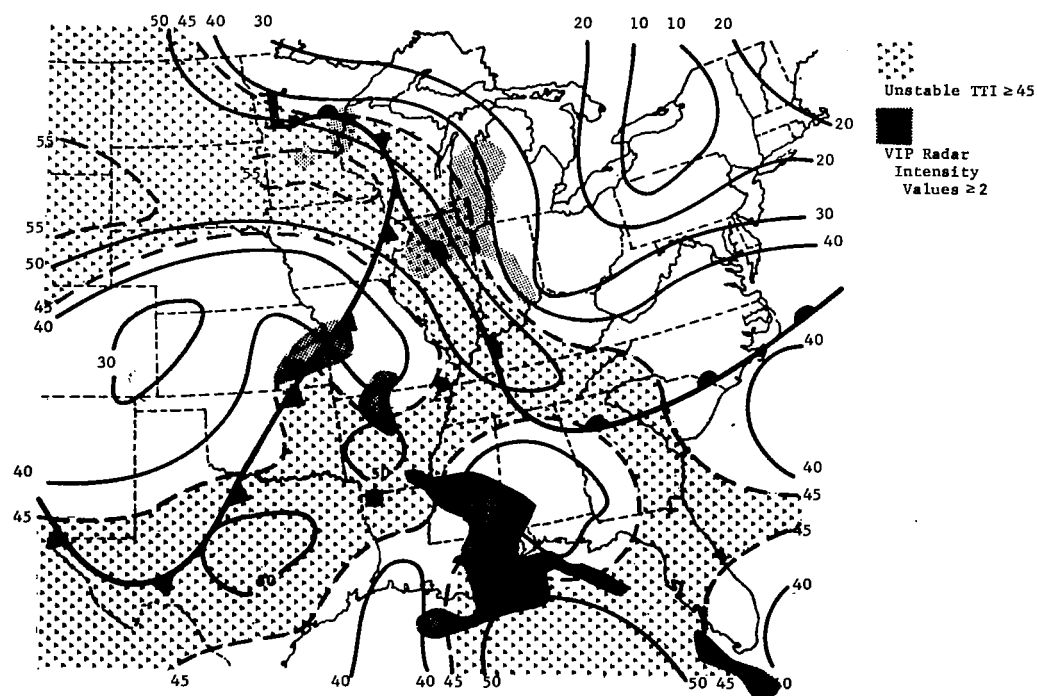
(a)   1200 GMT, 11 May 1974.
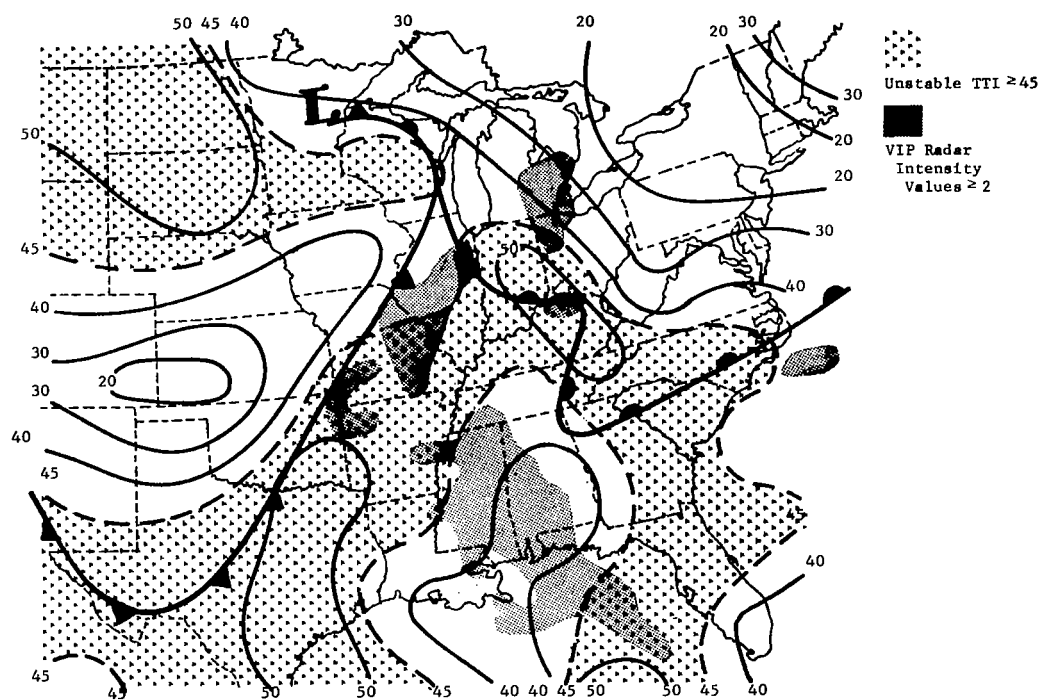
(b)   1500 GMT, 11 May 1974.

Fig. 58.   Objectively analyzed fields of TTI.
          (Superimposed are surface frontal positions).
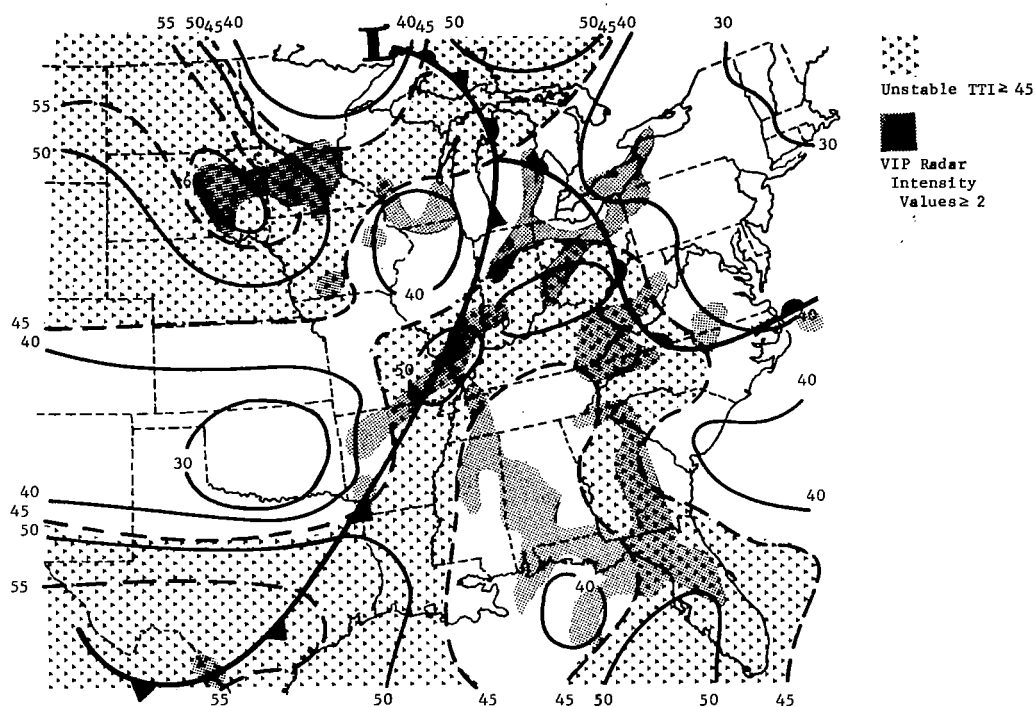
(c)   0000 GMT, 12 May 1974.

Fig. 58.   (Continued)

chart, and were determined from digital radar data in which MDR $\geq$ 2.
Unstable areas where TTI $\geq$ 45 are indicated by the lighter shading.

To compare the changes in stability that occur over 3- and 12-h
time periods, Fig. 59 shows objectively-analyzed fields of 3- and 12-h
changes in TTI that were computed from the TTI fields in Fig. 58.
Areas of convection and frontal positions appear on each time change
chart for the end of the time period.

While the magnitude of the largest change in TTI values over the
12-h period exceeded that of the 3-h period, the general spatial distri-
bution of the 3-h changes was similar to that observed over the 12-h
period.   In addition, well-defined centers of increasing or decreasing
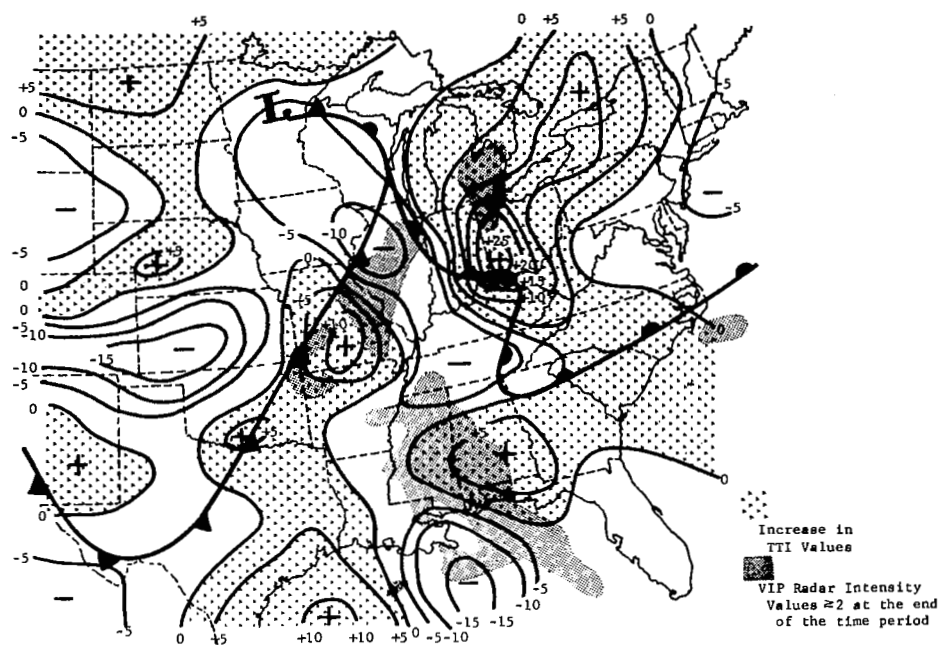
(a)   3-h change between 1200 GMT and
      1500 GMT, 11 May 1974.
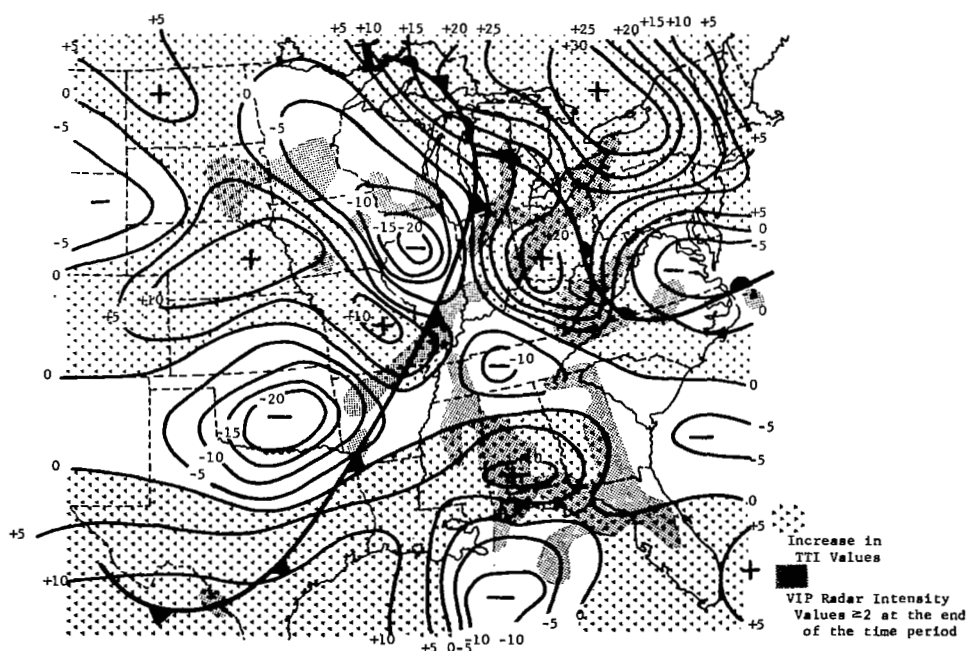
(b)   12-h change between 1200 GMT, 11 May
      and 0000 GMT, 12 May 1974.

Fig. 59.   Time changes in TTI determined from charts
           in Fig. 58. (Superimposed are surface frontal
           positions for the end of the time change period).

stability appear in the fields with the magnitude of some 3-h changes
exceeding the 12-h changes. These large changes in TTI values over the
3-h period indicate the extreme variability of the atmosphere not
measured with 12-h rawinsonde data. Also, the well-defined centers of
stability change, along with the observed convection, suggest the
presence of subsynoptic-scale features or systems, moving within the
large-scale synoptic field, that create the large variability over a
period of 3 h.

3. Variability of some basic synoptic-scale parameters over
3, 6, 9, and 12 h

To measure the variability of some basic rawinsonde parameters over
all the nine time periods of AVE II, cumulative frequency distributions
of changes in these parameters were computed and plotted for intervals of
3, 6, 9, and 12 h. An example of the results for stability measurement
is shown in Fig. 60 using the TTI.
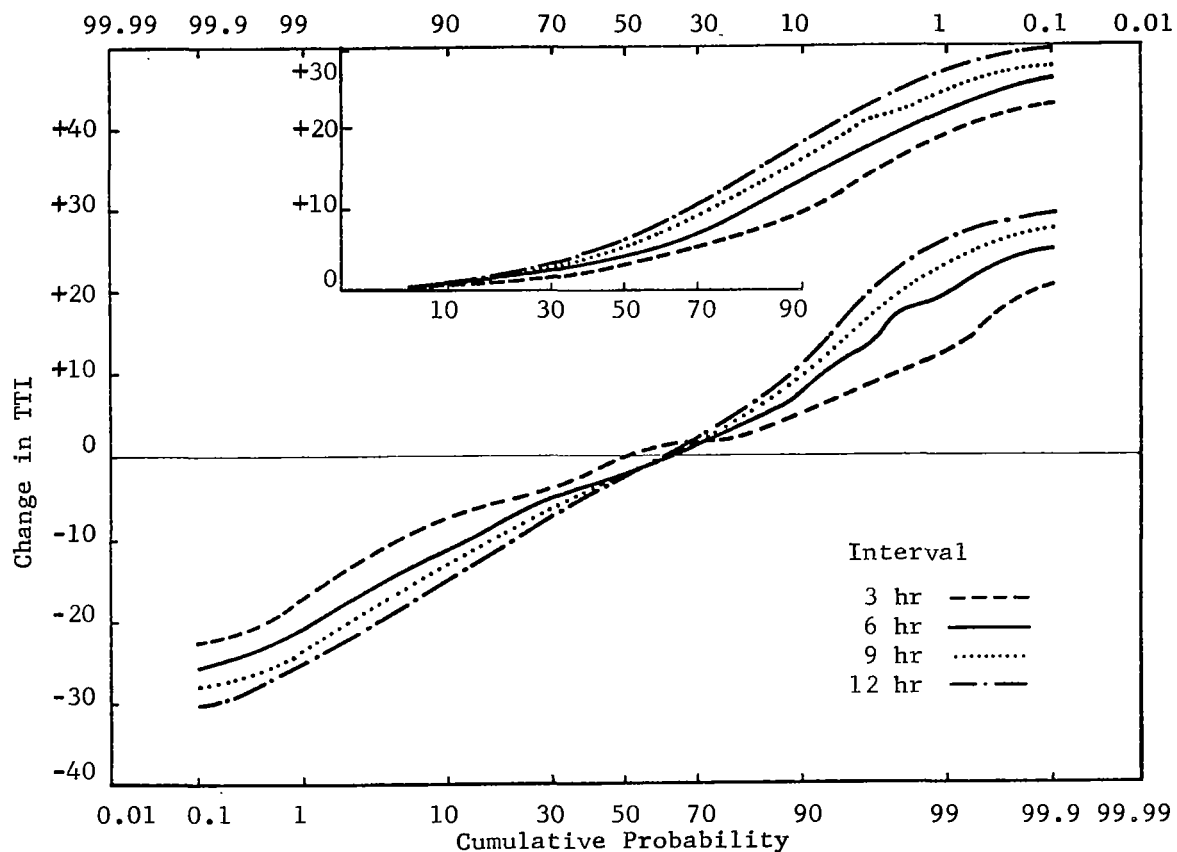
Fig. 60. Cumulative frequency distributions of
changes in TTI in AVE II.

The cumulative frequency distributions were computed from the nine objectively analyzed fields of a particular parameter by calculating all possible combinations of 3-, 6-, 9-, and 12-h change fields. Then grid point values in the time change fields were used to compute each cumulative frequency distribution.

The two sets of four curves give the probability of occurrence for either a certain magnitude change (upper curves) or a plus-or-minus change (lower curves) for the 3-, 6-, 9-, and 12-h time intervals. Both sets of curves indicate that, for all probability values, more than 50% of the total changes in TTI values occurred during a 3-h interval while the largest changes still existed over a 12-h period. For example, during AVE II, 10% of the magnitude changes in TTI exceeded 10 index values over a 3-h period while 10% of the magnitude changes exceeded only 16 index values over a 12-h period. Therefore, almost 2/3 of the change occurred over a 3-h period. In addition, the lower curves show that approximately 60% of the changes in TTI for all time change intervals were negative so that, during the AVE II experiment, the atmosphere was becoming more stable overall.

Table 1 contains values from the cumulative frequency distributions of changes in moisture, temperature, geopotential height, and vector wind for the 850- and 500-mb levels for 3-, 6-, 9-, and 12-h time intervals. Parameters calculated are listed in the left-hand column and the probability values for the four time intervals are listed along the top. Again, these data indicate that generally 30-60% of the total observed change in the basic parameters for a given probability level occurred over a 3-h period. This further suggests that subsynoptic-scale features or systems are responsible for the large variability of basic atmospheric parameters over periods of less than 12 h. In addition, direct measurement of this variability is lost between the 12-h synoptic rawinsonde runs and, therefore, not usually available for use in forecasting convection.

The importance of the short-period changes in parameters is illustrated in Fig. 52 when considered in light of the results which related vertical motion, stability, and observed convection. In Fig. 52, the probability of convection could change by a factor of 8 or

Table 1. Time changes for selected parameters and probability levels over 3-, 6-, 9-, and 12-h periods during AVE II.

% LEVEL	1%				5%				16%				50%				84%				95%				99%			
PARAMETER	3	6	9	12	3	6	9	12	3	6	9	12	3	6	9	12	3	6	9	12	3	6	9	12	3	6	9	12
Time change in mixing ratio at 850 mb	-6	-8	-9	-9	-3	-4	-6	-6	-1	-2	-3	-4	-1	-1	-1	-1	+1	+2	+2	+3	+2	+3	+4	+5	+4	+6	+7	+8
500 mb	-2.0	-2.5	-2.8	-3.2	-1.2	-1.8	-2.0	-2.3	-0.6	-0.9	-1.2	-1.5	0.0	-0.1	-0.2	-0.2	+0.4	+0.6	+0.7	+0.8	+1.0	+1.2	+1.6	+1.6	+1.8	+2.0	+2.4	+2.5
Time change in temperature at 850 mb	-4.0	-5.7	-7.0	-8.0	-2.3	-4.0	-5.3	-6.0	-1.6	-2.7	-4.0	-4.3	-0.2	-0.3	-1.0	-1.5	+1.0	+1.2	+1.7	+2.0	+2.0	+3.7	+4.2	+4.8	+4.0	+6.0	+6.9	+8.2
500 mb	-3.2	-5.5	-8.2	-9.8	-2.3	-3.5	-4.7	-6.8	-1.0	-2.0	-2.6	-3.6	0.0	-0.1	-0.2	-0.3	+0.8	+1.0	+1.5	+1.8	+1.8	+2.0	+2.7	+3.4	+2.7	+4.1	+5.0	+5.0
Time change in geopotential height at 850 mb	-35	-55	-70	-85	-25	-40	-60	-70	-15	-25	-40	-50	0.0	0.0	0.0	-5	+15	+20	+30	+40	+20	+35	+45	+55	+30	+40	+60	+80
500 mb	-60	-85	-125	-145	-40	-70	-100	-120	-25	-45	-65	-85	0.0	-5	-10	-15	+15	+20	+30	+35	+25	+35	+50	+65	+35	+50	+75	+85
Time change in magnitude of the vector wind at 850 mb	---	---	---	---	1.0	1.5	2.0	3.0	1.5	2.5	4.0	5.5	4.0	6.0	8.5	10.0	7.0	11.0	14.0	17.5	11.0	16.0	20.0	24.0	17.0	24.0	29.0	32.0
500 mb	---	---	---	---	1.0	2.0	3.0	4.0	2.0	4.0	5.0	6.0	4.0	7.0	9.0	11.0	7.0	11.0	16.0	17.0	11.0	16.0	22.0	26.0	17.0	24.0	30.0	34.0
Time change in Total Totals index. ± change	-17	-21	-24	-24	-11	-14	-16	-18	-6	-9	-10	-12	0.0	-2	-2	-2	+3	+5	+6	+8	+8	+12	+15	+17	+12	+19	+23	+26
absolute value change	---	---	---	.	.5	.5	.5	.5	1.0	1.2	1.5	1.5	3	4	5	6	8	11	13	15	13	16	20	21	19	22	24	27

more in just 3 h with large changes in either the TTI values or the
vertical fields or both.

d.   Analysis of a post-frontal area of convective storms

A moderately strong line of thunderstorms developed during AVE II
around 1800 GMT on 11 May behind the cold front in the north central
Plains States.   In association with this area of convection, an isolated
center of unstable air was indicated by the TTI at 0000 GMT on 12 May
(Fig. 58), and a strong 12-h increase in TTI was measured from 1200 GMT
on 11 May to 0000 GMT on 12 May (Fig. 59).   This system was studied in
detail using the 3-h rawinsonde data to determine what combination of
changes in the structure of the atmosphere occurred as the convective
system developed and moved eastward.   Therefore, both the variability
and structure of synoptic-scale parameters associated with convection
were combined in studying this subsynoptic- or convective-scale system.

The surface analysis at 2100 GMT on 11 May (Fig. 61) shows a well-
defined pressure trough behind the cold front extending from north-
western Kansas northeastward into Minnesota.   The observed convection
at 2200 GMT on 11 May is shown in Fig. 62.   To establish the variability
and structure of the atmosphere resulting from this convective area,
time cross-sections of various parameters associated with convection
were analyzed using the nine time periods of the experiment.   Omaha,
Nebraska was used since the system passed over the station around 2200
GMT.

Figure 63 shows nine consecutive temperature soundings at Omaha.
A well-defined frontal zone and tropopause is established and other
stable layers are trackable in time using potential temperature surfaces.
Large fluctuations in the position of the frontal zone and tropopause
occur during the experiment as the tropopause appears to subside into
the frontal zone while the convective system passes over the station
around 2200 GMT on 11 May.

The time cross section containing wind and isotach analysis, dew-
point depression, and TTI is shown in Fig. 64.   Figure 65 contains the
vertical motion calculated from Eqs. 17 and 18 for the same cross
section.   From 1200 GMT to 1800 GMT on 11 May subsidence is indicated
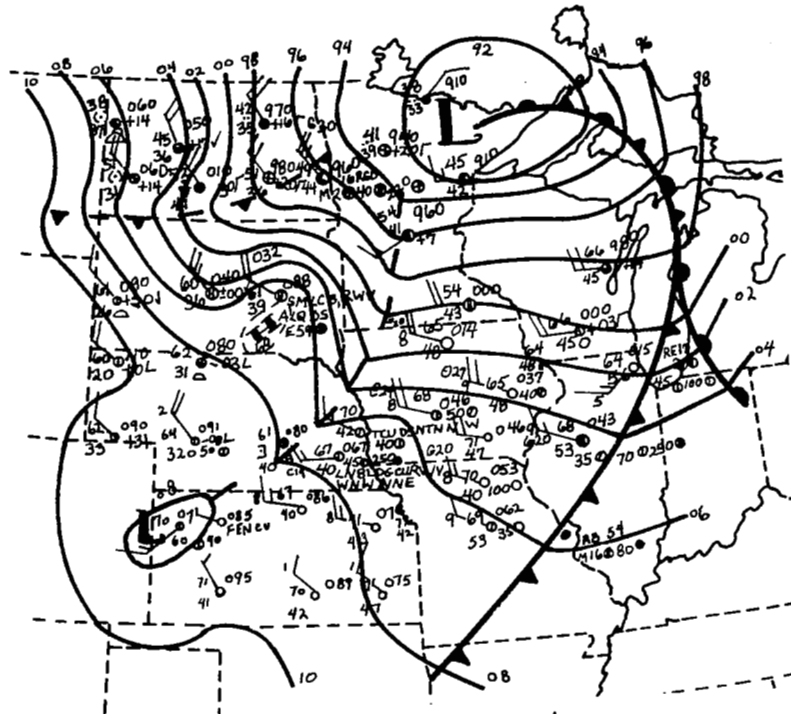
Fig. 61. Surface analysis at 2100 GMT, 11 May
1974.
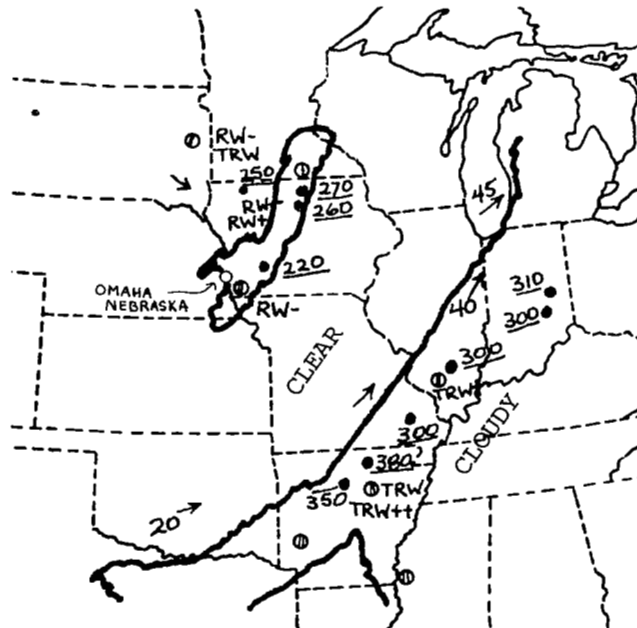
Fig. 62. Satellite and radar composite at
2200 GMT, 11 May 1974.
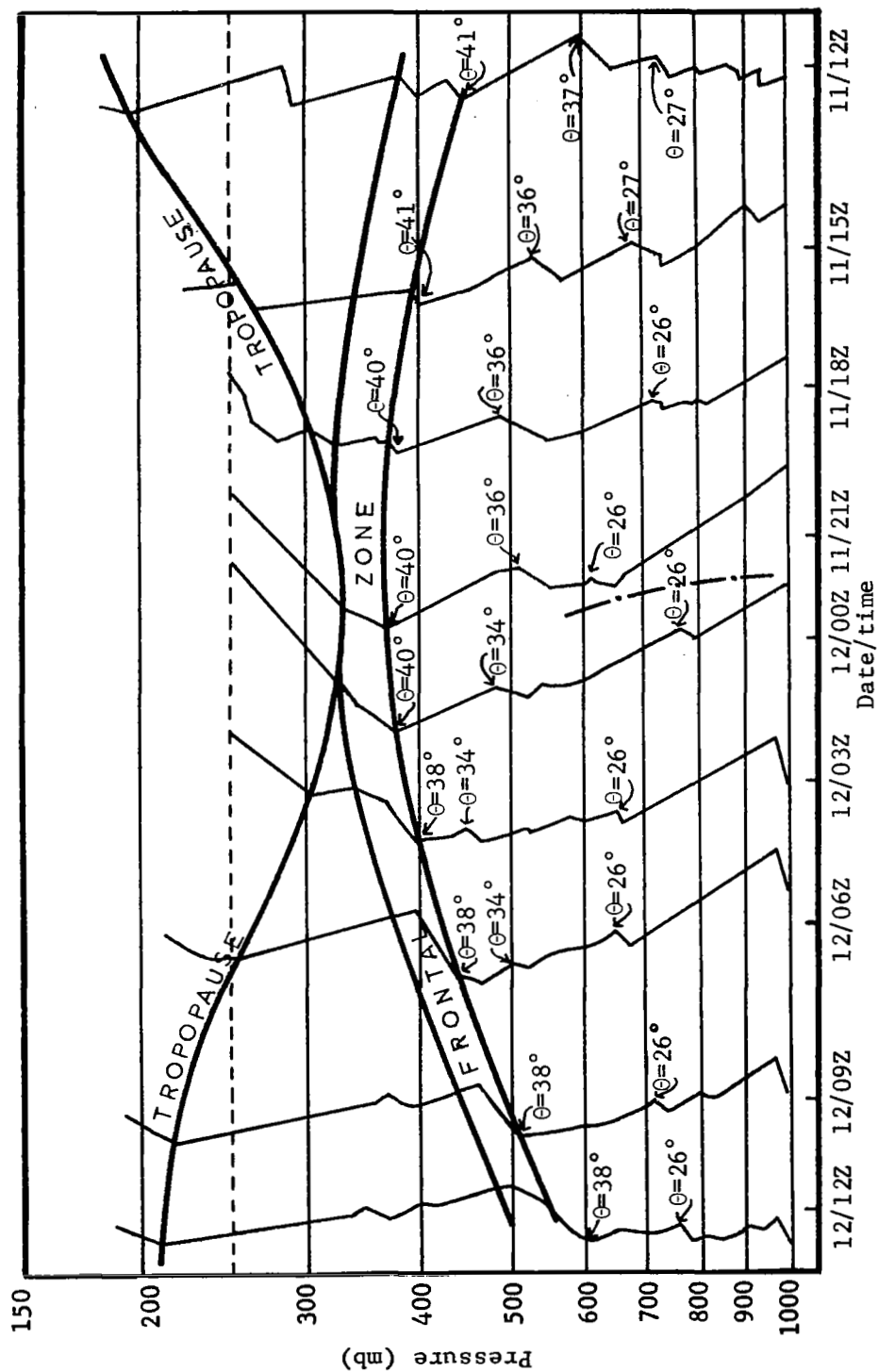
Fig. 63. Consecutive temperature soundings at Omaha, Nebraska on 11 and 12 May 1974.
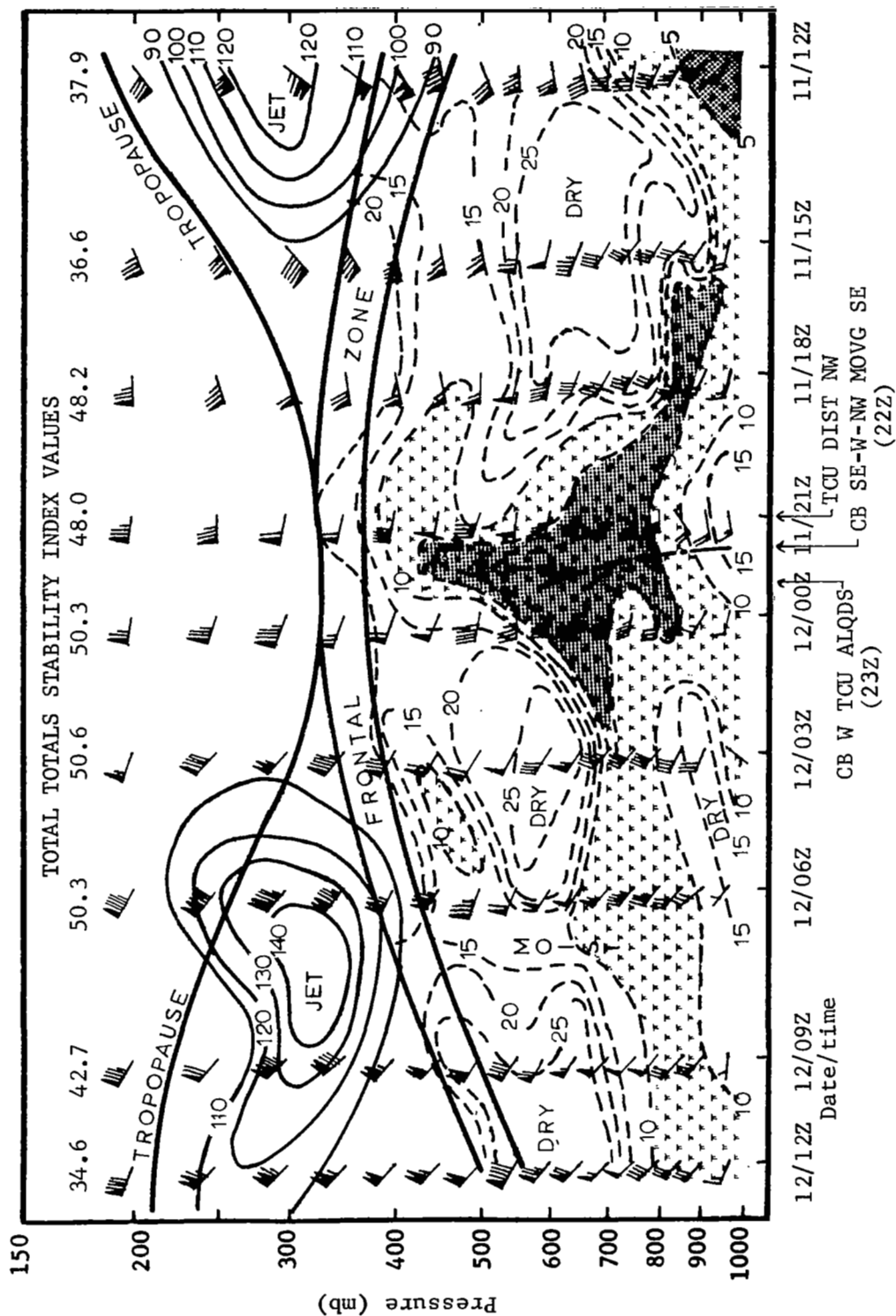
Fig. 64. Time cross-section of dew point depression and wind for
Omaha, Nebraska on 11 and 12 May 1974.
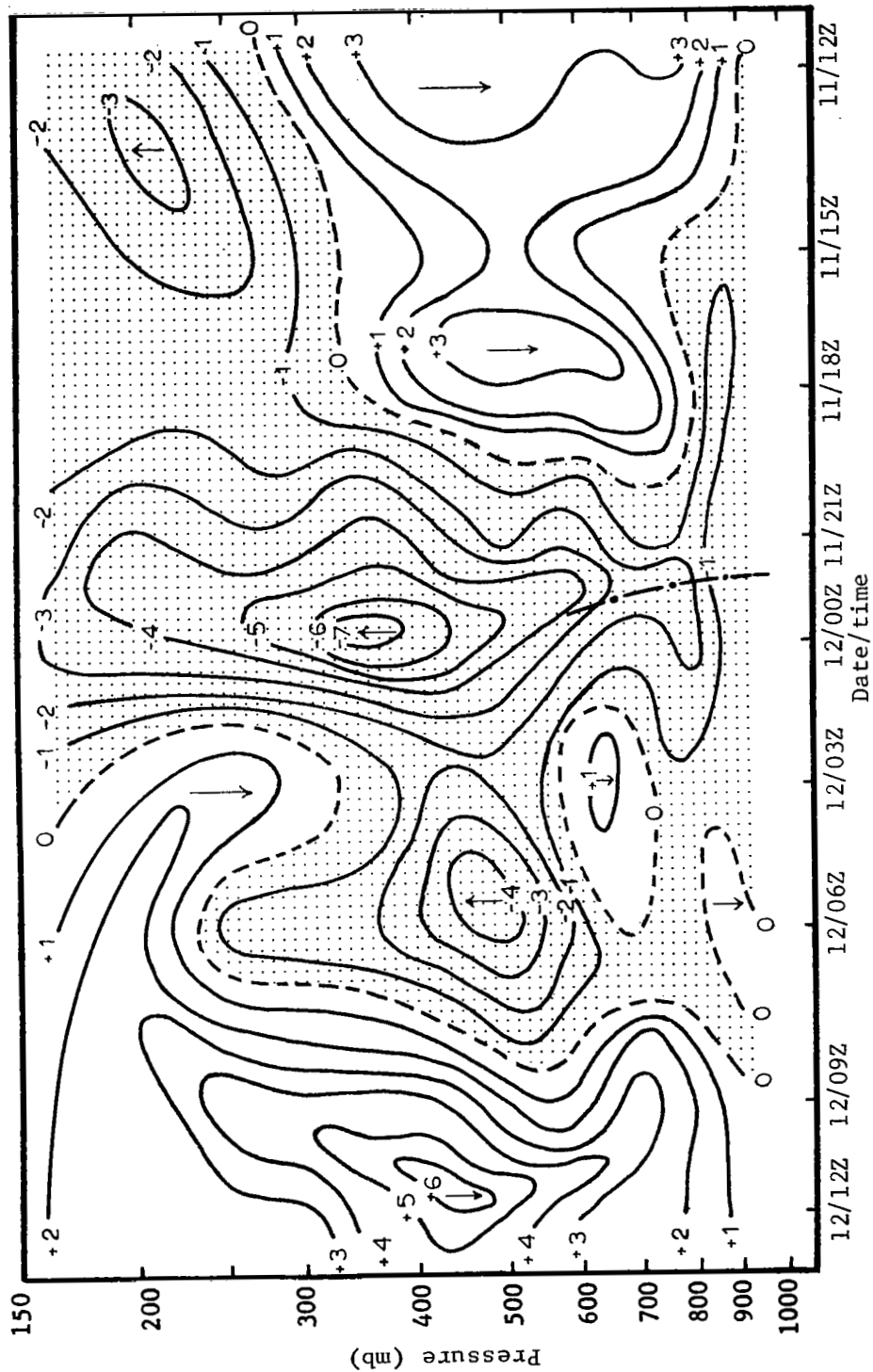
Fig. 65. Time cross-section of vertical motion (μbars s^{-1}) for Omaha, Nebraska on 11 and 12 May 1974.

under the frontal zone and dry air is present, producing a decreasing TTI. The polar jet also appears between the tropopause and frontal zone. Strong increases in moisture in the mid-troposphere occur between 2100 GMT on 11 May and 0000 GMT on 12 May as the convective system passed. Backing winds between 1800 GMT and 2100 GMT on 11 May signaled the approach of the pressure trough and strong positive vertical motion which, in combination with unstable air indicated by the TTI values, released the potential instability and produced convection. Subsidence followed at 0300 GMT on 12 May and the air dried but another weaker system (also seen in Fig. 44), containing no weather, developed and passed Omaha around 0600 GMT on 12 May. A center of upward vertical motion and higher moisture developed with the weaker system. From 0900 GMT to 1200 GMT on 12 May, the polar jet is seen again as the tropopause separated from the frontal zone and strong subsidence dried the air again under the frontal zone.

The analysis of this convective system substantiates the previous statements that *subsynoptic-scale systems, moving within the large-scale synoptic field, are important in both releasing potential instability and producing the large variability of parameters associated with convection over time intervals shorter than 12 h.*

6. SUMMARY AND CONCLUSIONS

a. Summary

An objective analysis of the structure and variability of the atmosphere relative to radar-observed convection has been carried out using the 3-h AVE II rawinsonde data, surface data, and manually digitized radar data. The analysis of moisture, vector wind, divergence of the wind, vertical motion, moisture divergence, and stability was accomplished using data of unique accuracy and sampling interval. These analyses were then compared to the radar-observed convection to determine the interrelationships between synoptic-scale parameters and convective-scale systems. The variability of synoptic-scale parameters was also computed over 3-, 6-, 9-, and 12-h periods, and a particular example of convection formation was analyzed to show the time changes in atmospheric structure that occur in convection areas over time intervals less than 12 h.

b. Conclusions

The following conclusions were reached for the 24 h AVE II experiment:

1. Moisture and convective storms

Usually surface dew point temperature exceeded 50°F and the mean relative humidity from the surface to 500 mb exceeded 60% in areas of convective activity. In addition, the boundary layer and lower troposphere (below 700 mb) are usually moist in areas of convective storms so that $\overline{RH}_{SFC - 850 \text{ mb}}$ and $\overline{RH}_{850 - 700 \text{ mb}}$ values > 70% and > 60%, respectively, occur in areas of convective activity.

2. Stability and convective storms

The stability index alone is only a fair indicator of convective activity but the KI appears to be superior over the LI and TTI for identifying areas of convective storms. Also, the atmosphere is usually convectively unstable in the lower troposphere but severe convective activity is found in areas with values of $\dfrac{-\Delta \Theta_e}{\Delta p}$ exceeding about -15C/25 mb.

3. <u>Divergence of wind and moisture relative to convective storms</u>

Convective activity is usually found in areas of both wind and moisture convergence at the surface with **stronger** convective activity usually associated with stronger surface moisture convergence. Above the surface, convective activity is usually associated with both wind and moisture convergence in the lower troposphere while stronger convective activity is associated with stronger moisture convergence within the boundary layer. In addition, wind divergence in the middle and upper troposphere (above 700 mb) is usually found over areas of convective storms.

4. <u>Vertical motion and convective storms</u>

The magnitude and sign of terrain-induced vertical motion correlate poorly with areas of convective storms but upward vertical motion just above the surface, computed from both terrain-induced vertical motion and surface wind divergence, is usually found in areas of convective activity. Above the ground, convective storms are found in areas where upward vertical motion exists somewhere in the lower troposphere while above about 700 mb upward vertical motion is not a necessary condition for convective activity to form and maintain itself. In addition, convective storms form many times within upward vertical motion along a cold front or above a warm frontal surface, while strong convective activity occurs in areas where strong upward vertical velocity extends throughout the low and middle troposphere.

5. <u>Interrelationships between parameters and convective storms</u>

When a measure of potential instability and upward vertical motion in the lower troposphere is combined, areas of convective storms can be accurately delineated about 80% of the time when the atmosphere is unstable while the probability of convective activity is < 20%, independent of the potential instability, when subsidence is occurring in the lower troposphere. Also, areas of convective storms can be most accurately outlined by combining those areas in which the boundary layer is moist, the low and middle troposphere is potentially and convectively unstable, and moisture convergence is present either at the surface or within the boundary layer.

6.   Variability of parameters and convective storms

The variability of synoptic-scale parameters over periods from 3 to 12 h indicates that 30-60% of the total change observed in a parameter over a 12-h period occurs within a 3-h period. As a result, the large variability of potential instability and vertical motion can allow the probability of convective activity to change by a factor of 8 or more in 3 h. Accurate 3-h rawinsonde data can be used to identify and follow subsynoptic-scale systems that produce convective storms and sometimes create the large variability of the atmosphere over time periods as small as 3 h.

REFERENCES

Barnes, S. L., 1964: A technique for maximizing detail in numerical weather map analysis. J. Appl. Meteorol., 3, 396-409.

Barr, S., W. K. Widger, Jr., I. A. Miller, and R. Stanton, 1971: Objective subsynoptic upper level analysis. J. Appl. Meteorol., 10, 410-417.

Berkofsky, L., and E. A. Bertoni, 1955: Mean topographical charts of the entire earth. Bull. Amer. Meteor. Soc., 36, 350-354.

Bonner, W. D., R. M. Reap, and J. E. Kemper, 1971: Preliminary results on severe storm prediction by screening regression using forecast predictors. Preprints of Papers, Seventh Conf. on Severe Local Storms, Kansas City, 36-41.

Byers, H. R., 1959: General Meteorology. McGraw-Hill, New York, 144-192.

Charba, J. P., 1975: Operational scheme for short range forecasts of severe local weather. Preprints of Papers, Ninth Conf. on Severe Local Storms, Norman, 252-261.

Chien, H., and P. J. Smith, 1973: On the estimation of kinematic parameters in the atmosphere from rawinsonde wind data. Mon. Wea. Rev., 101, 252-261.

David, C. L., 1973: An objective method for estimating the probability of severe thunderstorms using predictors from the NMC (PE) numerical prediction model and from observed surface data. Preprints of Papers, Eighth Conf. on Severe Local Storms, Denver, 223-225.

Endlich, R. M., and R. L. Mancuso, 1968: Objective analysis of environmental conditions associated with severe thunderstorms and tornadoes. Mon. Wea. Rev., 96, 342-350.

Fankhauser, J. C., 1969: Convective processes resolved by a mesoscale rawinsonde network. J. Appl. Meteorol., 8, 778-798.

Foster, D. S., and R. M. Reap, 1973: Archiving of manually-digitized radar data, Techniques Development Laboratory Office Note 73-6, National Weather Service, Silver Springs, Md., 12 pp.

Fuelberg, H. E., 1974: Reduction and error analysis of the AVE II pilot experiment data. NASA CR-120496, NASA Marshall Space Flight Center, Huntsville, Alabama, 131 pp.

Galway, J. G., 1956: The lifted index as a predictor of latent instability. Bull. Amer. Meteor. Soc., 39, 574-582.

George, J. J., 1960: Weather Forecasting and Aeronautics, New York, Academic Press, 410-415.

Jarvis, E. C., and T. Agnew, 1970: A note on the computation of terrain and frictionally induced vertical velocities. J. Appl. Meteorol., 9, 942-946.

Kaplan, M. L., D. A. Paine, and N. J. Tetrick, 1973: The results of a mesoscale numerical prediction of the squall-line organizing the Palm Sunday Tornadoes. Preprints of Papers, Eighth Conf. on Severe Local Storms, Denver, 320-327.

Kung, E. C., 1973: Note on design of an optimized computation scheme for kinematic vertical motion fields. Mon. Wea. Rev., 101, 685-690.

Lewis, J. M., Y. Ogura, and L. Gidel, 1974: Large-scale influences upon the generation of a mesoscale disturbance. Mon. Wea. Rev., 102, 545-560.

Maddox, R. A., 1973: A severe thunderstorm surface potential index (SPOT). Preprints of Papers, Eighth Conf. on Severe Local Storms, Denver, 252-256.

Miller, R. C., 1967: Notes on analysis and severe-storm forecasting procedures of the Military Weather Warning Center. AWS Tech. Report 200, 94 pp.

Ninomiya, K., 1971: Mesoscale modification of synoptic situations from thunderstorm development as revealed by ATS III and aerological data. J. Appl. Meteorol., 10, 1103-1121.

O'Brien, J. J., 1970: Alternate solutions to the classical vertical velocity problem. J. Appl. Meteorol., 9, 197-203.

Ostby, F. P., 1975: An application of severe storm forecast techniques to the outbreak of June 8, 1974. Preprints of Papers, Ninth Conf. on Severe Local Storms, Norman, 7-12.

Overall, J. W., and J. R. Scoggins, 1975: Relationships between motion on isentropic surfaces from 3-h rawinsonde data and radar echoes. NASA CR-2558, NASA Marshall Space Flight Center, Huntsville, Alabama, 59 pp.

Palmén, E., and C. W. Newton, 1969: Atmospheric Circulation Systems. New York, Academic Press, 390-425.

Reap, R. M., 1975: Thunderstorm and severe weather probabilities based on model output statistics--No. 3, Technical Procedures Bulletin No. 138, National Weather Service, Silver Springs, Md., 4 pp.

_____, and D. S. Foster, 1975: New operational thunderstorm and severe storm probability forecast based upon model output statistics (MOS). _Preprints of Papers, Ninth Conf. on Severe Local Storms_, Norman, 58-63.

Reiter, E. R., 1963: _Jet-Stream Meteorology_. University of Chicago Press, p. 29.

Scoggins, J. R., and O. E. Smith, 1973: data for the first NASA atmospheric variability experiment (AVE I), Part I: Data tabulation. NASA TM X-2938, NASA Marshall Space Flight Center, Alabama, 681 pp.

_____, and R. E. Turner, 1975: 25-mb sounding data and synoptic charts for NASA's AVE II pilot experiment. NASA TN D-7832, Washington, D. C., 530 pp.

_____, and J. E. Wood, 1971: Factors in the formation and prediction of convective clouds and thunderstorms. _Preprints of Papers, Seventh Conf. on Severe Local Storms_, Kansas City, 110-117.

Smith, P. J., 1971: An analysis of kinematic vertical motions. _Mon. Wea. Rev._, _99_, 715-724.

APPENDIX I

Rawinsonde Stations Participating in AVE II Pilot Experiment

Station Identifier	Location
11001 (MSF)	Marshall Space Flight Center, Alabama
22001 (OUN)	Norman, Oklahoma
22002 (FSI)	Ft. Sill, Oklahoma
22003 (LNS)	Lindsay, Oklahoma
22004 (FTC)	Ft. Cobb, Oklahoma
22005 (CHK)	Chickasha, Oklahoma
201 (EYW)	Key West, Florida
202 (MIA)	Miami, Florida
208 (CHS)	Charleston, South Carolina
211 (TPA)	Tampa, Florida
213 (AYS)	Waycross, Georgia
221 (VPS)	Eglin AFB, Florida
226 (MGM)	Montgomery, Alabama
232 (BVE)	Boothville, Louisiana
235 (JAN)	Jackson, Mississippi
240 (LCH)	Lake Charles, Louisiana
248 (SHV)	Shreveport, Louisiana
250 (BRO)	Brownsville, Texas
255 (VCT)	Victoria, Texas
260 (SEP)	Stephenville, Texas
261 (DRT)	Del Rio, Texas
265 (MAF)	Midland, Texas
304 (HAT)	Hatteras, North Carolina
311 (AHN)	Athens, Georgia
317 (GSO)	Greensboro, North Carolina
327 (BNA)	Nashville, Tennessee
340 (LIT)	Little Rock, Arkansas
349 (UMN)	Monett, Missouri
363 (AMA)	Amarillo, Texas
402 (WAL)	Wallops Island, Virginia
405 (IAD)	Dulles Airport, Virginia
425 (HTS)	Huntington, West Virginia
429 (DAY)	Dayton, Ohio
433 (SLO)	Salem, Illinois
451 (DDC)	Dodge City, Kansas
456 (TOP)	Topeka, Kansas
486 (JFK)	Kennedy Airport, New York
494 (CHH)	Chatam, Massachusetts
518 (ALB)	Albany, New York
520 (PIT)	Pittsburgh, Pennsylvania
528 (BUF)	Buffalo, New York
532 (PIA)	Peoria, Illinois
553 (OMA)	Omaha, Nebraska
562 (LBF)	North Platte, Nebraska
606 (PWM)	Portland, Maine
637 (FNT)	Flint, Michigan

APPENDIX I (Continued)

Rawinsonde Stations Participating in AVE II Pilot Experiment

Station Identifier	Location
645 (GRB)	Green Bay, Wisconsin
654 (HON)	Huron, South Dakota
655 (STC)	St. Cloud, Minnesota
662 (RAP)	Rapid City, South Dakota
712 (CAR)	Caribou, Maine
734 (SSM)	Sault Sainte Marie, Michigan
747 (INL)	International Falls, Minnesota
764 (BIS)	Bismarck, North Dakota